Hydrodynamic Performances Analysis and Design of a Containership Propeller

Daniel Javier Orona Cobos

Master Thesis

presented in partial fulfillment
of the requirements for the double degree:
“Advanced Master in Naval Architecture” conferred by University of Liege
"Master of Sciences in Applied Mechanics, specialization in Hydrodynamics, Energetics and Propulsion” conferred by Ecole Centrale de Nantes

developed at "Dunarea de Jos" University of Galati
in the framework of the

“EMSHIP”
Erasmus Mundus Master Course
in “Integrated Advanced Ship Design”

Ref. 159652-1-2009-1-BE-ERA MUNDUS-EMMC

Supervisor:	Prof. Mihaela Amoraritei, "Dunarea de Jos" University of Galati
Reviewer:	Prof. Lionel Gentaz, “École Central de Nantes”

Galati, February 2014

TABLE OF CONTENTS

TABLE OF FIGURES

Declaration of Authorship

I declare that this thesis and the work presented in it are my own and have been generated by me as the result of my own original research.

Where I have consulted the published work of others, this is always clearly attributed.

Where I have quoted from the work of others, the source is always given. With the exception of such quotations, this thesis is entirely my own work.

I have acknowledged all main sources of help.

Where the thesis is based on work done by myself jointly with others, I have made clear exactly what was done by others and what I have contributed myself.

This thesis contains no material that has been submitted previously, in whole or in part, for the award of any other academic degree or diploma.

I cede copyright of the thesis in favour of the University of .....

Date: 22/01/2014 *Signature*

ABSTRACT

Hydrodynamic Performances Analysis and Design of a Containership Propeller.

By Daniel Javier Orona Cobos

Since its emergence as a propulsive element of the vessel, the importance of the propeller has a direct influence on ship propulsive performances due to its direct influence on the cost and effectiveness of ship operation.

Ship propellers need to be efficient. This implies that the energy supplied to the propeller is converted to thrust in order to overcome the ship resistance with minimum of losses. Additionally, the device should not generate unwanted vibration and inboard noise. Finally, the propeller should not suffer from erosion damage due to cavitation. Finding the right balance between these demands is a major task of the designer.

The propeller design is an activity which nowadays presents ever increasing challenges to the designer. The choice of an optimum marine propeller is an important issue in Naval Architecture.

This Master thesis will be focused on the design procedure of a marine propeller for 800 **TEU's* containership in order to find the optimum propeller characteristics involved by taking into account following stages:

1) The preliminary design (using standard series data);
2) The detailed design using the lifting line theory (lifting line method with lifting surface corrections).

Moreover, an analysis regarding hydrodynamic performances for the designed propeller will be developed, by studying the behavior of the geometry in off design conditions; all of this, through theoretical methods.

**TEU's: twenty-foot equivalent unit of cargo capacity*

1. INTRODUCTION.

The design of the most appropriate propeller for a specific vessel implies, as all Hydrodynamic aspects related with the project, a compromise solution in order to address different needs, many of them conflicting.

However, there are clear objectives which shall be covered:

a) The propeller must provide sufficient thrust power to propel the ship with a given range of speed determined before by the owner. This range of celerity includes the desired or optimal speed which the vessel will operate correctly. All of this, with a yield as high as possible, i.e., the power absorbed by it is the minimum that can be achieved. This leads to a lower installed power and thus, lower fuel consumption.
b) No cavitation should occur, or, at least, must be reduced up to admissible limits.
c) Mechanical/structural strength of the propulsion device has to be the adequate to allow it to work along its life subjected to efforts made on its blades without risk of breakage or deformation.
d) No vibrations induced by the propeller are allowable due to an improper location of the component at the aft part of the vessel and rudder. This phenomenon would provoke ruptures on weldings for example.

Nowadays, two main methods exist for a proper propeller design

1. The use of systematic series.
2. By “direct” calculation using lifting line method with lifting surface corrections.

However, a study of the behavior of the propeller will be performed in steady flow conditions with C.F.D. methods. This open-water hydrodynamic performances analysis has the objective to validate it as well as to determine how the propeller will act under certain conditions.

The present Master thesis pretends to be focused on the entire design process of a marine propeller for an 800 TEU’s container vessel. It will be designed in order to absorb minimum power with maximum efficiency, all of this, without cavitation, noise and vibrations.

2. PROBLEM DESCRIPTION.

2.1 GENERAL DATA

A marine propeller for a small feeder container vessel will be designed and analyzed in off design conditions.

Generally speaking, we could say that the propeller design procedure starts right after total ship resistance is determined for a range of velocity including the desired speed (optimal) by using either a statistical method or numerical methods.

To proceed, first of all it is necessary to know main particularities of the project; based on this, total ship resistance as well as powering prediction must be estimated with the following ship main particulars and form coefficients:

.

MAIN PARTICULARS			
TEU's	800		No. of Twenty Feet Unit
L_{OA}	140.64	[mt]	Length over all
L_{WL}	136.8	[mt]	Length weater-line
L_{PP}	130.0	[mt]	Length btwn perpendiculars
B	21.8	[mt]	Breadth
D	9.5	[mt]	Depth
T	7.3	[mt]	Mean Draft
∇	13311.00	[m^3]	Volumetric displacement
Δ	13644	[tons]	Displacement
V_S	18.5	[knots]	Service speed
DWT	9500.00	[tons]	Deadweight
LGHTWT	3811.00	[tons]	Ligthtweight

Table 1. 800 TEU's containershi p particularities.

FORM COEFFICIENTS		
C_M	0.966	Midship coeff
C_B	0.643	Block coeff
C_P	0.665	Prismatic coeff
C_W	0.833	Watrplane coeff

Table 2. Form coefficients.

3. THE TOTAL SHIP RESISTANCE PREDICTION.

The accurate prediction of ship resistance is important to ensure that it is kept to a minimum and to establish the power needed to propel the ship at different speeds.

In order to get the total resistance, the designer has many options available. Next graph shown below presents four different methodologies of approach to the issue; the traditional and standard series, the regression based procedures; the direct model test and numerical simulations.

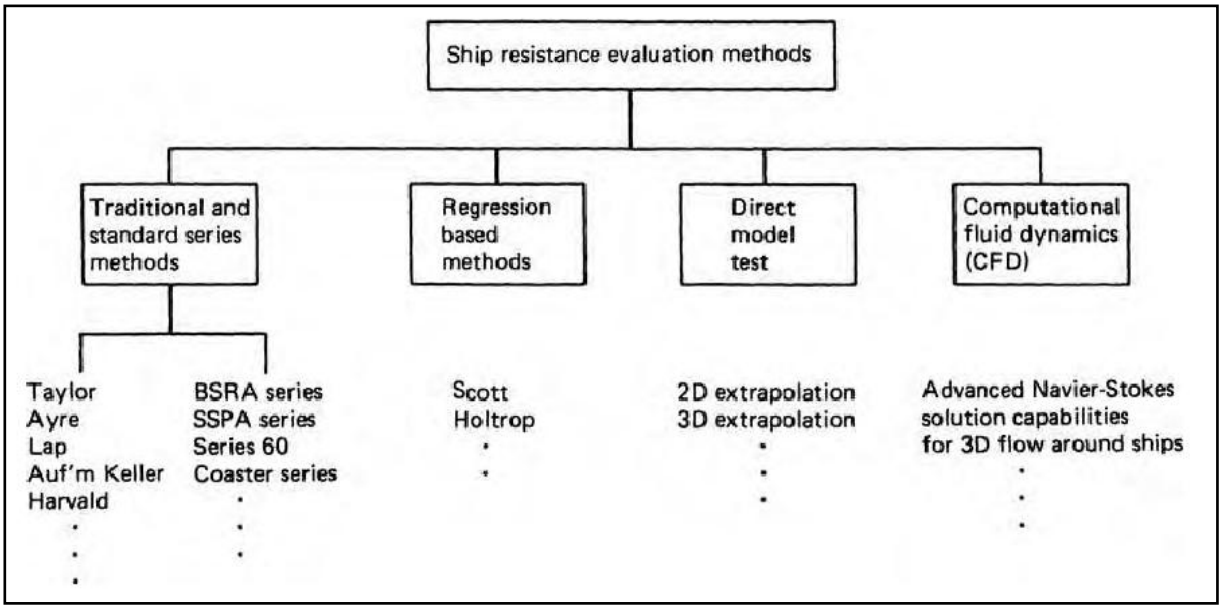

Figure 1. Ship resistance evaluation methods.

The first two evaluation methods are based on what naval architect traditionally will do, by taking main dimensions such as length, breadth, draft; longitudinal centre of buoyancy, speed of the vessel; parameters of hull forms such as block coefficient $[C_B]$, prismatic coefficient $[C_P]$ and so on.

At the early stages of the project, when only few main characteristics of the ship are known, experimental methods (direct model test) would be very expensive but also, they would be impossible due to the absence of lines plan on the early design phase. On these cases, the use of a statistical/analytical method is the most effective in order to predict ship resistance.

To apply one of these methods we must choose from the available information, paying special attention to the characteristics of our vessel by checking if our project 'fits' in the range of limitations given from selected prediction method.
It should be noted that these methods do not replace experimental results inasmuch as these are more accurate regarding ship resistance but statistical approximations give reliable values in order to continue further calculations.

Furthermore, experimental results will provide other items to proceed on the correct design of propulsion system, the arrangement of appendages, and so on; being able to make small modifications on the forms in order to improve the hydrodynamic behavior of the hull.

The majority of these computations are done based on statistical methods (regression analysis of statistical data). The most typical method of finding the resistance for a container vessel is the $Holtrop\ \&\ Mennen$ statistical method. The power required to propel the vessel through the water will depend upon the resistance given by the water itself and the air.

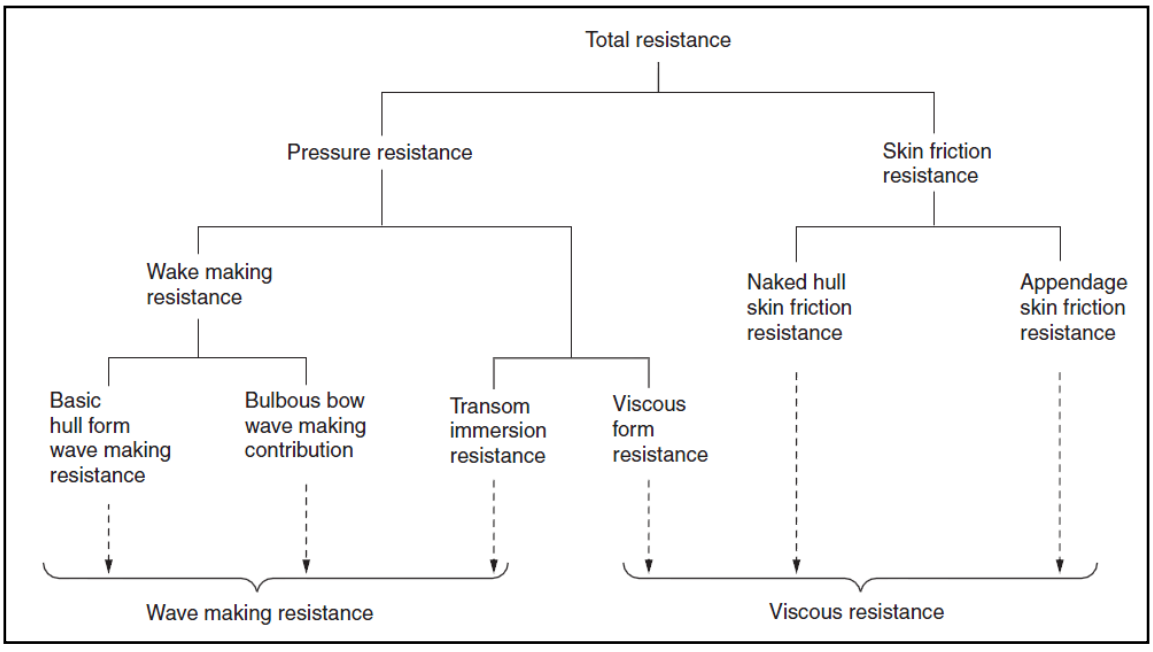

Figure 2. Components of the total ship resistance

By computing total ship hull resistance, the wave-making resistance, form resistance, eddy resistance and air resistance are concentrated into a force named as residuary resistance $[R_R]$. On the other hand, frictional resistance $[R_F]$ is determined with friction coefficient$[C_F]$ from ITTC-1957 formulae we have:

$$R_T = R_R + R_F \tag{1}$$

Where:

$$R_F = \frac{1}{2} C_F \rho S V^2 \tag{2}$$

$$C_F = \frac{0.075}{(log_{10} R_n - 2)^2} \tag{3}$$

On the other hand the resistance prediction issue can be solved with numerical methods as well. The appeal of a numerical method for estimating ship hull resistance is in the ability to seek the 'best' solution from many variations in shape. The development of these methods and their success is documented in the series of proceedings at the I.T.T.C. (International Towing Tank Conference). Nevertheless for having a benchmark, C.F.D. methods have been compared against high quality experimental tests done at the I.T.T.C. international workshops in order to see its capability and to approve reliable results from ship hull resistance point of view. One advantage over traditional towing tank tests and statistical methods is in the level of flow field detail which can be clearly observed. If correctly interpreted, this brings a greatly enhanced level of understanding to the designer on the physical behavior that occurs on the hull and the flow which surrounds it.

However, for our study case we have used *"An Approximate Power Prediction Method – 1982"* by J. Holtrop & G.G.J. Mennen in order to proceed with total ship resistance prediction due to our project is well suited into the application range given by this method and it provides reliable results on the early phases of design so that we can continue with power design.

SHIP TYPE	Max. F_n	C_p		L/B		B/T	
		Min	Max	Min	Max	Min	Max
TANKERS / BULK-CARRIERS	0.24	0.73	0.85	5.10	7.10	2.40	3.20
TRAWLERS / COASTERS / TUGS	0.38	0.55	0.65	3.90	6.30	2.10	3.00
CONTAINERSHIPS / DESTROYER TYPES	**0.45**	**0.55**	**0.67**	**6.00**	**9.50**	**3.00**	**4.00**
CARGO LINERS	0.30	0.56	0.75	5.30	8.00	2.40	4.00
RO-RO SHIPS / CAR FERRIES	0.35	0.55	0.67	5.30	8.00	3.20	4.00
800 TEU's CONTAINER VESSEL	**0.25**	**0.67**		**6.28**		**3.00**	

Table 3. Holtrop & Mennen power prediction method limitations with 800 TEU's container vessel project values.

From main particulars whose were described before on table 1, total ship resistance prediction has been performed with Holtrop & Mennen-1982 method which is presented on next table for ship's working range including its operational velocity.

V_S [knot]	R_T [kN]
15	363
16	430
17	482
18	542
18.5	**581**
19	661
20	798
21	925
22	1033

Table 4. Total ship resistance for different velocities including design speed.

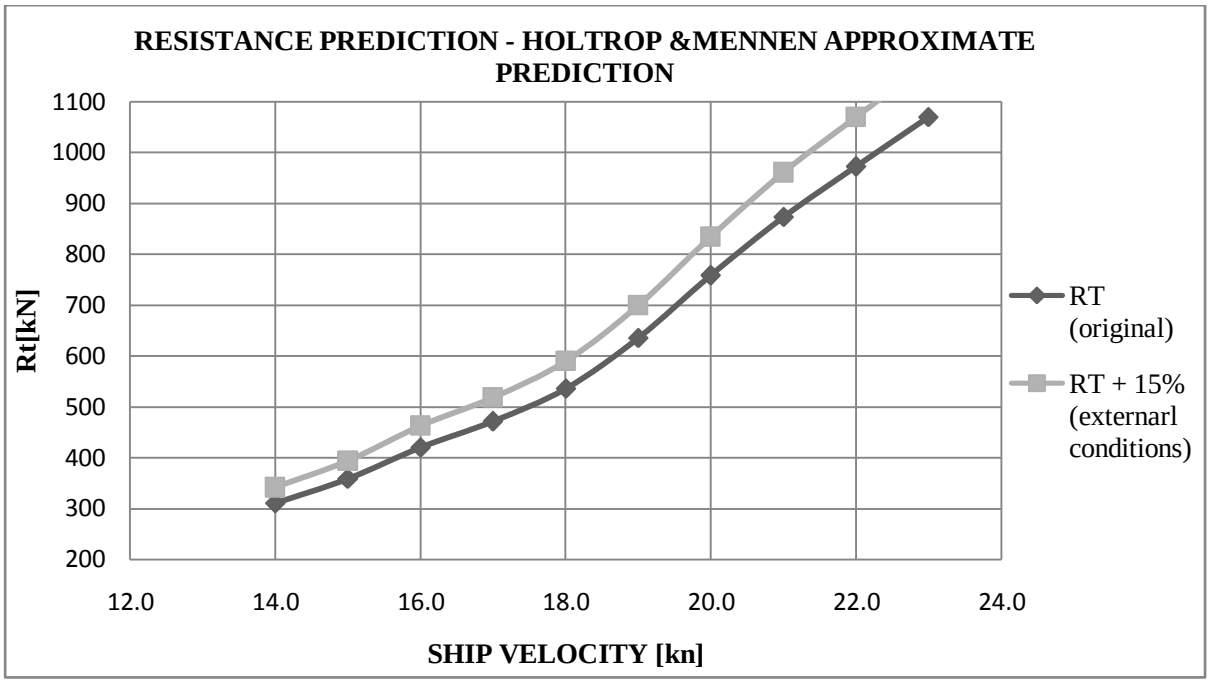

Figure 3. 800 TEU's containership total resistance.

Moreover, a prediction of the global wake fraction coefficient [w] as well as thrust deduction factor [t] and relative rotative efficiency [η_R] were performed by statistical methods, these were "Troost for cargo ships" and "Holtrop & Mennen 1978" respectively.

$$w = 0.25 + 2.5(C_B - 0.6)^2 \tag{4}$$

$$t = 0.001979\left(\frac{L}{B(1-C_P)}\right) + 1.0585\frac{B}{L} - 0.00524 - \frac{0.1418D^2}{BT} \tag{5}$$

$$\eta_R = 0.9922 - 0.05908\left(\frac{A_E}{A_0}\right) + 0.07424(C_P - 0.0225lcb) \tag{6}$$

Where,

lcb = longitudinal centre of buoyancy = 2.02% aft of $\frac{1}{2}L_{pp}$

PROPULSION FACTORS (hull-propeller interaction coefficients)		
w	0.25	Mean wake fraction coefficient
t	0.16	Thrust deduction coefficient
η_R	0.99	Relative rotative efficiency

Table 5. Hull-propeller interaction factors.

4. PROPULSIVE POWER ESTIMATION.

One of the most important problems in Naval Architecture during the early phases of the project is the determination of the propulsive power required for the vessel to overcome its resistance and to be capable to sail at the design speed.

For this starting point, a 'rough' proposal for propeller characteristics was established with empirical formulas in order to proceed with powering prediction. Following table provides information regarding propeller particulars as a starting point.

PROPELLER CHARACTERISTICS.			
D	[mt]	5.4	Initial propeller diameter
Z		4	Blade number
h	[mt]	4.7	Height from the water line to the center line of the shaft
A_E/A_O		0.8	Initial Expanded Area Ratio (Keller's formulation)

Table 6. 800 TEU's containership 'first' propeller particularities.

1. The propeller diameter [D]: data obtained as a result of the formulae proposed by MAN-DIESEL & TURBO engine manufacturer on its article entitled *"Basic Principles of Ship Propulsion"* which states:

   draft / D < approximately 0.74

2. The blade number [z]: there is no restriction regarding number of blades. Propellers may be manufactured with 2 up to 6 blades depending on the project. We have to keep in mind that the fewer the number of blades are, the higher the propeller efficiency will be. Nevertheless for reasons of strength, propellers which are subjected to heavy loads cannot be manufactured with only 2 or 3 blades. Normally 4, 5 and 6-bladed propellers are used for merchant ships. Also, the selection of number of blades has a direct impact regarding number of cylinders of the diesel engine, which could lead to vibrations issues.
3. The height from the water line to axis of the shaft [h]: measured directly from the lines plan.
4. The expanded area ratio [A_E/A_O]: an initial value determined by Keller's formulae which states:

"The blade area ratio can be determined from e.g. Keller's formulae:

$$\frac{A_E}{A_0} = K + \frac{(1.3 + 0.3Z)T}{(p_o + \rho gh - p_v)D^2} \tag{7}$$

In this formula [T] is the propeller thrust, [p_v] is the vapour pressure, [$p_o + \rho gh$] is the static pressure at the shaft centre line and [K] is a constant to which the following figures apply:

K = 0 to 0.1 for twin-screw ships;
K = 0.2 for single-screw ships. "

Once the 'early' propeller characteristics as well as the effective power that we would have to use to tow the ship without propulsive system is known [$P_E = R_T V_S = 5531 kWatt$] thanks to resistance calculation, the next step will be to compute different efficiencies such as shaft efficiency [η_S], reduction gear efficiency [η_G] (if applicable), **open-water efficiency [η_O]** relative rotative efficiency [η_R], hull efficiency [η_H], quasi-propulsive efficiency [η_D] and so on; as well as performances such as shaft power [P_S], thrust power [P_T], delivered power [P_D]; and losses along the drive-train that precede thus, to obtain an approximation of the minimum

required power for the prime mover named as brake power [P_B] and the moment generated by the propeller [Q].

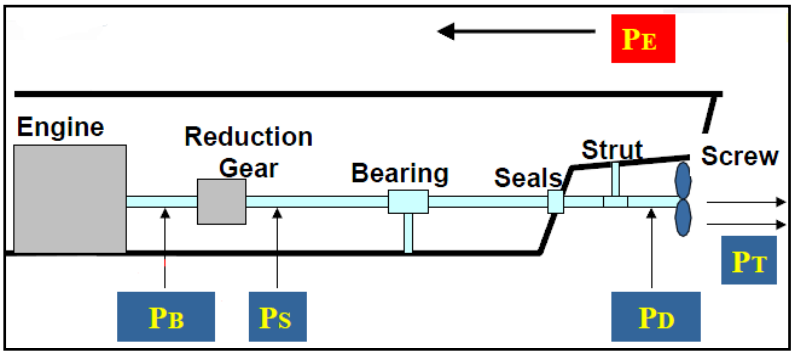

Figure 4. Ship's drive-train and Power description.

In order to estimate the 'brake power' [P_B]; then, to select the marine engine and finally, to fix the diameter [D] as well as the revolution rate [N], it is necessary to know of among other terms, the open water efficiency [η_0] by using on our case, the Wageningen B-series diagrams employing the propeller characteristics described before (see Table 6).

Starting from

$$P_T = \frac{P_E}{\eta_H} = TV_A = P_D\eta_B \tag{8}$$

$$P_D = \frac{P_T}{\eta_0\eta_R} = 2\pi nQ \tag{9}$$

$$\eta_B = \eta_0\eta_R = \frac{P_T}{P_D} \tag{9.1}$$

We then have,

$$P_B = \frac{P_D}{\eta_S} \tag{10}$$

Finally, [P_B] is dependant ofamong other factors, the open water efficiency [η_0] expressed as,

$$P_B = \frac{P_E}{\eta_S\eta_H\eta_R\eta_0} = \frac{P_E}{\eta_S\eta_H\eta_B} = \frac{P_E}{\eta_S\eta_D} \tag{10.1}$$

Where,

$$P_E = R_T V_S = 5531 kWatt \tag{11}$$

$\eta_S =$ 0.97 (our case)

$\eta_R =$ 0.99 (computed before by Holtrop-Mennen expression)

$$\eta_D = \eta_B \eta_H \tag{12}$$

$$\eta_B = \eta_0 \eta_R = \frac{P_T}{P_D} \tag{13}$$

$$\eta_H = \frac{1-t}{1-w} > 1 = \frac{1-0.16}{1-0.25} = 1.12 \tag{14}$$

$$\eta_0 = \left(\frac{K_T}{K_Q}\right)\left(\frac{J}{2\pi}\right) \tag{15}$$

$$K_T = \frac{T}{\rho n^2 D^4} \tag{15.1}$$

$$K_Q = \frac{Q}{\rho n^2 D^5} \tag{15.2}$$

$$J = \frac{V_A}{nD} \tag{15.3}$$

$$V_A = V_S(1-w) \tag{16}$$

WhereK_T,K_Q, η_0 and J are known vith the B-Wageningen diagrams. To predict these values, it is possible to use the method of multiple linear regression analysis for B-Wageningen series by programming the *regression polynomials expressions* which are presented later on.

The polynomials for torque and thrust coefficients derived with multiple regressions with a Reynolds number $\boldsymbol{R_n = 2x10^6}$ analysis used on our case are then:

$$K_T = \sum_{s,t,u,v} C^T_{s,t,u,v} (J)^s (P/D)^t (\frac{A_E}{A_0})^u (Z)^v \tag{16.1}$$

$$K_Q = \sum_{s,t,u,v} C^Q_{s,t,u,v} (J)^s (P/D)^t (\frac{A_E}{A_0})^u (Z)^v \tag{16.2}$$

Where,

Coefficients $[C^T_{s,t,u,v}]$ and $[C^Q_{s,t,u,v}]$ are written on following table.

THRUST K_T					**TORQUE K_Q**				
$C_{s,t,u,v,}$	**s**	**t**	**u**	**v**	**$C_{s,t,u,v,}$**	**s**	**t**	**u**	**v**
	[J]	**[P/D]**	**A_E/A_O**	**[z]**		**[J]**	**[P/D]**	**A_E/A_O**	**[z]**
0.01	0.00	0.00	0.00	0.00	0.00379368	0	0	0	0
-0.20	1.00	0.00	0.00	0.00	0.00886523	2	0	0	0
0.17	0.00	1.00	0.00	0.00	-0.03224100	1	1	0	0
0.16	0.00	2.00	0.00	0.00	0.00344778	0	2	0	0
-0.15	2.00	0.00	1.00	0.00	-0.04088110	0	1	1	0
-0.48	1.00	1.00	1.00	0.00	-0.10800900	1	1	1	0
0.42	0.00	2.00	1.00	0.00	-0.08853810	2	1	1	0
0.01	0.00	0.00	0.00	1.00	0.18856100	0	2	1	0
-0.05	2.00	0.00	0.00	1.00	-0.00370871	1	0	0	1
0.01	0.00	1.00	0.00	1.00	0.00513696	0	1	0	1
0.06	1.00	1.00	0.00	1.00	0.02094490	1	1	0	1
-0.01	0.00	0.00	1.00	1.00	0.00474319	2	1	0	1
0.01	1.00	0.00	1.00	1.00	-0.00723408	2	0	1	1
-0.13	0.00	3.00	0.00	0.00	0.00438388	1	1	1	1
0.01	0.00	6.00	0.00	0.00	-0.02694030	0	2	1	1
0.00	2.00	6.00	0.00	0.00	0.05580820	3	0	1	0
0.17	3.00	0.00	1.00	0.00	0.01618860	0	3	1	0
-0.05	0.00	0.00	2.00	0.00	0.00318086	1	3	1	0
0.09	2.00	0.00	2.00	0.00	0.01589600	0	0	2	0
-0.05	3.00	0.00	2.00	0.00	0.04717290	1	0	2	0
0.01	1.00	6.00	2.00	0.00	0.01962830	3	0	2	0
-0.01	2.00	6.00	2.00	0.00	-0.05027820	0	1	2	0
-0.01	0.00	3.00	0.00	1.00	-0.03005500	3	1	2	0
0.02	1.00	3.00	0.00	1.00	0.04171220	2	2	2	0
0.00	3.00	3.00	0.00	1.00	-0.03977220	0	3	2	0
-0.03	0.00	3.00	1.00	1.00	-0.00350024	0	6	2	0
0.02	1.00	0.00	2.00	1.00	-0.01068540	3	0	0	1
0.00	0.00	2.00	2.00	1.00	0.00110903	3	3	0	1
0.00	0.00	0.00	0.00	2.00	-0.00031391	0	6	0	1
0.00	1.00	0.00	0.00	2.00	0.00359850	3	0	1	1
0.00	2.00	0.00	0.00	2.00	-0.00142121	0	6	1	1
0.00	3.00	0.00	0.00	2.00	-0.00383637	1	0	2	1

0.00	1.00	2.00	0.00	2.00	0.01268030	0	2	2	1
0.00	1.00	6.00	0.00	2.00	-0.00318278	2	3	2	1
0.00	2.00	6.00	0.00	2.00	0.00334268	0	6	2	1
0.00	0.00	0.00	1.00	2.00	-0.00183491	1	1	0	2
0.00	0.00	3.00	1.00	2.00	0.00011245	3	2	0	2
0.00	3.00	6.00	1.00	2.00	-0.00002972	3	6	0	2
0.00	0.00	3.00	2.00	2.00	0.00026955	1	0	1	2
					0.00083265	2	0	1	2
					0.00155334	0	2	1	2
					0.00030268	0	6	1	2
					-0.00018430	0	0	2	2
					-0.00042540	0	3	2	2
					0.00008692	3	3	2	2
					-0.00046590	0	6	2	2
					0.00005542	1	6	2	2

Table 7. Coefficients for polynomials: thrust [K_T] an torque [K_Q] respectively

Its range of application covers:

2	**z**	7
0.3	$\mathbf{A_E/A_O}$	1.05
0.5	**P/D**	1.40

Table 7.1. Regression polynomials application range.

By programming the hydrodynamic characteristics of the screw propeller on *EXCEL* application based on polynomial regressions expressions explained before and entering data such as: a) the expanded area ratio [$\frac{A_E}{A_0} = 0.85$]; b) number of blades [Z = 4]; c) pitch ratio [$\frac{P}{D} = 0.1 \sim 1.4$] we have obtained following charts (B4.85 diagrams) and the maximum open-water efficiency for our case.

The curve plotted on diagrams is given by:

$$\frac{K_T}{J^2} = \frac{T}{\rho V^2 D^2} \tag{17}$$

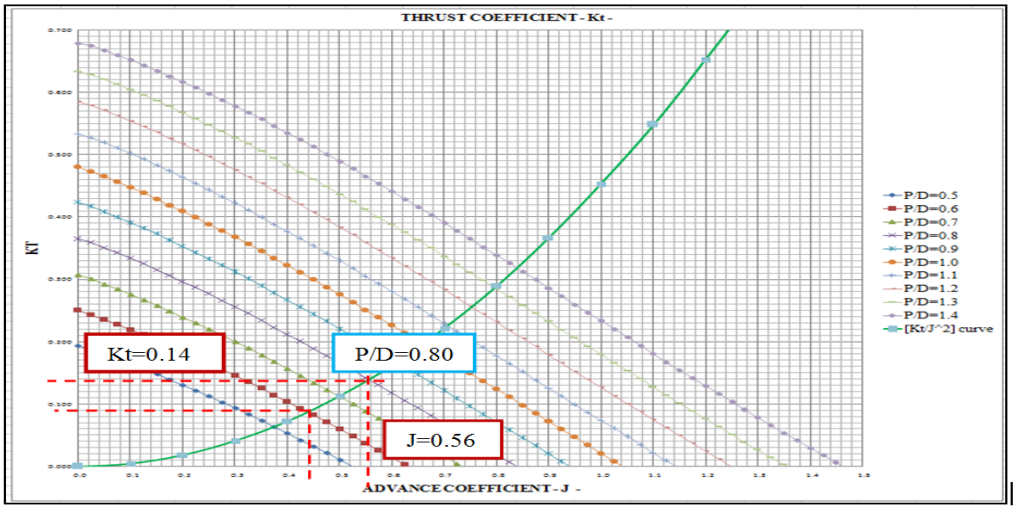

Figure 5.1. Thrust coefficient – advance coefficient diagram [Kt-J] (B4.85 diagrams).

Once we know the advance coefficient as well as thrust coefficient by intersecting all P/D values against the $[\frac{K_T}{J^2}]$ curve; it is now possible to get torque coefficient. This coefficient can be known by looking on the [Kq-J] diagram shown below. By entering with the result of each advance coefficient [J] read on the [Kt-J] diagram with the correspondent intersection point of each curve which represents each P/D value. These values will be then, torque coefficients

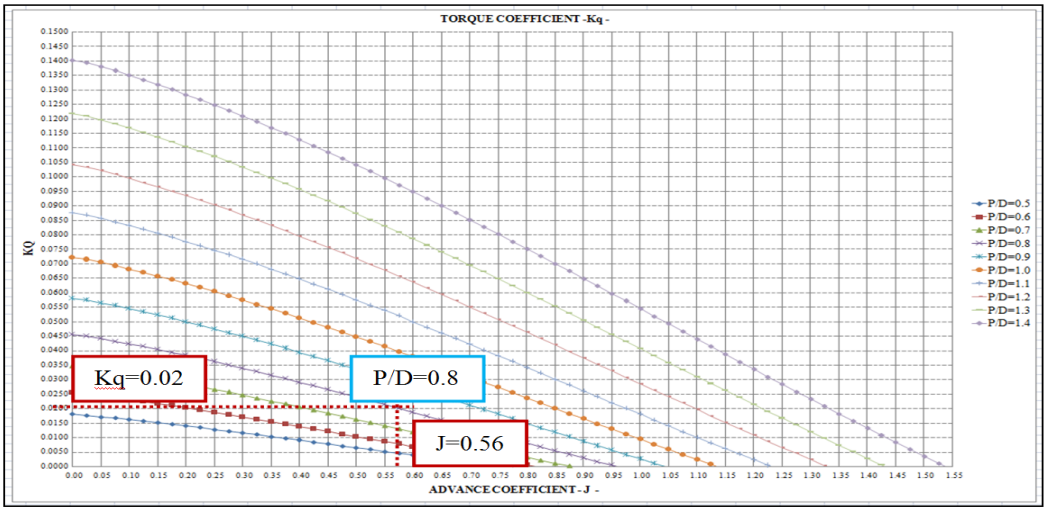

Figure 5.2. Torque coefficient – advance coefficient diagram [Kq-J] (B4.85 diagrams).

Later on, the open water efficiencies $[\eta_0]$ may be known either by reading directly the value on the following chart using the resultant advance coefficient [J] extracted on [Kt-J] diagram for each P/D value and the intersection point with the $[\frac{K_T}{J^2}]$ curve crossing its respective efficiency curve; or by computing with the empirical formula (equation 15).

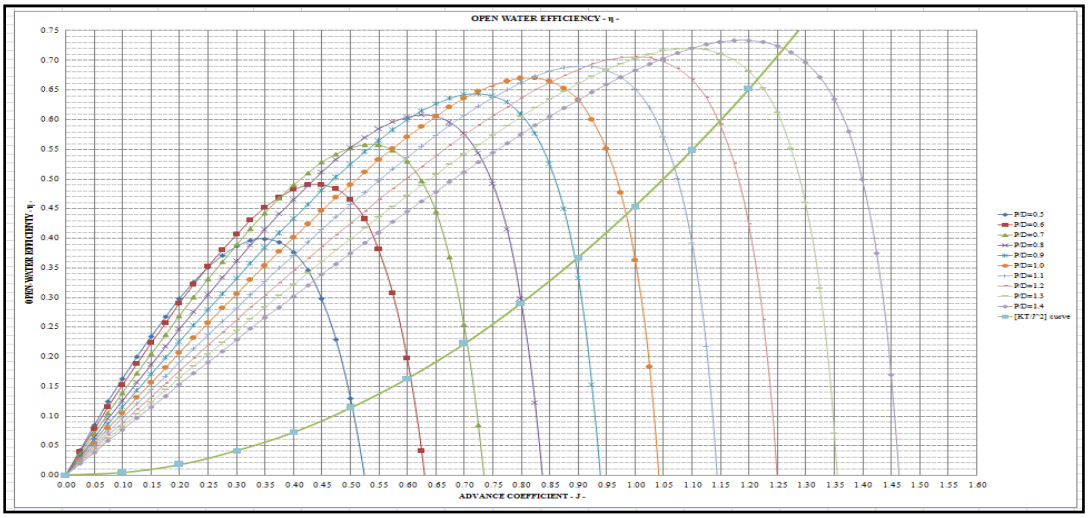

Figure 5.3. Open water efficiencies diagram [η_0-J] (B4.85 diagrams).

THRUST	WATER DENSITY	SHIP VELOCITY	ADVANCE VELOCITY	THRUST DEDUCTION	GLOBAL WAKE COEFFICIENT	DIAMETER	PITCH RATIO	CURVE	ADVANCE COEFFICIENT	THRUST COEFFICIENT	TORQUE COEFFICIENT	OPEN WATER EFFCICIENCY	RELATIVE ROTATIVE EFFICIENCY
T [kN]	ρ [ton/mt^3]	V_S [m/sec]	V_A [m/sec]	t	w	D [mt]	P/D	k_T	J	k_T	k_Q	η_O	η_R [%]
690	1.025	9.52	7.14	0.16	0.25	5.40	0.00						0.99
							0.10						
							0.20						
							0.30						
							0.40						
							0.50	0.11	0.38	0.07	0.01	0.39	
							0.60	0.16	0.44	0.09	0.01	0.504	
							0.70	0.22	0.50	0.12	0.02	0.60	
							0.80	**0.29**	**0.56**	**0.14**	**0.02**	**0.623**	
							0.90	0.37	0.61	0.17	0.03	0.619	
							1.00	0.45	0.66	0.20	0.03	0.61	
							1.10	0.55	0.71	0.227	0.04	0.60	
							1.20	0.65	0.75	0.26	0.05	0.60	
							1.30	0.77	0.80	0.29	0.06	0.60	
							1.40	0.89	0.84	0.32	0.07	0.60	

Table 8. Results.

Results highlighted represent values obtained for the maximum open water efficiency possible [η_0]. This information obtained will be considered as input data for estimating the required power to be installed on board.

REMARK : It should be noted that we have assumed a new value of Expanded Area Ratio [A_E/A_0] different from the one which was approximated before thanks to Keller's formulae (see table 6) due to Keller's approximation formulae as it is called, it provides an estimated value in order to proceed with further calculations but, it does not ensure the right one and as a consequence, it does not provide any information regarding minimum value to avoid cavitation criteria determined with Burrill diagrams for example; an increment of expanded area ratio [A_E/A_0] value does not ensure the absence of cavitation phenomenon but it helps in order to do not be far from the real expanded area ratio value. After computations are done, an interpolation could be executed in order to approach the results obtained with the "experience" value taken of E.A.R. to the real one which is provided on our case, from Burrill diagrams if for example, the E.A.R. used were smaller than the one proposed by any methodology regarding cavitation criteria. Based on this, we have performed previous computations with the highlighted Expanded Area Ratio value shown below:

A_E/A_O	0.797	E.A.R. calculated from KELLER's formulae
A_E/A_O	**0.850**	**E.A.R. taken after Keller's prediction (by experience)**

Table 9. E.A.R. value (experience).

Before determining the engine brake power [P_B] necessary, we have to take in consideration that the estimation of resistance at the beginning corresponds to still water and ideal weather conditions; on the other hand related to the hull, we consider that it is not fouled. Throughout the years, its resistance will increase due to fouling phenomenon. It is possible to take into account following 'design' factors during the design process which are described below:

- The sea margin (S.M.): which represents a power increasing traditionally of 15%; it is applied when determining the required engine power. However, for large container vessels, 20%-30% may sometimes be used. Here, fouling effect is within this margin.

- The engine margin (E.M.): besides the sea margin the so-called engine margin, is defined as the maximum power which the engine is designed to work as a continuous manner, fulfilling the requirements of the Classification Society. Regularly on diesel engines this value ranges between 85% and 95% of its power known as Maximum Continuous Rating (M.C.R.) frequently added as an operational margin for the prime mover. This fraction of power requirement is usually determined by the customer.

Once the propeller has been designed, it has a point of operation, a revolution rate [n] and a delivered power to the propeller [P_D]; considering performance estimation on shaft line, this means a brake power for given revolutions. This point is known *design point* [DP]. On the diagram shown below, it can be seen the propeller working lines (line 6).

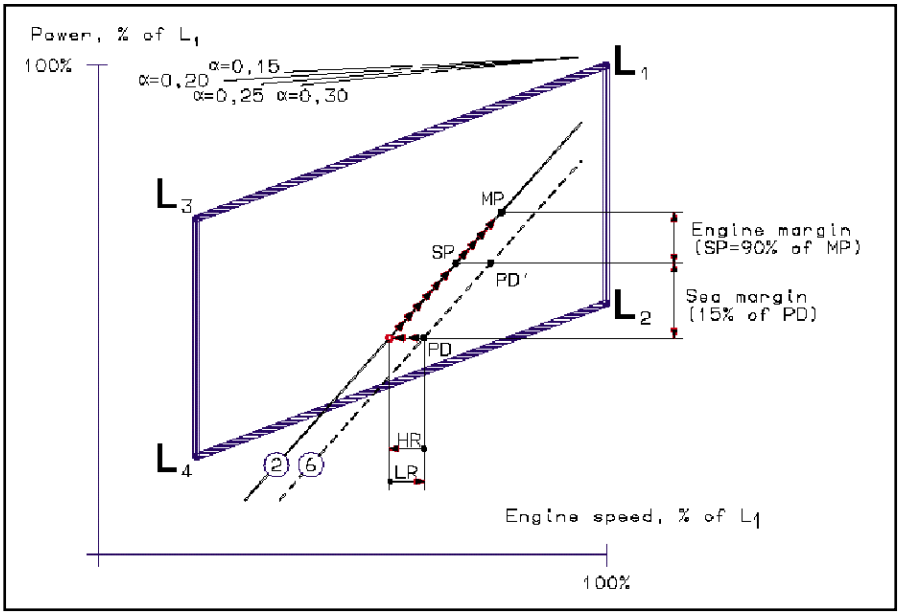

Figure 6. Working diagram (propeller-engine).

When the vessel has sailed for some time, the hull and propeller are fouled and therefore the resistance is increased for the same speed. Therefore, the power output must increase to maintain speed or slow down if you cannot increase the power. In either case, the propeller thrust is increased. This is called "loaded propeller". Operating propeller line is moved to the left (line 2).

If the propulsor device is destined to operate at its (M.C.R; ideal conditions), the propeller will be working at its best condition; later on, after some years on service, the propeller will

now be working at its Normal Continuous Rate (N.C.R.) which comprehends a percentage between 85%-90% of its (M.C.R.) as stated before.

In general it is recommended for engine selection that the operation diagram covers not only the propeller operating line for light running (trial condition) but also the line which is shifted to the left between 3% and 7% of the revolutions in heavy running condition.

Then, taking into account previous parameters and input data necessary, we may now determine the brake power demanded four our four-bladed 'stock 'propeller.

V_S [knot]	R_T [kN]	η_R [%]	η_H [%]	η_S [%]	η_B [%]	η_D [%]	P_E [kW]	P_D [kW]	$P_{B\ final}$ [kW]
15	363								
16	430								
17	482								
18	542								
18.5	**581**	**0.99**	**1.12**	**0.97**	**0.62**	**0.694**	**5531**	**7970**	**9921**
19	661								
20	798								
21	925								
22	1033								

Table 10. Efficiencies and power prediction for 800 TEU's container vessel.

Where,

$$P_B final = P_B + 15\% + 5\% \quad (18)$$

4.1 ENGINE SELECTION.

The selection of propulsion machinery will depend on design features such as space, weight and noise levels, together with overall requirements including areas of operation, running costs and maintenance. All of these factors will depend on the ship type, its function and operational patterns.

Main factors to consider on the prime mover selection are:

a) Compactness and weight: Extra deadweight and space. Engine dimensions are important for all types of ships, especially for merchant ships due to the big the payload space is, the more rentable vessel will be.
b) Initial cost.
c) Type of fuel and consumption: Influence on running costs and bunker capacity (deadweight and space).
d) Grade of fuel (lower grade/higher viscosity, cheaper).
e) Level of emission of NOx, SOx and CO2.
f) Noise and vibration levels.
g) Maintenance requirements/costs, costs of spares.
h) Rotational speed: lower propeller speed plus larger diameter generally leads to increased efficiency.

One of the most efficient machinery available and used for merchant vessels is the diesel engine. Around 90 percent of merchant ships, specifically, container vessels are powered by diesel engines due to this type of fuel is considered as inexpensive as well as the fuel quality does not affect the performance of the engine (most of the case). Other advantages are related to low maintenance requirements for long working periods; simple technology.

Depending on the type of vessel and its operational profile, the most favorable solution must be chosen in the earliest conceptual design stage.

However, due to the facility regarding diesel engine manufacturers, easy to find spare parts, low fuel cost and consumption, the absence of gear box requirement, coupled directly on the shaft line with a fixed pitch propeller (F.P.P.) working at low revolution rate among others, 2-stroke diesel engine has been chosen as a prime mover of propulsion machinery for our case.

With the propeller working layout presented before (figure 6), it is also presented the engine working layout diagram provided by the engine manufacturer. Engine power is specified in kWatt for each cylinder number and layout points $L_1, L_2, L_3,$ *and* $L4$.
L_1 designates the nominal (M.C.R.) at 100% engine power and full speed. L_2, L_3, L_4 designate layout points at the other three corners of the layout area, chosen easy for reference.

The engine should be capable to work at all points (revolution rate/power) within the parallelepiped.

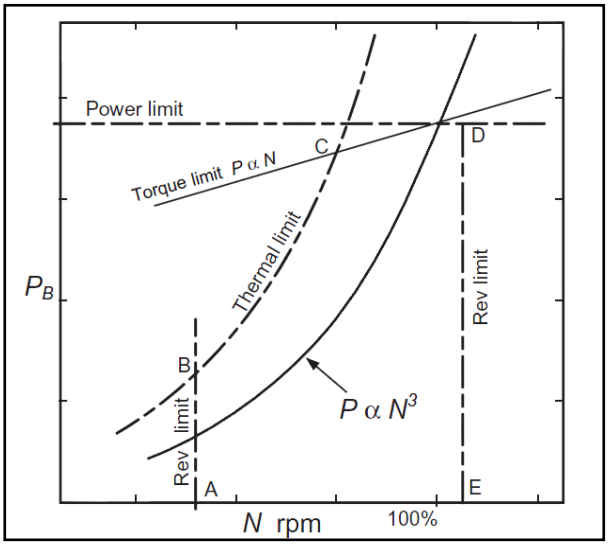

Figure 7. Typical diesel engine limits.

Having previous knowledge of engine selection as well as the input data necessary to choose it, the following step will be then, to find an engine which fits with the requirements of the project's brake power.

A low speed engine "*MAN B&W S50ME-B8*" from MAN DIESEL manufacturer was selected. Following chart illustrates the information regarding engine particulars provided by the builder as well as the specifications respectively.

ENGINE SELECTION						
MAN B&W S50ME-B8			LOW SPEED ENGINE			
			2 STROKES			
			6 CYLINDERS			
N [RPM]	n [rps]	P_B [kW]	L_1	L_2	L_3	L_4
108	1.80	9960	1660	1330	1410	1130
127	2.12					

Table 11. Selection of the engine.

MAN B&W S50ME-B8

Cyl.	L_1 kW
5	8,300
6	9,960
7	11,620
8	13,280
9	14,940

Stroke: 2,000 mm

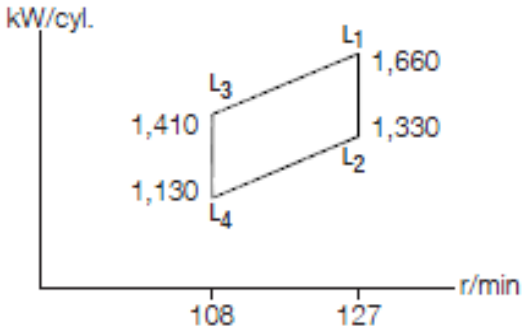

SFOC for engines with layout on L_1 - L_3 line [g/kWh] — L_1/L_3 MEP: 20.0 bar

SFOC optimised load range	Tuning	50%	75%	100%
High load (85%-100%)	-	168.5	166.0	169.0
Part load (50%-85%)	ECT	167.5	165.0	172.0
	VT	165.5	164.5	169.5
	EGB	165.5	164.5	170.5
Low load (25%-70%)	ECT	166.0	165.5	170.5
	VT	163.5	165.5	169.5
	EGB	163.5	165.5	170.5

SFOC for engines with layout on L_2 - L_4 line [g/kWh] — L_2/L_4 MEP: 16.0 bar

SFOC optimised load range	Tuning	50%	75%	100%
High load (85%-100%)	-	164.5	160.5	163.0
Part load (50%-85%)	ECT	163.5	159.5	166.0
	VT	161.5	159.0	163.5
	EGB	161.5	159.0	164.5
Low load (25%-70%)	ECT	162.0	160.0	164.5
	VT	159.5	160.0	163.5
	EGB	159.5	160.0	164.5

The SFOC excludes 1 g/kWh for the consumption of the electric HPS

Specifications

Dimensions:	A	B	C	H_1	H_2	H_3
mm	850	3,150	1,088	9,050	8,500	8,250

Cylinders:	5	6	7	8	9	
L_{min} mm	5,924	6,774	7,624	8,474	9,324	
Dry mass t	189	215	241	276	314	

Figure 8. MAN B&W S50ME-B8 main particulars. MAN DIESEL manufacturer catalogue (source 2013).

Later on, after the required brake power [P_B] is known, the following stage will be to find the best solution regarding optimum diameter for the revolution rate provided by the selected engine. This step is generally considered on the propeller design loop as the preliminary design of the marine propeller using standard series data.

5. THE PROPELLER DESIGN PROCESS.

Since its emergence as a propulsive element of the vessel, the importance of the propeller has grown continuously due to its direct influence on the cost and effectiveness of ship operation.

As theoretical knowledge in the field of naval hydrodynamics has grown, the attention has been focused as well to the propeller design and efforts have been intensified in order to develop mathematical tools to predict the behavior of a propeller in a 'field' of variable speeds.

The most important issues regarding propeller design and its consequences of 'a poor design' are the presence of vibrations on the hull, on the shaft line, propeller erosion/cracks due to cavitation, propeller blade breakage, among others. These problems have grown unfortunately, as a result of increasing the use of power of the propulsion engines installed on ships.

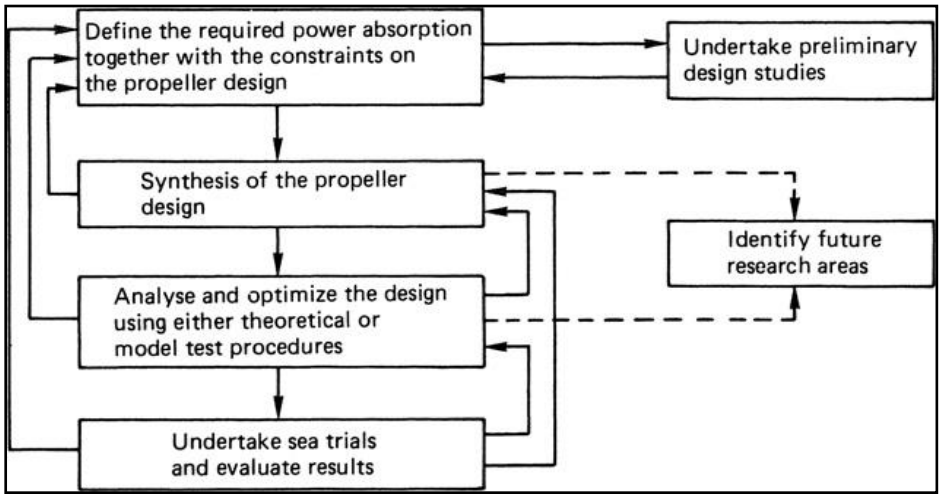

Figure 9. Stages on propeller design.

5.1 THE SELECTION OF THE MARINE SCREW PROPELLER.

On this section we present two different solutions regarding propulsion system devices that are currently in use; however, it is important to gain an overview of the subject prior discussing the propeller design process. Accordingly, principal propeller types are then briefly reviewed according to merchant ships by outlining their major features and characteristics together with their general areas of application.

5.1.1 Fixed pitch propeller.

Made from a single casting; usually they have an efficiency, cost and simplicity advantage over other type of propellers. F.P. propellers are most efficient at one speed (constant) and therefore ideal for long voyages.

For a fixed pitch propeller the choice of blade number, notwithstanding considerations of blade-to-blade clearances at the blade root to boss interface, is largely an independent variable and is normally chosen to give a mismatch to the range of hull superstructure and machinery vibration frequencies which are considered likely to cause concern. Additionally, blade number is also a useful parameter in controlling unwelcome cavitation characteristics. Blade numbers generally range from two to seven, although in some naval applications, where considerations of radiated noise become important, blade numbers greater than these have been researched and used to solve a variety of propulsion problems. For merchant vessels, however, four, five and six blades are generally favored.

Figure 10. Fixed Pitch Propeller of a merchant ship.

A F.P. propeller must use a reversing system (transmission) in order to be able for making astern movements.

5.1.2 Controllable pitch propeller.

Unlike fixed pitch propellers whose blades are fixed to the hub, the controllable pitch propeller provides an extra degree of freedom in its ability to change blade pitch.

C.P. propeller has installed inside the hub a mechanical or hydraulic system which makes rotate the blades around its vertical axis in order to control the pitch at different service conditions. This movement does not affect the performance of the vessel due to the propeller pitch may be change while the propeller rotates and develop thrust.

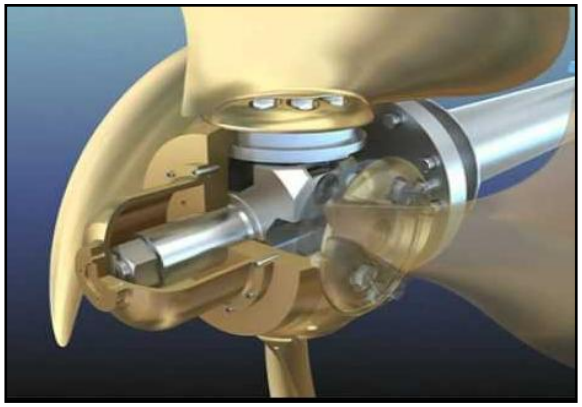

Figure 11. Controllable Pitch Propeller with mechanical mechanism.

A controllable pitch propeller allows the use of full engine throttle at given RPM's under all operational conditions.

One of its best advantages is that controllable pitch propellers provide highest propulsive efficiency over a wide range of RPM's for different velocities and load conditions by automatic adjusting. Another advantage is better maneuvering performances than fixed pitch propellers.
On the other hand controllable pitch propellers are more expensive than fixed pitch propellers due to its mechanical/hydraulic mechanism inside the hub as well as the manufacturing process is relatively expensive. Also the blade area and the length of the blade section of a controllable pitch propeller are limited to ensure blade reversibility.

However, there are different options regarding propulsion system devices depending on the project. Nonetheless, we have presented the most common options available to merchant ships.

Moreover, due to its advantages such as relatively low manufacturing cost, easy to manufacture as well as a high efficiency and a good performance for long voyages among others, a Fixed Pitch Propeller was selected from different options on market.

5.2 FIRST STAGE: THE PRELIMINARY PROPELLER DESIGN.

Traditionally, propeller design was based on standard series data, by using the systematic propellers series. These are a set of different propeller forms whose geometrical characteristics have been varied systematically so that its performances and behavior (on cavitation) are optimal and results are disposed.

Several systematic propellers series are available for the designer. We can highlight the following series:

1. A & B series from Wageningen.
2. M.A.U. series from Japan.
3. K.C.B. series from Newcastle University.
4. Gwan series.

The most used propellers series are the Wageningen B-series propellers. These charts, were created by testing several number of model propellers on open-water conditions (120) at the Netherlands Ship Model Basin in Wageningen (N.S.M.B.) and also, they have been transformed into polynomial expressions (see equations 16.1 and 16.2**)** allowing easy interpolation and optimization within the traditional propeller geometries.

Furthermore, the derived polynomials were presented in traditional formats as today are well known (diagrams) giving the Torque (K_Q) and Thrust (K_T) coefficients in unction of blade number (Z), blade area ratio$\left(\frac{A_E}{A_0}\right)$, pitch ratio$\left(\frac{P}{D}\right)$ and advance coeffient (J) for Reynolds number = $2.0x10^6$.

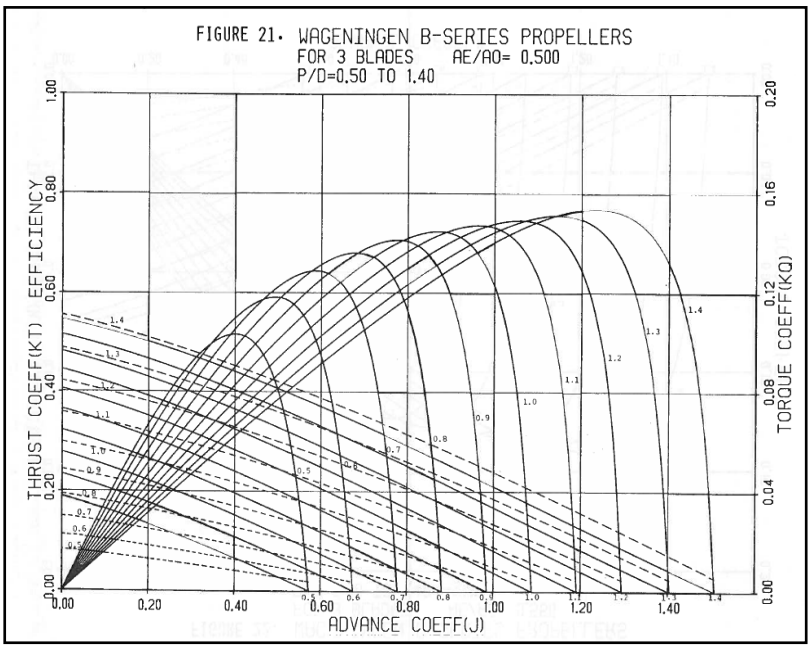

Figure 12. B-Wageningen open-water efficiency propeller diagram example (B3.50).

Today is still used as a popular starting point for modern propeller design process due to it is one of the most complete series. The preliminary propeller design stage has been accomplished based on B-Wageningen series diagrams with the polynomial expressions.

5.2.1 Drawbacks on the definition of the propeller using systematic series.

a) There is no control over the radial load distribution. Therefore, it is possible for loaded propellers in general that at the blade ends, produce vortices generated due to overloading, which produce energy dissipation vibration and noise. Besides the excessive loading, the occurrence of laminar cavitation. All of this decreases, in general, the performance of the propeller operating at modern sterns from the theoretical calculated according to the systematic series;
b) There is no control over the thickness distribution on each profile. Therefore, there is no control on the thrust generated by each profile. This precludes the use of new materials for propellers.
c) We cannot act on the pitch radial distribution. Therefore, if the stern of the vessel provides a distribution different from that designed for systematic series propeller wake, the flow velocity, and the angle of incidence in each profile are different from the optimum, so that the efficiency is reduced;

d) We cannot act on the radial distribution of strings. The relationship between expanded area $[A_E]$ and disc area $[A_0]$ is given by a fixed criteria of cavitation, sometimes it is not satisfied;
e) The detailed study of the mechanical strength of the propeller is not allowed;
f) A modification regarding rake and skew can be done in some series, but overall this is a fixed parameter, which cannot adapt if we anticipate problems of vibrations or space on modern skegs;
g) They allow only to develop a global study of cavitation phenomenon through certain criteria such as Burrill or Keller, forcing overall performance by losing aspects that may be particular to a profile.
h) Unable to act on the radial distribution of loads we obtain a 'disturbing' propeller, condition that is aggravated with high loaded propellers such as tugs and fishing vessels; ships whose water lines are finished too high and propellers with limited diameter because of the height of the stern part;
i) The performance at aft part with different shapes from traditional is greatly reduced due to not having control over the distribution of pitch;
j) The development of cavitation is excessive because the distribution of constant pitch leads to blade tip vortices, the flow influences on blade profiles and it affects the $[A_E/A_0]$ ratio due to this flow has an incidence on profiles without an optimum angle; as a consequence, the expanded area ratio$[A_E/A_0]$ ratio cannot be optimized unable to act on the radial distribution, so that the resulting disk area-ratio depends on the most critical section;
k) With systematic series cannot be designed propellers with high skew.

Priority considerations imposed either by the design theme or by the purpose of the vessel make sometimes difficult to fulfill all the requirements that are related to the performances of a new ship such as maximization of cargo capacity, minimize fuel consumption, maximize speed performances, low noise and vibrations level.

These considerations require continuous improvement of the propeller design methods, which involves theoretical methods, numerical techniques and experimental investigations.

As we have referred previously, the design of a propeller, which operates on reality into a non-uniform flow behind the ship "never finalizes", due to it is an iterative procedure having one objective: to provide maximum thrust to propel the vessel with minimum power consumption without vibration, cavitation and other restrictive conditions. During this process, the efficiency plays an important role on the design-loop because, how high the efficiency is, how greater the thrust will be. That is why we are looking for the highest value of efficiency without forgetting the restrictions. This is also related with a low fuel-consumption which is very important parameter for merchant ships.

For the performance of the ship, propeller efficiency is related to velocity, cavitation risk, noise and unsteady forces induced by the propeller which are:

- Bearing forces: forces transmitted via the shaft to ship hull structure.
- Surface forces: forces transmitted via the water to ship hull structure.

5.2.2 Optimum diameter.

Considered as a main output will be the diameter of the propeller, which is the optimum value whose fits on the space available for propulsion device. Furthermore these computations will give an average pitch ratio $\frac{P}{D}$ which is a representative value.

On the preliminary phase of propeller design as we have said before, up to now 3 terms are known:

- The delivered power [P_D],
- The marine engine particulars (brake power [P_B], revolution rate at M.C.R. [N,rpm]),
- The advance velocity [V_A],

With this information and using following formulae, we will obtain then, the maximum and optimum diameter possible which will develop the maximum thrust possible in order to overcome the ship resistance. Optimum diameter [D_{Opt}] may be eliminated from the diagrams by plotting K_Q/J^5 versus advance coefficient [J] instead of torque coefficient [K_Q] versus advance coefficient [J] as follows:

$$\frac{K_Q}{J^5} = \left[\frac{Q}{\rho n^2 D^5}\right]\left[\frac{nD}{V_A}\right]^5 = \frac{Qn^3}{\rho V_A^5} \tag{19}$$

Clearing the formula we have,

$$K_Q = \left[\frac{Qn^3}{\rho V_A^5}\right] J^5 \tag{20}$$

Knowing that torque is cleared from equation 9,

$$Q = \frac{P_D}{2\pi n} \tag{21}$$

$$K_Q = \left[\frac{(\frac{P_D}{2\pi n})n^3}{\rho V_A^5}\right] J^5 \tag{21}$$

Finally we get,

$$K_Q = \left[\frac{P_D n^2}{2\pi\rho V_A^5}\right] J^5 \tag{22}$$

As we can see, all coefficients are known and are used on charts of Wageningen B-series; on the other hand, the advance coefficient [J] is a variable value, from 0.1 up to 1.4.

By entering with revolutions per second [n= 127rps], delivered power [$P_D = 7970\ kW$] and computing the torque coefficient expression (equation 15.2), we have plotted this time, employing *MATLAB* application for developing the new B-Wageningen charts for our particular case (B4.85 diagrams). In contrary for the first propeller design described before, our unknown value is now the optimum diameter[D_{opt}].

The curve plotted on B4.85 Wageningen diagrams has been computed with equation (22)

$$\frac{K_Q}{J^5} = 0.30$$

Once we have plotted the $\left[\frac{K_Q}{J^5}\right]$ overlapped on $[K_Q - J]$ diagram for B4.85, we have read the values of torque coefficient (on the 'y' axis) as well as advance coefficient [J] where the curve intersects each P/D value for all P/D ratios (0.5-1.4) .

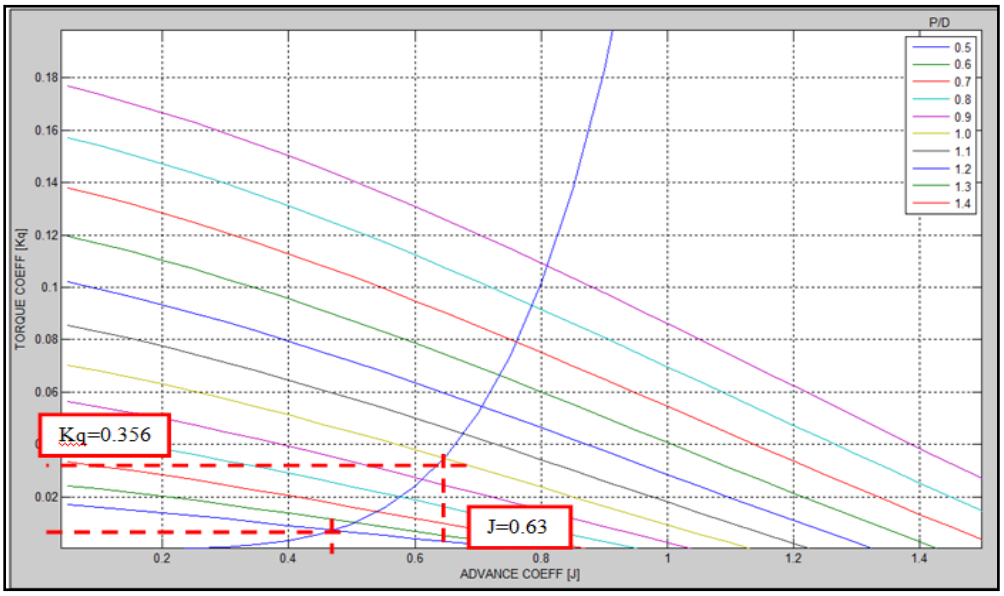

Figure 13.1. Torque coefficient – advance coefficient diagram [Kq-J].

Then, with advance coefficients [J] read before on [Kq-J] diagram, we locate each [J] value on 'x' axis crossing the respective P/D to read now on 'y' axis the thrust coefficient [Kt] for all P/D ratios (0.5-1.4).

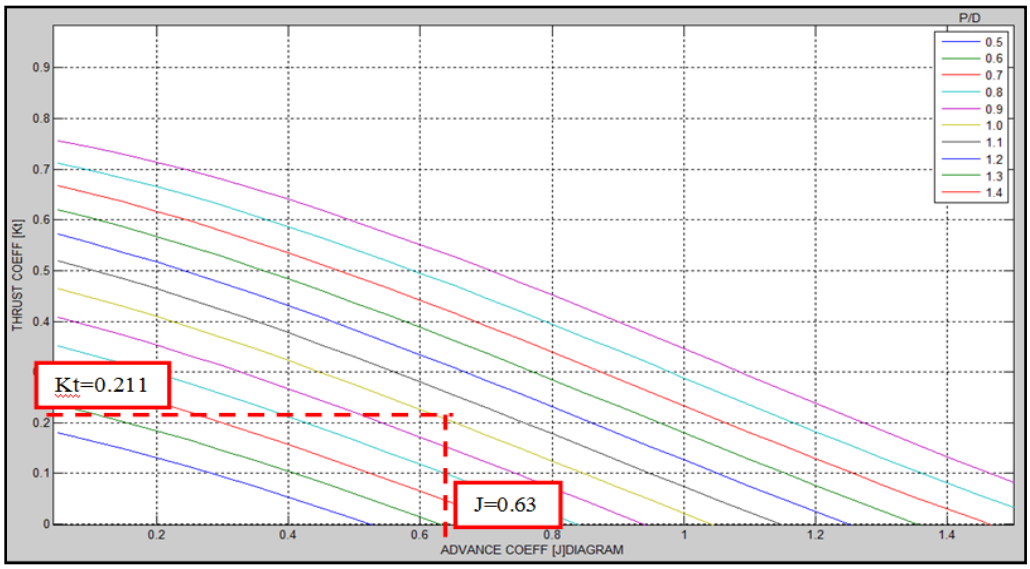

Figure 13.2. Thrust coefficient – advance coefficient diagram [Kt-J].

Efficiency has been evaluated with empirical formulae (equation 15).

THRUST	WATER DENSITY	SHIP-VELOCITY	ADVANCE SPEED	THRUST DEDUCTION coefficient	WAKE FRACTION coefficient	REVOLUTION RATE		PITCH RATIO	ADVANCE COEFFIENT	THRUST COEFFICIENT	TORQUE COEFFICIENT	OPEN-WATER EFFICIENCY
T [kN]	ρ [ton/mt^3]	V_S [m/sec]	V_A [m/sec]	t	w	n [rps]	N [RPM]	P/D	J	k_T	k_Q	**η_0**
690	1.025	9.52	7.14	0.16	0.25	2.12	127	0.1				
								0.2				
								0.3				
								0.4				
								0.5	0.460	0.028	0.007	0.27
								0.6	0.494	0.063	0.011	0.47
								0.7	0.528	0.099	0.015	0.56
								0.8	0.564	0.135	0.021	0.592
								0.9	0.600	0.172	0.027	**0.60**
								1.0	0.630	0.211	0.0355	**0.596**
								1.1	0.661	0.249	0.045	0.58
								1.2	0.690	0.288	0.056	0.57
								1.3	0.717	0.328	0.068	0.55
								1.4	0.744	0.369	0.081	0.54

Table 12. Results for open water efficiency [η_0] calculation.

On previous table, we can observe two highlighted rows with yellow and green color respectively. Yellow line represents the maximum value obtained from Wageningen B-series statistical method regarding the open-water efficiency [η_0]. Green line represents the second maximum value obtained from Wageningen B-series statistical method regarding the open-water efficiency [η_0].

There is a small difference between open water efficiencies but, making computations in order to know the value for the optimum diameter by using [D_{opt}] expression, we have found a lack of necessary space for the diameter of the propulsion device.

New values for delivered power and torque,

P_D 'new' [kWatt]	Q 'new' [kN*mt]
8212	617

Where,

$$P_D = (P_B)(\eta_S)(15\%) \tag{23}$$

With a pitch ratio $[\frac{P}{D}]$ value = 0.90 we have,

$$D_{opt} = \sqrt[5]{\frac{Q}{\rho n^2 K_Q}} \tag{24}$$

$$D_{opt} == \sqrt[5]{\frac{617\ kN*mt^2}{\left(1.025\ \frac{ton}{mt^3}\right)(2.12\ rps)(0.027)}} = 5.50\ mt.$$

With a pitch ratio $[\frac{P}{D}]$ value = 1.0 we have,

$$D_{opt} = \sqrt[5]{\frac{617\ kN*mt^2}{\left(1.025\ \frac{ton}{mt^3}\right)(2.12\ rps)(0.0355)}} = 5.20\ mt.$$

Taking into account the clearance available that we have measured from lines plan, we have 5.32 meters as a maximum space available for the propeller at the aft part of the vessel. As a conclusion we have selected following results providing open-water efficiency equals to 0.596 with the maximum possible diameter:

- Pitch ratio $[\frac{P}{D}]$: 1.0
- Advance coefficient [J]: 0.630.
- Thrust coefficient [k_T]: 0.211.
- Torque coefficient [k_Q]: 0.0355.
- Optimum diameter [D_{opt}]: 5.20mts.

It should be noted that during the preliminary stage using systematic charts, information regarding hull-propeller interaction coefficients such as the global wake coefficient [w], it has been determined with empirical equation (see table 5, "Propulsion factors") due to no account is taken of the variation of the wake over the propeller disk; we require only a rough knowledge of them.

5.2.3 Preliminary stage verification.

For fixed diameter, it must be calculated in function of the desired radial distribution and the blade area ratio, the performance of the propeller (isolated) corresponding to the design speed, so that the propeller provide the required thrust in order to overcome total ship resistance. For this, we have verified if the proposed propeller and its characteristics combined with the brake power and its revolution rate given by the engine will provide the design velocity required by the containership.

Following equation express delivered power provided by the designed propeller and torque coefficient,

1) Delivered power is then:

$$P_D = P_B \eta_S \eta_{gear-box} C_U \tag{24}$$

$C_U = 0.85$ For delivered power including sea margin = 15 %;
$\eta_{gear-box}$ = no gear box for our case = 1

2) P/D ratio was extracted from B- Wageningen charts (A.E.R. = 0.85, z = 4) by entering first with advance coefficient [J] and the resultant of [K_Q] value which is on this case, constant. Values were interpolated (see figure14.1 and 14.2).
3) Then, by entering with [P/D] ratios obtained before and the advance coefficient values, the intersection between them gives K_T values shown on figure 14.3.

Results are shown later on.

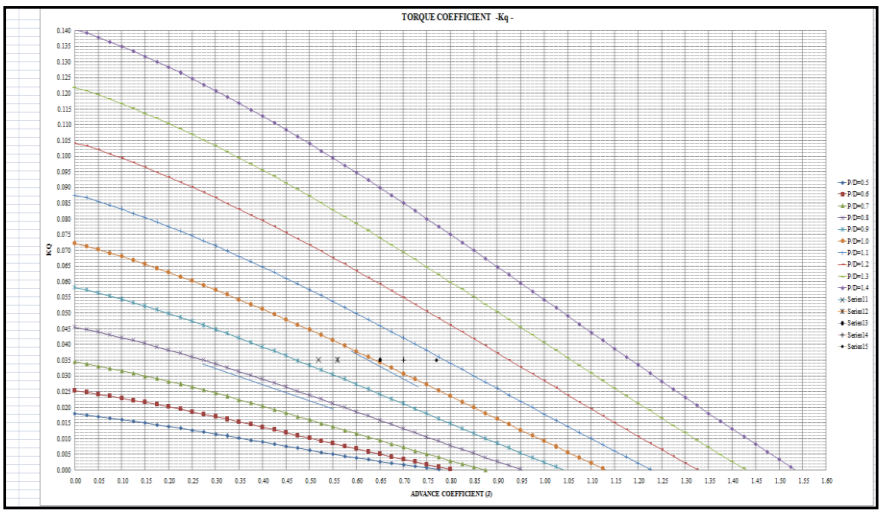

Figure 14.1. Torque coefficient – advance coefficient diagram [Kq-J].

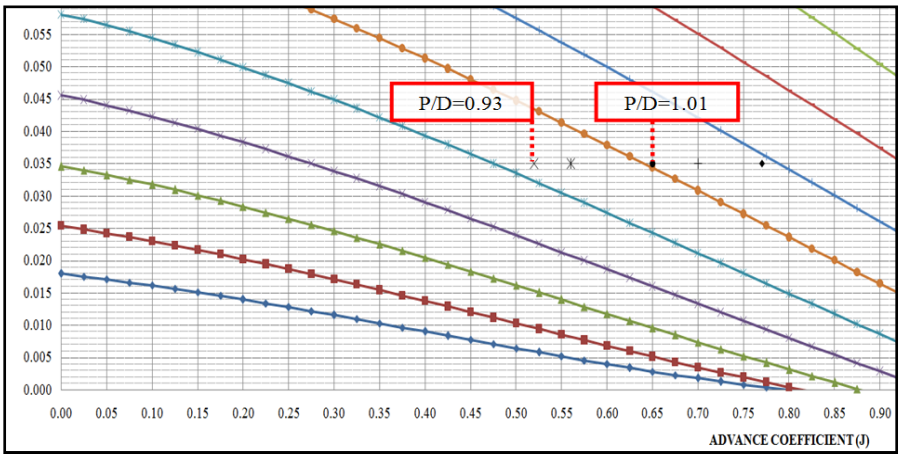

Figure 14.2. Torque coefficient – advance coefficient diagram [Kq-J] (zoomed view).

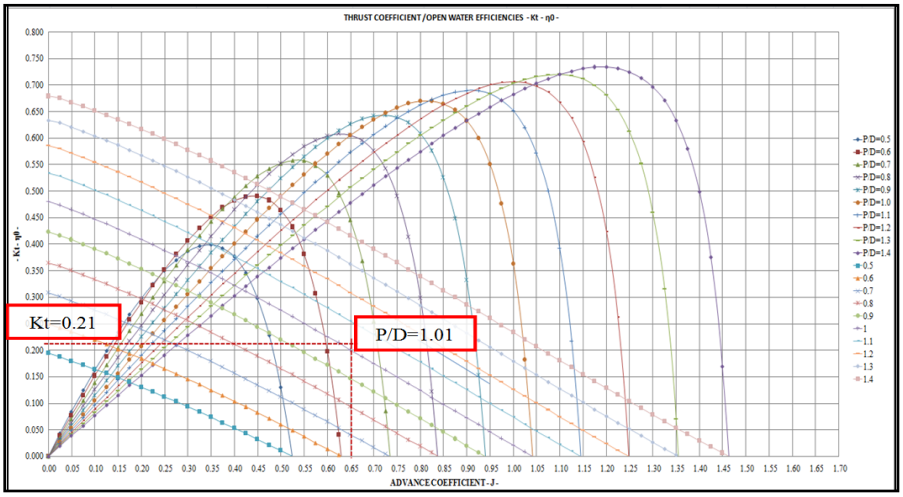

Figure 14.3. Thrust coefficient – advance coefficient – open water efficiencies diagram [Kt-J-η0].

SHIP VELOCITY	Vs	[kn]	15	16	18.5	20	22
	Vs	[m/s]	7.72	8.23	9.52	10.29	11.32
ADVANCE VELOCITY	V_A		5.79	6.17	7.14	7.72	8.49
PROPELLER DIAMETER	D	[mt]	5.20				
WAKE FRACTION COEFFICIENT	*w*		0.25				
THRUST DEDUCTION FACTOR	*t*		0.16				
ADVANCE COEFFICIENT	J		0.52	0.56	0.65	0.70	0.77
SHIP RESISTANCE	R_T	[kN]	363	430	581	798	925
THRUST	T	[kN]	431	511	690	948	1099
BRAKE POWER (ENGINE)	P_B	[kW]	9960				
REVOLUTIONS PER SECOND (ENGINE)	n	[rps]	2.12				
TORQUE COEFFICIENT	K_Q	[%]	0.035				
PITCH RATIO	P/D		0.93	0.95	1.01	1.04	1.09
THRUST COEFFICIENT	K_T		0.23	0.22	0.205	0.20	0.18
OPEN WATER EFFICIENCY	η_O	[%]	0.55	0.56	0.60	0.62	0.62
RELATIVE ROTATIVE EFFICIENCY	η_R	[%]	0.99				
HULL EFFICIENCY	η_H	[%]	1.12				
BEHIND-HULL EFFICIENCY	η_B	[%]	0.55	0.56	0.60	0.62	0.62
PROPULSIVE EFFICIENCY	η_D	[%]	0.61	0.62	0.67	0.69	0.70
EFFECTIVE POWER	P_E	[kW]	2801	3539	5529	8210	10468
DELIVERED POWER	P_D	[kW]	4581	5673	8226	11817	14999
DELIVERED POWER	P_D	[kW]			8212		

Table 13. Results (verification preliminary stage).

The result of this verification will be that the propeller must provide the required power to reach the design speed. A tolerance of ± 0.2 knots is acceptable.

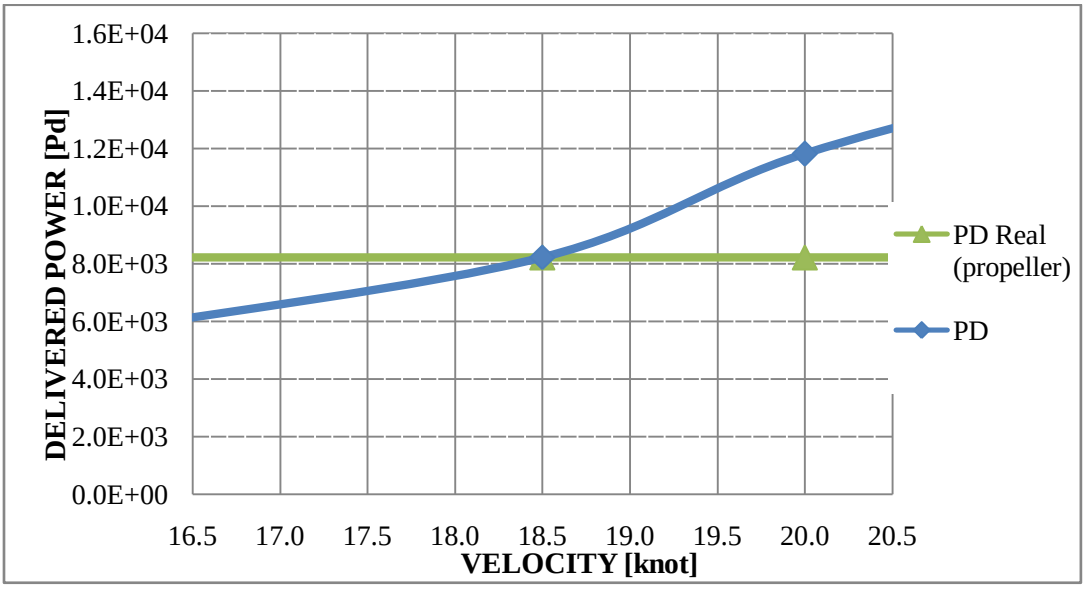

Figure 15. Propeller speed verification.

Pervious figure represents the delivered power: 1) given by the propeller at different speeds (curve colored on blue); 2) given by the propeller at the design speed (curve colored on green). As we can observe, we can establish that the propeller design during the preliminary stage will provide the required thrust to overcome the resistance encountered during its sailing.

The result of optimum diameter will be fixed on 5.20 meters. This value will be the input data for further calculations. Later on, cavitation test will be performed as well as to find the minimum blade area ratio permitted.

5.2.4 Cavitation check.

When a profile corresponding to the propeller blade moves in the water, it may occur that at certain points over the surface local speed reaches high values. These high speeds give rise to low pressures. If the local pressure at that point reaches the vapour pressure corresponding to the temperature of working water, it is vaporized on those areas forming steam bubbles. These bubbles are dragged by the flow and when they have reached higher pressure areas, same phenomenon occurs but this time in reverse.

The change from vapour to liquid has the particularity that, since the specific volume is much greater than fluid, vapour bubble is reduced to a much smaller droplet size. As a consequence, it occurs an empty area (where steam had before now there is nothing) that is quickly filled by the rest of the surrounding liquid; finally bubbles collapse. This implosion process results in crowd shocks of kinetic energy on very small surface areas of not inconsiderable magnitude acting, resulting in vibrations, noises (typical boiling water noise), surface damage of the blades, thrust reduction . In extreme cases have come to breakage caused by material fatigue.

For ship propellers, the velocities around the profiles of the blade may be sufficiently high to decrease the local pressures to trigger cavitation. Due to the hydrostatic pressure, the total pressure (if we imagine a clock on propeller axis), will be higher on a blade at the 6 o'clock position than at the 12 o'clock position. Consequently, cavitating propellers will then have regions on a blade where alternating cavitation bubbles are formed (near the 12 o'clock position) and collapse again.

Cavitation may be classified by:

- Location: tip cavitation, hub cavitation, root cavitation, leading edge or trailing edge cavitation, suction side (back) cavitation, face cavitation etc.
- Cavitation form: sheet cavitation, cloud cavitation, bubble cavitation, vortex cavitation.
- Dynamic properties of cavitation: stationary, non-stationary, migrating.

Cavitation phenomenon is explained with Bernoulli's equation:

$$p_1 + \frac{1}{2}\rho V_1^2 = p_0 + \frac{1}{2}\rho V_0^2 \tag{25}$$

And the change in pressure is,

$$\delta_p = p_1 - p_0 = \frac{1}{2}(V_0^2 - V_1^2) \tag{25.1}$$

At some point 'x' near the leading edge of the section, the velocity $[V_1]$ is zero. This point 'x' is called "stagnation point" and the pressure at 'x' is,

$$q = \frac{1}{2}\rho V_0^2 \tag{25.2}$$

The pressure $[p_1]$ at some point on the back of the blade will become zero if,

$$\delta_p = -p_0 \tag{25.3}$$

Since water cannot support tension, the flow will break down at this point with the creation of bubbles and cavities, cavitation phenomenon is the result. On reality, this occurs when $[p_1]$ is close to vapour pressure of water (vapor pressure when it begins to boil and form empty spaces in water). This criteria is then,

$$p_v = \delta_p + p_0 \tag{25.4}$$

$$\delta_p = -(p_0 - p_v) \tag{25.5}$$

Dividing by the stagnation point pressure [q], cavitation will occur when,

$$-\frac{\delta_p}{\rho} \geq \frac{P_o - P_v}{q} \tag{25.6}$$

Previous expression will determine as we know "the local cavitation number". Local cavitation number represented as $[\sigma_{0.7R}]$ is a non-dimensional parameter to estimate the likelihood of cavitation in a flow:

$$\sigma_{0.7R} = \frac{P_o - P_v}{q} = \frac{(P_o - P_v) + \rho g h}{\frac{1}{2}\rho V_0^2} \tag{26}$$

Where,

$q =$ total pressure incident on the blade, consisting of the axial and rotational (dynamic pressure).

$P_o =$ total static pressure

$$P_o = P_{atmosp\ heric} + P_{hydrostatic} \tag{26.1}$$

$P_{atmosp\ heric} =$ atmospheric pressure (measured at sea level) = 98.10 kPa*

$$P_{hydrostatic} = \rho g h \tag{26.2}$$

ρ = salt water density.

g = gravity.

h = height from the water-line to the axis of the shaft = 4.70mt.

P_v = Vapor pressure = 1.75 kPa*

$$V_{0.7R} = \sqrt{V_A^2 + (0.7\pi nD)^2} \tag{26.3}$$

$V_{0.7R}$= corresponding reference speed value of the local velocity at radii section 0.7

* : Values for sea water at 15 ºC as reference.

This means that cavitation number [σ] depends on the absolute pressure in the area where we are, since $[P_o]$ is the sum of atmospheric pressure and hydrostatic pressure [ρgh]. Also depends on the vapor pressure $[P_v]$ and velocity of advance $[V_A]$ as the incident flow velocity. This is, the profile depends not only on the mechanical characteristics of the flow.

For cavitation number corresponding to vapor pressure ($\sigma < P_v$), the flow will be free of cavitation in an ideal fluid. On reality, one introduces a safety factor and sets a higher pressure than vapor pressure as the lower limit.

Cavitation is predominantly driven by the pressure field in the water. Cavitation avoidance consequently strives to control the absolute pressure minimum in a flow. This is achieved by distributing the thrust on a larger area, either by increasing the diameter or the expanded area ratio [$\mathbf{A_E/A_O}$].

Cavitation is thus a local phenomenon, which must be studied in all areas of the blades and different positions that can occupy them.
For this purpose the local cavitation number $[\sigma_{0.7R}]$ to consider will vary from point to another. It is usual to study cavitation in determined radii sections [r/R] of the propeller, but local cavitation values which are often used (0.7 R and 0.8 R), are the sections that in practice, have the most cavitation risk, for being the sections that supply more thrust.

Among different methods to choose the minimum [$\mathbf{A_E/A_O}$] necessary to evade dangerous cavitation such as Keller diagrams for example, we have used *Burrill methodology* proposed

by Profr. L.C. Burrill; the most popular approach to estimate the danger of cavitation regarding merchant vessels.

From the experience gained in many cavitation tunnel tests, Burrill has estimated maximum thrust per unit of projected area for the propeller would had an acceptable value which has fixed no more than 5% of the blade itself.

Burill procedure uses the coefficientτ_c,

$$\tau_c = \frac{T}{q_{0.7R} A_p} \tag{27}$$

Where,

$$q_{0.7R} = \frac{1}{2}\rho V_{\frac{r}{R}=0.7R}^2 \tag{27.1}$$

$$A_p = (1.067 - 0.229\frac{P}{D})A_E \tag{27.2}$$

$\frac{P}{D} = 1.0\ (selected)$

$\frac{A_E}{A_0} = 0.85\ (selcted)$

$$A_0 = \frac{\pi D^2}{4} \tag{27.3}$$

T = Thrust;

A_p= projected propeller area;

n = revolution rate of the engine (rps);

D = propeller diameter;

$V_{0.7R}$ = the absolute value of the local velocity at radii section 0.7.

Computing cavitation number $[\sigma_{0.7R}]$ and coefficient $[\tau_c]$ with equations given before we have,

$$\sigma_{0.7R} = \frac{(P_o - P_v) + \rho g h}{\frac{1}{2}\rho V_0^2} = 0.44$$

$P_v = 1.75\ kPa$,

$P_{atmosp\ heric}$ = 98.10 kPa

$P_{hydrostatic} = \rho g h = \left(1.025 \frac{ton}{mt^3}\right)\left(9.81\ \frac{mt}{sec^2}\right)(4.70\ mt) = 47.26\ kPa$

h = height from the water-line to the axis of the shaft = 4.70mt.

$V_{0.7R} = \sqrt{(7.14\, mt/sec)^2 + [(0.7)(\pi)(2.12 rps)(5.20 mt)]^2}\ V_{0.7R} = 25.27\ mt/sec$

$$\tau_c = \frac{T}{q_{0.7R} A_p} = 0.14$$

$q_{0.7R} = \frac{1}{2}\rho V_{r/R}^2 = \frac{1}{2}(1.025 \frac{ton}{mt^3})(25.27\ mt/sec)^2 = 327kN$

$A_p = (1.067 - 0.229 \frac{P}{D}) A_E$ = [1.067 – (0.229*1.0)] [18.04mt²] = 15.11 mt²

$\frac{A_E}{A_0} = 0.85;\ A_E = (0.85)(21.23 mt^2) = 18.04\ mt^2$

$A_0 = \frac{\pi D^2}{4} = \frac{(\pi)(5.20\ mt)^2}{4} = 21.23\ mt^2$

$\frac{P}{D} = 1.0$

From the experience gained in many cavitation tunnel tests, Burrill has estimated maximum thrust per unit of projected area for the propeller would had an acceptable value which has fixed no more than 5% of the blade itself.

Later on, we can predict the cavitation done in percentage thanks to Burrill diagrams. From abscissa axis we read local cavitation number; on the other hand, ordinate axis presents coefficient [τ_c]. Making an intersection between both on Burrill diagram (see figure 16).

There exists around 5% of cavitation presented on the designed propeller for our project.

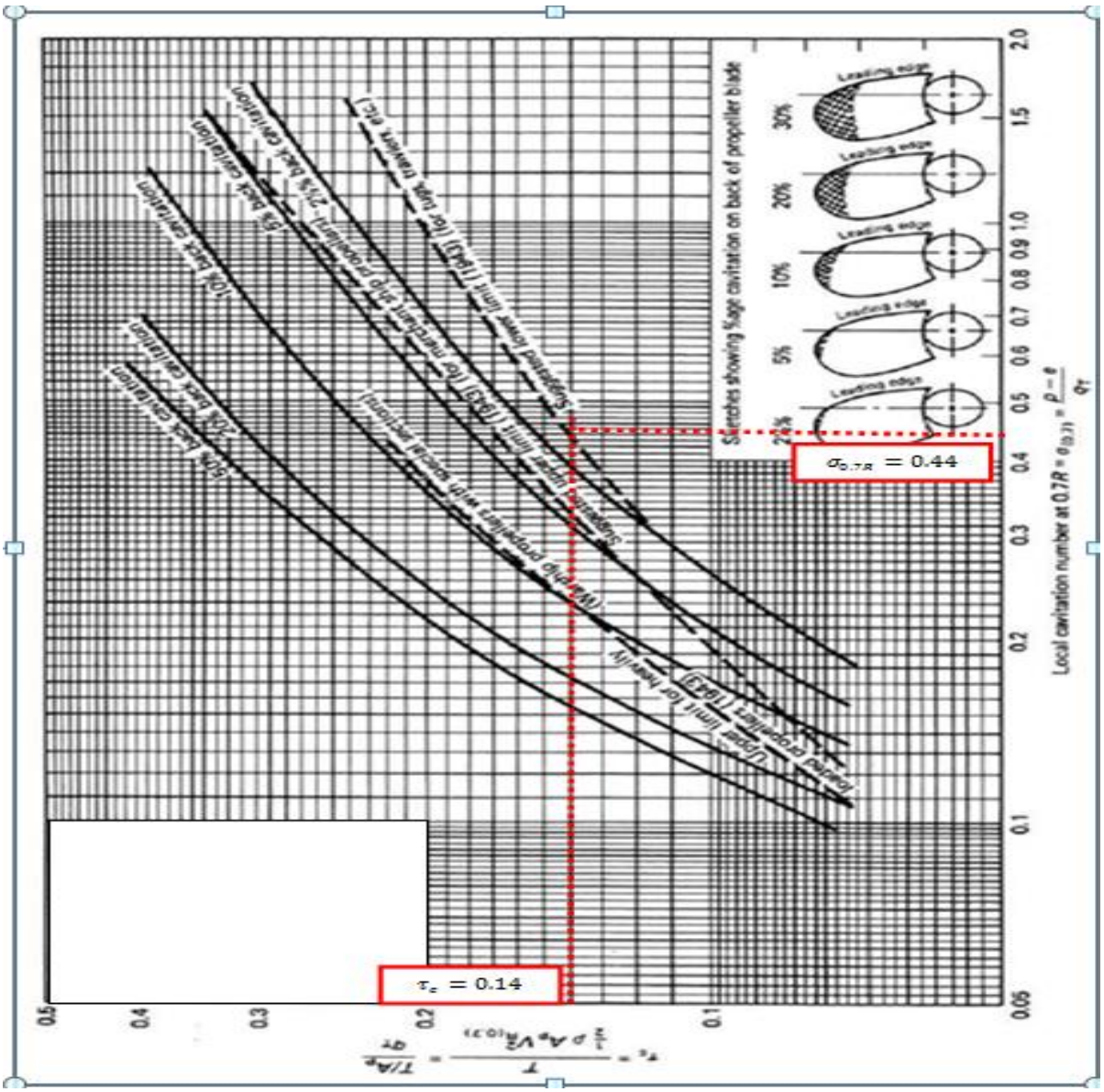

Figure 16. Burrill diagram.

5.2.5 Estimation of expanded area ratio to prevent cavitation.

The primary procedure, and therefore most widely used to prevent the occurrence of cavitation, is the choice of a sufficiently large [$\mathbf{A_E/A_O}$] ratio. Nevertheless for an optimum propeller design, it must be considered that the blade area ratio is as minimum as possible in order to avoid dangerous cavitation, inasmuch as propeller efficiency decreases when blade area ratio increases due to larger surface of the blade is subjected to friction.

The minimum Expanded Area Ratio allowable in order to prevent dangerous cavitation has been computed as follows:

$$\sigma_A = \frac{(P_o - P_v) + \rho g h}{\frac{1}{2}\rho V_A^2} \tag{28}$$

$$\sigma_A = \frac{98.10kPa - 1.75kPa + 47.26kPa}{\left(\frac{1}{2}\right)\left(1.025\frac{ton}{mt^3}\right)\left(7.14\frac{mt}{sec}\right)^2} = 5.50$$

$$\sigma_R = \frac{\sigma_A}{\Upsilon_7} \tag{29}$$

$$\sigma_R = \frac{5.50}{12.51} = 0.44$$

$$\Upsilon_7 = 1 + (\frac{\delta}{46.1})^2 \tag{29.1}$$

$$\Upsilon_7 = 1 + (\frac{156.40}{46.1})^2 = 12.51$$

$$\delta = \frac{101.3}{J} \tag{29.2}$$

$$\delta = \frac{101.3}{\frac{7.14\ mt/sec}{(2.12\ rps)(5.20\ mt)}} = 156.40$$

"Load factor"[K_v] expressed as,

$$K_v = \frac{T}{\rho D^2 V_{0.7R}^2} \tag{30}$$

$$K_v = \frac{690kN}{(1.025\ ton/mt^3(5.20mt)^2(25.27mt/sec)} = 0.04$$

Minimum Expanded Area ratio permitted is given by next expression,

$$a_E = 0.34a_D\left(2.75 + \frac{a_D}{z}\right) = \frac{A_E}{A_0} \tag{31 }$$

Where disk ratio coefficient $[a_D]$ is read from the following chart.

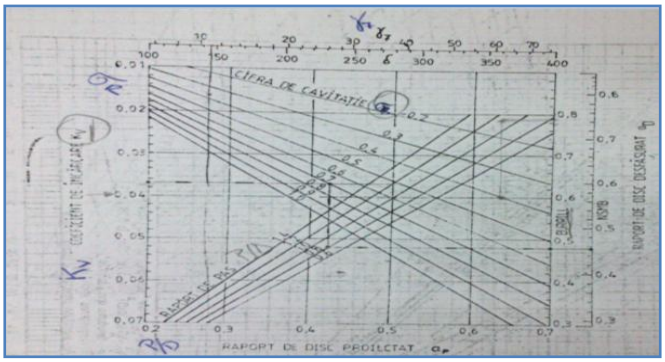

Figure 16.1. Burrill diagram for a_D coefficient.

In order to read it, it is necessary to enter with load coefficient $[K_v = 0.04]$ read it on ordinate axis; then, we have to do an intersection between the value of cavitation number $[\sigma_R = 0.44]$. Later on, we have to cross now, the value of selected pitch ratio [P/D] which is 1.0. As a result, $[a_D]$ disk ratio is read on right side axis, $a_D = 0.813$.

If we use $[a_D]$ coefficient we finally have the minimum value allowed to avoid risk cavitation,

$$a_E = (0.34)(0.813)\left(2.75 + \frac{0.813}{4}\right) = 0.816 = \frac{A_E}{A_0}$$

As we can observe, for all computations in order to find the optimum diameter for our propeller, we have used an $\frac{A_E}{A_0}$ =0.85. Comparing the blade area ratio proposed by Burrill diagrams against the blade area ratio used before, we can eliminate the possibility to have dangerous cavitation in our propeller. However, during the detailed design which involves different theories such as Lifting Line Method with Lifting Surface corrections, we can establish the correct value for expanded area ratio due to, although the proposed propeller design up to now is far of risk of cavitation, we have more blade area which is traduced on losses regarding propeller efficiency as well as a decrement on thrust.

Nevertheless, to get information regarding cavitation phenomenon and to satisfy the required pressure conditions, it is necessary to carry out model experiments in a depressurized towing tank or in a cavitation tunnel. The outputs of model tests which are important from propeller design point of view are:

- The nominal wake distribution (axial and tangential velocities in propeller disk plane) provided by wake measurement tests.
- The hull-propeller interaction coefficients such as the effective wake fraction [w]; thrust deduction factor [t]; relative rotative efficiency [η_R], obtained by self propulsion test with a stock propeller.

However, an explanation regarding the use of global wake distribution on each r/R section will be on the detailed design stage.

	SHIP VELOCITY	V_S	[knot]	18.5
			[mt/sec]	9.52
	ADVANCE SPEED	V_A	[mt/sec]	7.14
	TOTAL SHIP RESISTANCE	R_T	[kN]	581
	THRUST	T	[kN]	690
	RELATIVE ROTATIVE EFF.	η_R	[%]	0.99
	HULL EFF.	η_H	[%]	1.12
	SHAFT EFF.	η_S	[%]	0.97
	BEHIND-HULL EFF.	η_B	[%]	0.59
	QUASIPROPULSIVE EFF.	η_D	[%]	0.67
	EFFECTIVE POWER	P_E	[kW]	5531
	DELIVERED POWER	P_D	[kW]	8212
	TORQUE	Q	[kN*mt]	617
	GLOBAL WAKE DISTRIBUTION	w		0.25
	THRUST DEDUCTION FACTOR	t		0.16
ENGINE SPECS.	BRAKE POWER	P_B		9960
	REVOLUTION RATE	n	[rps]	2.12
		N	[RPM]	127
PROPELLER PARTICULARS	NUMBER OF BLADES	z		4
	EXPANDED AREA RATIO			0.85
	PITCH RATIO	P/D		1.0
	ADVANCE COEFFICIENT	J		0.63
	THRUST COEFFICIENT	k_T		0.211
	TORQUE COEFFICIENT	k_Q		0.0355

	OPEN-WATER EFF.	η_0	[%]	0.60
	FINAL DIAMETER	**D**	**[mt]**	**5.20**
(Minimum to avoid dangerous cavitation)	**EXPANDED AREA RATIO**	**A_E/A_O**		**0.816**

Table 14. Results for propeller design at preliminary stage.

On the final phase of preliminary design stage of the propeller, it can be possible to generate the B-Wageningen *'open-water characteristics'* for the estimated propeller using the output data such as P/D=1.0, A.E.R =0.85, Z=4 plotted in *EXCEL* application.

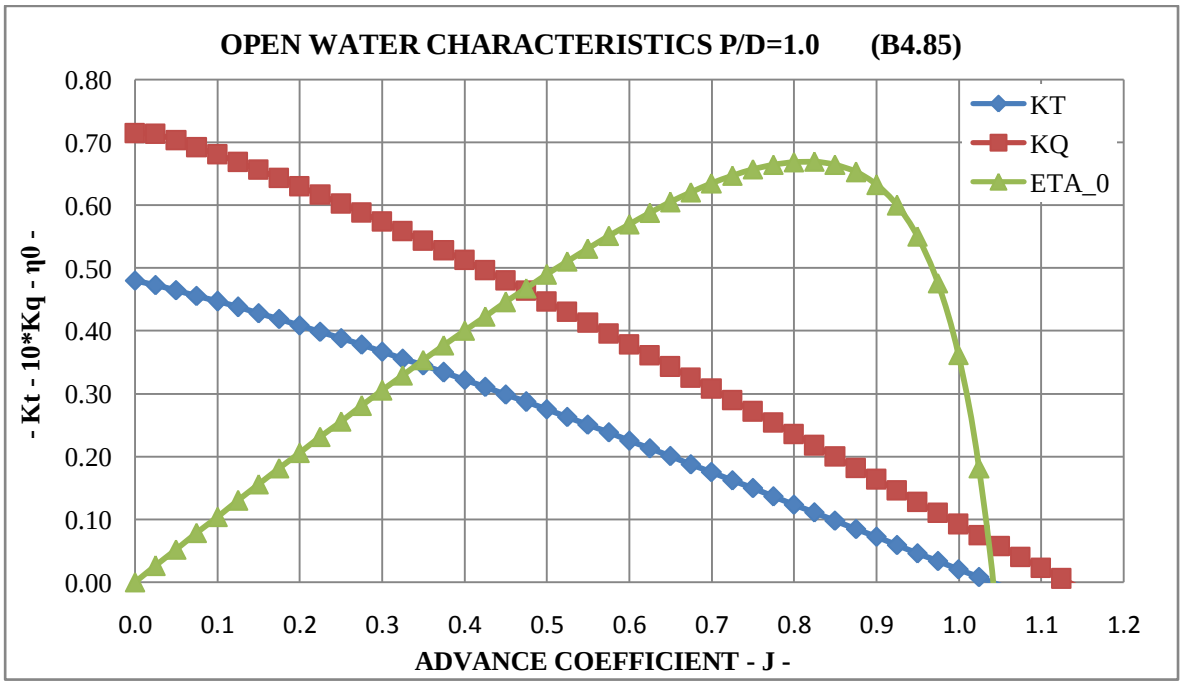

Figure 17. Theoretical B-Wageningen open-water characteristics diagram for P/D=1.0; A.E.R. =0.85; Z=4.

As a conclusion on preliminary stage of propeller design, the performances of the propulsion device designed based on standard series and empirical formulations are considered as insufficient nowadays; the information obtained during preliminary phase give good agreement between ship speed, engine power, shaft power, propeller revolutions and so on; they are considered as starting point and will be useful for following design phases. The propeller is then, "not adapted" for a real wake field due to we are supposing with its open water characteristics results, that the given information is the best solution if the customer would like to use a stock propeller from B-Wageningen series for example.

5.3 SECOND STAGE: THE DETAILED DESIGN.

The propeller is essentially an energy exchanger which employs energy received from power drive train to increase the amount of axial movement and the angular momentum of the water flowing through the propeller itself per unit of time.
The performance of energy conversion depends on the pressure distribution established on both sides of the propeller. In turn, the radial distribution of the pressure difference on the propeller disc leads to the radial distribution of the thrusts exerted by the propeller.

The purpose of making detailed design of the propeller named "direct calculation" as well is to find the optimum propeller diameter and the radial distribution of thrust which is deemed most appropriate taking into account some parameters such as mean wake for each [r/R] section. Likewise, it is also intended that each section has an adequate annular configuration so that its contribution to the total thrust is to be assigned, the viscous resistance is minimal and the development of cavitation is minimized without any danger of erosion of the blade. Naturally, the mechanical strength of the designed propeller must be fully guaranteed.

At the preliminary phase, the designed propeller is a result of, among other characteristics, hull-propeller coefficients computed by empirical formulas; nevertheless for the detailed design stage this is not possible due to now, the propeller is adapted to the water flow modified by the stern shape of the vessel. The inflow of the propeller is assumed to vary radially and the objective is to find blade geometry for the specified radial wake distribution. The result during this stage will be then, the so-called “wake adapted propeller”.

As we have said previously, to get information about the wake radial distribution, it is necessary to perform a “propeller test” behind hull (without propeller). The flow distribution at the propeller disk is measured with a Pitot test tube installed at the propeller plane on the ship model.

The results of these measurements are usually displayed on a chart known as wake field distribution (wake distribution diagram, see picture 19).

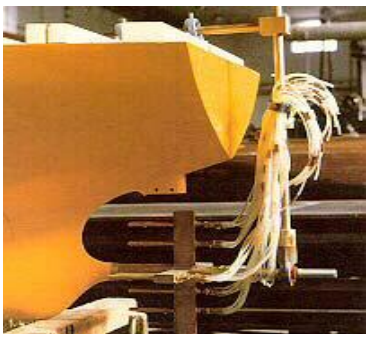

Figure 18. Wake measurement with a Pitot test tube.

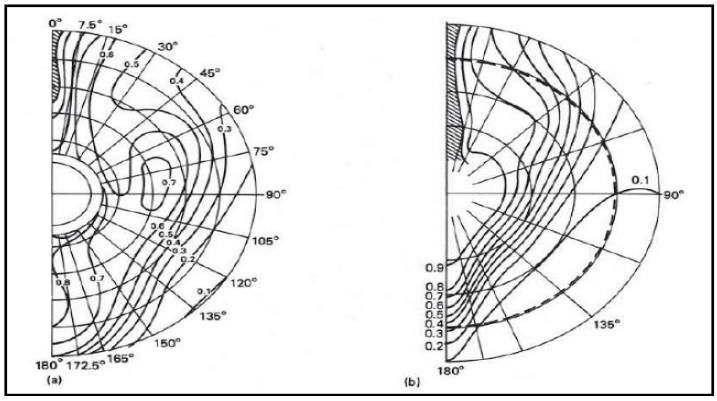

Figure 19. Radial wake distribution diagram.

The output information provided by model tests will be useful for detailed design phase which gives:

- The axial and tangential velocities in the propeller plane (nominal wake distribution).
- Hull-propeller coefficients [w, t, η_R] determined on self-propulsion test (with a stock propeller).

Following next chart presents the mean wake field distribution [w(ϒ)] at each [r/R] section for our project.

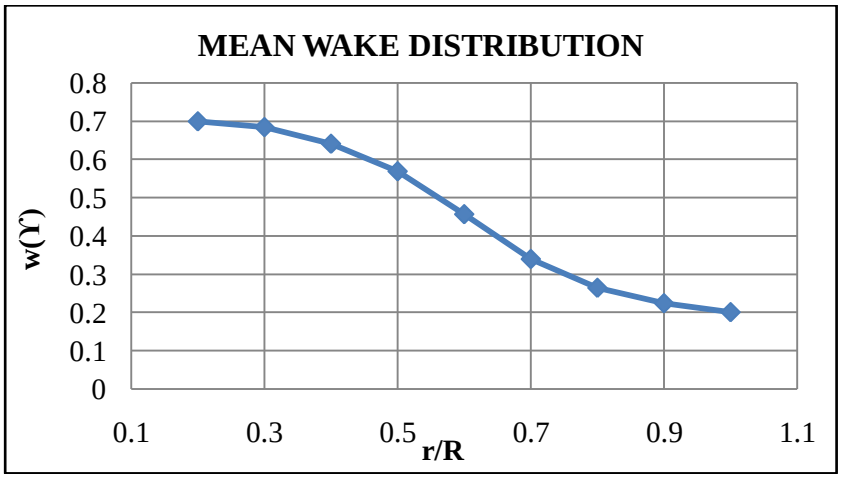

Figure 20. Mean wake distribution at each radii section [w(ϒ)].

It should be noted that the wake [w (ϒ, θ)] varies at different location on the propeller plane in function of radius and angular position.

After the determination of mean wake distribution values we can proceed with the detailed design stage. On this stage, analytical methods based on circulation theories such as lifting line method/surface corrections and/or lifting surface based theories are used.

5.3.1 Propeller theory.

Before, we can summarize that the early propeller theory had two currents:

1. The Momentum Theory, declares that the production of thrust thanks to propeller (regarded as an actuator disk)was based on axial (and rotational) changes acting in the fluid flow;
2. On the other hand, the blade element Theory states that the thrust produced by the propeller (composed of a series of blade elements) is obtained was obtained by analyzing hydrodynamic forces acting on different blade sections.

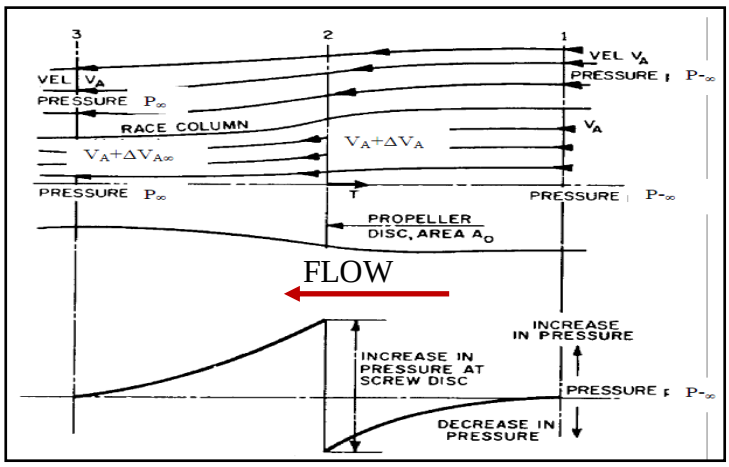

Figure 21. Representation of the momentum theory where uA and uj are the speeds before and after the propeller.

Nowadays many modern theories are based on:

1. The Circulation Theory (vortex), which provides more reliable explanation regarding propeller hydrodynamics describes that the lift is produced by each blade, similar to an aircraft wing.

   Considering a fluid flow which particles have circular movement such a flow is known as a vortex flow and its axis about which fluid particles move in 3-D is known as a vortex line.

   Helmholtz states in his theorem that "*In an ideal fluid, a vortex line cannot end abruptly inside the fluid but must either form a closed curve or end on the boundary of the fluid*". If for example, we place a cylinder in a uniform flow (ideal fluid) with a vortex flow, the cylinder will experience on one side an increment on the resultant velocity; on the other side a decrement regarding pressure. This has a result of lift force normal to the direction of the fluid flow.

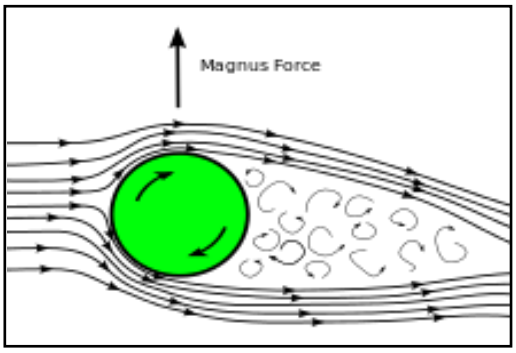

Figure 22. Cylinder with an ideal fluid flow.

The circulation obtained by taking the line integral around the circle radius [r] (the cylinder for ex.) is:

$$\Gamma = \oint v ds = \int_0^{-2\pi} \frac{k}{r} r d\theta = 2\pi k \tag{32}$$

Where tangential velocity to a circle of radius r is $v = k/r$.

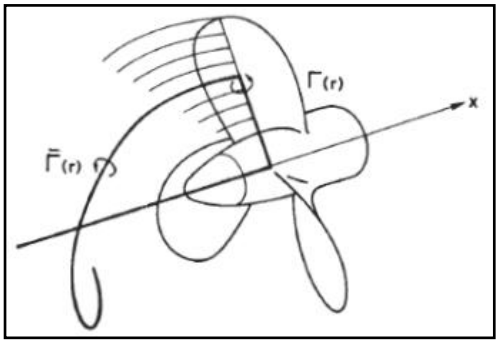

Figure 23. Circulation representation on the propeller.

This also explains how the flow behaves during its pass through an airfoil; the asymmetry of the component provokes the lift. This lift per unit of length is stated as:

$$dL = \rho \Gamma V_R dr = \rho \frac{2\pi r U_t}{Z} V_R dr \text{ (Kutta-Joukowski theorem).} \quad (33)$$

Where circulation is totally dependent on the form of the airfoil and consequently, its angle of attack. Also, the lift force is explained with Bernoulli theorem (pressure/velocity differences, see formula 25)

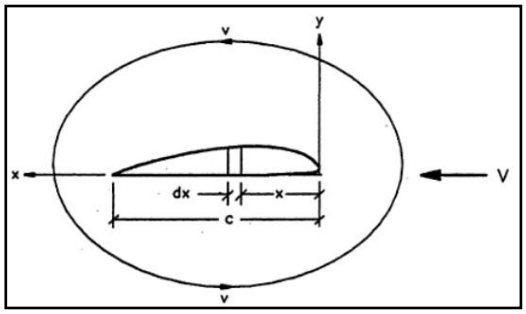

Figure 24. Circulation around an airfoil.

Finally, the lift produced by an airfoil per unit of length is then:

$$L = 1 \int_0^{x_1} \Delta p dx = \rho V \int_0^{x_1} 2v dx = \rho \left[\int_{x_1}^{0} -v dx \right] V = \rho \Gamma V \quad (34)$$

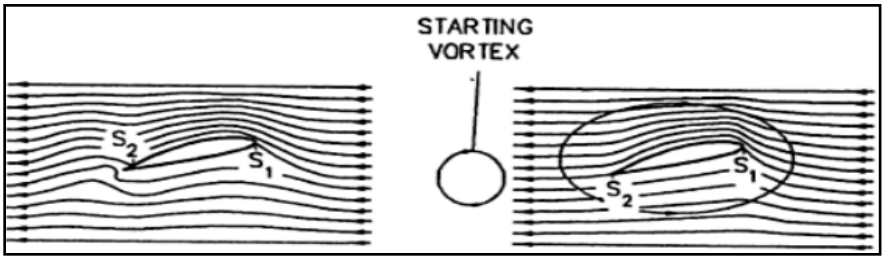

Figure 25. “Infinite aspect ratio wing section”; beginning of fluid flow (left); pass of flow (right).

Because the fluid is unstable, the starting vortex is formed due to change of pressure/velocity of the flow. Stagnation point [S_2] formed first on the “initiation of

the flow" (figure 25-left) at the trailing edge (upper part) of the airfoil section, then it moves below the trailing edge (figure 26-right). This movement causes the 'starting vortex' while the vortex associated with the circulation around the wing is named 'bound vortex'.

Now if we refer to a wing with finite aspect ratio [b/c] bound and starting vortex cannot end abruptly in the fluid; there must exist vortex lines which connect the ends of the starting vortex and the bound vortex (see figure 26). These vortex lines are known as trailing vortices. They are aligned parallel to velocity [V] producing no lift force and downward velocity in the flow behind the wing section.

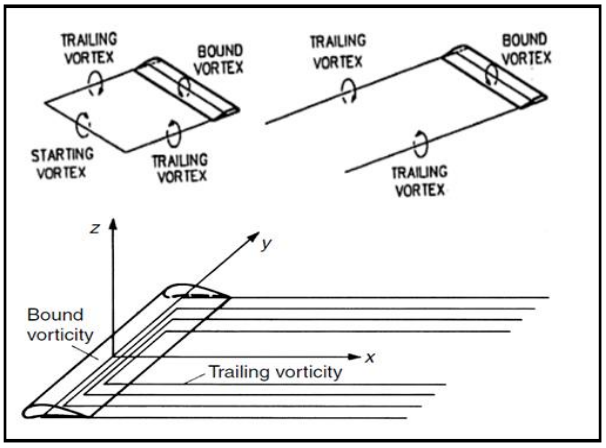

Figure 26. Vortex generation description on a finite wing.

Passing the time, the starting vortex is left far downstream of the wing and the vortex system has a 'horseshoe' form. The magnitude of that velocity far behind the airfoil is twice than at the airfoil because the trailing vortices extend infinitely in both direction far behind the wing while at the wing section the trailing vortices extend infinitely only in one direction.

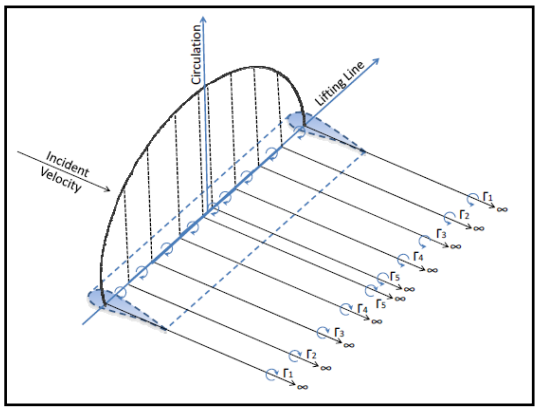

Figure 27. Vortex pattern representing lifting wing.

On previous figure we can observe a finite wing airfoil with a finite span. On reality the circulation of a wing decreases from a maximum mid-span up to zero at the extremes. It is taken to be as constant.

The trailing vortices are shed not only from the wing tips but from all along the trailing edge forming a vortex sheet. The strength of a free vortex shed from any element along the trailing edge is equal to the change in circulation across the element.

The phenomenon on the propeller has a similar behavior as a wing vortex system. Each blade is depicted as a vortex system; the vortex sheet is shed from the trailing edge. Also, the trailing vortex sheets have a helicoidally shape due to the propeller turns on its axis. It should be noted that there exist as many such vortex sheets as there are blades in the propeller.

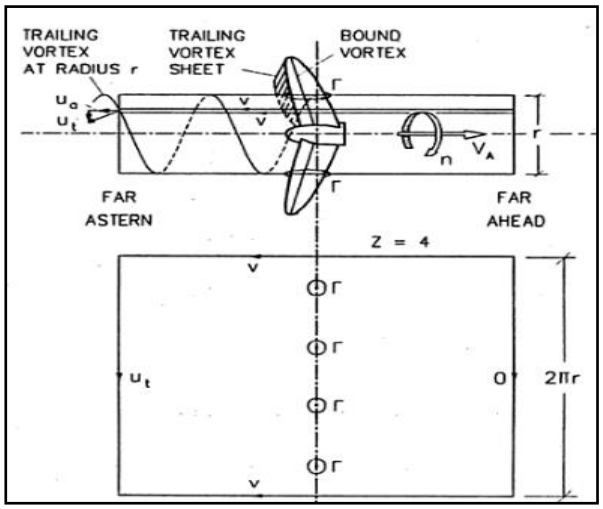

Figure 28. Vortices on the propeller.

These trailing vortex sheets produce induced celebrities that are normal to the vortex sheets; the induced velocity magnitude at the blade being half the induced speed far downstream.

The velocity represented along the circle far ahead is zero while along the circle far astern is $[U_t]$. For the propeller we have a circulation described as:

$$Z\Gamma = 2\pi r U_t \tag{35}$$

Where circulation is dependent on number of blades [Z], radius [r] and velocity far astern.

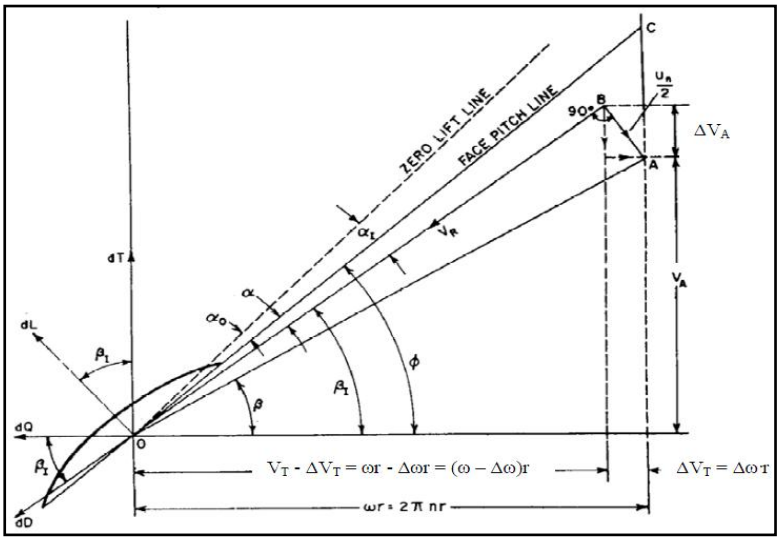

Figure 29. Forces and velocities presented on each blade profile of the propeller.

Figure from above represents forces and velocities existent on a blade profile. The velocities are taken relative to the blade element. The induced velocities at the blade profile are half those far behind the propeller; as a consequence, there is no drag due to there exist ideal fluid conditions (assumed to be inviscid). Lift force is described as [dL]; thrust [dT]; torque [dQ]; resultant velocity [V_R]; angle of attack [α]; hydrodynamic pitch angles excluding and ncluding the induced velocities respectively [β, β_1].

The lift on a blade of a propeller of length [dr] at radius [r] is obtained as Kutta-Joukowski theorem states (see equation 33).

Projecting the forces in the axial and tangential directions and calculating the moments thrust and torque both in function of profile radius we get:

$$dT(r) = dL(r)cos\beta_i - dD(r)sin\beta_i \tag{36.1}$$

$$dQ(r) = r[dL(r)sin\beta_i - dD(r)cos\beta_i] \tag{36.2}$$

Now the real thrust [T(r) dr] of the annular radius [r] is a product between thrust and the profile of the same radius [r] by the number of blades [Z]. The actual torque [Q(r) dr] is also the product of torque on the profile by the number of blades:

$$T(r) = Z[dL(r)cos\beta_i - dD(r)sin\beta_i r \tag{36.3}$$

$$Q(r) = Zr[dL(r)sin\beta_i - dD(r)cos\beta_i] \tag{36.4}$$

Where the incidence angle of the fluid having on consideration induced celerities [β_i] may be computed with:

$$tan\beta_i = \frac{V_A(r) + \Delta V_A(r)}{V_\Gamma(r) - \Delta V_\Gamma(r)} = \frac{V_A(r) + \Delta V_A(r)}{\Gamma[\omega - \Delta\omega(r)]} \tag{37}$$

On the other hand we have:

(Lift)

$$dL(r) = \frac{1}{2}\rho V_R^2 c C_L \tag{38.1}$$

(Drag)

$$dL(r) = \frac{1}{2}\rho V_R^2 c C_D \tag{38.2}$$

Where [c] is known as chord at specific section; [C_L] lift coefficient; [C_D] drag coefficient; [V_R] flow velocity is now given by following expression considering an ideal fluid (non-viscous):

$$V_R = \sqrt{(V_A(r) + \Delta V_A(r))^2 + (\omega - \Delta\omega(r))^2} \tag{39}$$

Substituting circulation[Γ] from equation $Z\Gamma$ (see equation 32, 35) we get:

$$Q_i = Z[dL(r)sin\beta_1] \text{ (radial torque distribution)} \tag{40.1}$$

$$T_i = Z[dL(r)cos\beta_1] \text{ (radial thrust distribution)} \quad (40.2)$$

To determine the expression of the efficiency of an ideal propeller, whereas rotation of the fluid, we assume that before reaching the disc and with enough distance from it, far from the propeller, the fluid has an axial velocity and a rotational speed of zero ($\omega_1 = 0$); when the fluid has reached the propeller, the propeller rotates at an angular velocity[ω] and the fluid keeps an axial velocity; once the fluid has traversed the propeller, the fluid acquires a certain rotational speed [Δω] in the same direction as the disk. Once enough distance drive past the propeller, the fluid will have an axial velocity ($\Delta V_A + V_{A\infty}$) as discussed before and an angular celerity we can write in the form: $\omega_3 = \Delta_{\omega\infty}$. These considerations give as a final expression:

$$\eta = \frac{TV_A}{\omega Q} = \frac{TV_A}{2\pi n Q} \quad (41)$$

We must consider that: *"the kinetic energy imparted to the fluid and not used by the propeller will then increased by the energy of rotation, resulting in a decrease in the value of the ideal efficiency"*.

Nonetheless, the propeller thrust is function of the circulation and the issue is to find optimum circulation Γ(r) to get the maximum efficiency (function of the induced velocities). Betz has solved for an ideal fluid which results in:

$$\eta_i = \frac{tan\beta}{tan\beta_i} \quad (42)$$

5.3.1.1 The lifting line theory with lifting surface corrections method.

The use of a design method based upon a theory permits the ability to account important information such as:

- Number of blades
- Radial blade loading
- Chordwise blade loading
- Blade shape and size
- Blade skew
- Wake adaption

Lifting-line methods with lifting surface corrections are nowadays an essential complement regarding detailed propeller design. These theories are used to find the radial distribution of optimum blade loading taking into consideration the efficiency as a first step to provide the corresponding blade geometry adapted at a specific wake. Also, these theories allow for computation of the optimum spanwise lift distribution over the propeller blade, the hydrodynamic pitch angle, the inflow velocity to each blade section, the total thrust which is produced, the power which is absorbed, and so on. Consequently the radial distribution of loading may be specified to determine the corresponding blade geometry (Lerbs (1952, 1954)). The methodology described by H.W. Lerbs is used to determine the circulation and induced velocity distributions for given values of advance coefficient using the hydrodynamic properties of the foil sections at specified radial distances along the propeller blade. If pressure distributions are either highly demanded or non realistic, there might be a mistake regarding the framework of the theory due to the solution does not show realistic output data or imply it has no solution due to this method, as all approaches, has limitations. Lifting line theory with surface corrections are able to design and analyze propellers without resorting to extensive empirical data.

5.3.1.2 Theoretical foundation.

Mathematical model for predicting the lift distribution over a three-dimensional wing based on its geometry. Lifting-line methods with lifting surface corrections used in propellers were adapted from lifting-line theory for straight foils; the vortex system of a propeller is similar to a wing with finite span (circulation theory); this theory essentially consists in replacing each propeller blade vortices by its own lifting line as described in the circulation theory with a

radial flow distribution. Propeller blades are helical wings of finite span moving in the fluid along a helical path, each blade is depicted by a bound vortex of strength varying along the length of it and a vortex sheet which is shed from the trailing edge. Lifting lines and trailing vortex systems generates the vortex system of the propeller; by varying the flow circulation with the radius of the blade, vortices are detached from the lifting line; the free vortices will be identical and spaced at constant angles to each other. The free vortex lines shed from the lifting line are not acted on by forces. Their directions, according to "wing theory", coincide with that of the resultant lifting system. These results in the free vortex lines are combined, they form a free vortex sheet that is in the form of a general helical surface aft of the propeller; the shape of the helicoidally sheets and their induced velocities are mutually dependant so certain assumptions about the shape of helicoidally sheets are demanded. It is considered that this surface comes to infinity downstream, in order to satisfy the Helmholtz's theorem.

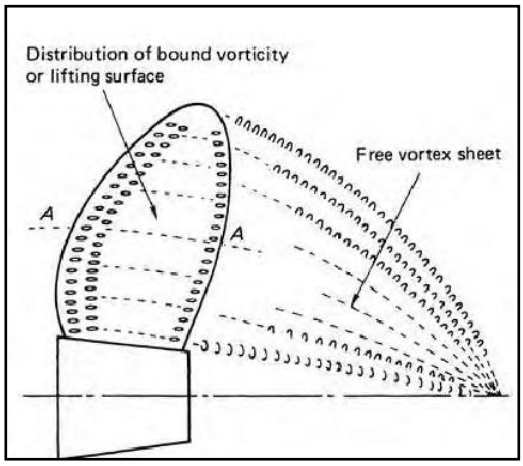

Figure 30. Vortex sheet wake.

According to Helmholtz theorem, a vortex filament cannot finish in the fluid. The variation in vortex strength is therefore assumed to result from superposition of a number of horseshoe shaped vortices (see figure 27).

The main hypotheses and assumptions of the lifting line concept can be summarized as follows:

1. The fluid is inviscid and incompressible. However, in the calculation procedure, allowance is made for the viscous drag of the blade by the use of some kind of strip theory.
2. The free stream velocity is axisymmetric and steady.
3. Each propeller blade is represented by a lifting line and the circulation varies along the radius. From vortex theory it follows that free vortices are shed from the lifting line

and, in a coordinate system that rotates with the propeller, these free vortices form a general helical surface behind the propeller.

4. Each of the free vortices is at a constant pitch in the downstream direction, but a radial variation in pitch is allowed. This means that effects of centrifugal force on the shape of the vortex sheets are ignored.
5. The lift characteristics of the blade are now described by the circulation expression[Γ].
6. The radial velocity induced at the hub is assumed small so that the effect of the hub on the pitch of the trailing sheets is ignored.
7. Lifting line calculation is always performed in steady conditions.
8. The velocity induced by the vortex system of the propeller can be determined by the law of Biot Savart or by Laplace's equation.

The lifting line results allow detailed cavitation and strength analysis. The preliminary estimates of thickness and chord distribution can now be checked and altered if necessary. It might be found that the optimum load distribution cannot be achieved. In particular, the tip might have to be unloaded. In this case, a non–optimum load distribution will have to be developed and the lifting line computation re-run.

Skew and rake are very important regarding the control in propeller vibrations. Vibration excitation results from both, the unsteady pressure forces acting on the hull and the unsteady bearing forces which result from the varying loading on the propeller. The rake is used to increase the distance between the propeller and the hull.

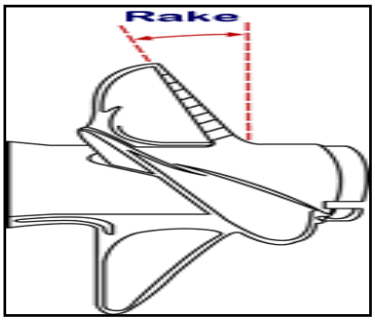

Figure 31. The rake angle.

On the other hand the skew permits a more gradual entry of the blade into the high wake region. Thus, both rake and skew tend to reduce the propeller excitation forces.

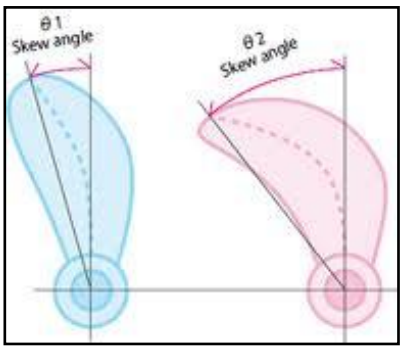

Figure 32. The skew angle.

The lifting line theory cannot recognize chordwise effects and thus it is not sufficient to use two dimensional section data to obtain the required angle of attack and camber for relatively broad bladed marine propellers. To obtain the chordwise effects, we must use a lifting surface method to compute the lifting surface corrections for the angle of attack and camber distributions. The previous lifting line theory assumptions hold for lifting surface, except now it is assumed that the bound vortices are distributed over the blade surface rather than concentrated at a lifting line, and the blade is allowed to have a finite thickness.

Moreover the propeller design based on the lifting line theory is divided as follows:

a) The hydrodynamic design phase which involves computations regarding the induced velocities, circulation resultant velocity, the chord length, the chord ratio as well as the hydrodynamic pitch angle varying at various r/R sections are determined.
b) Secondly, after the hydrodynamic design parameters are known [Γ,$U_A, U_T, \beta_i, c_L, c/D$], the final blade geometry can be known having in consideration that the final computation will provide the best solution (geometry) satisfying minimal cavitation issues at the shock angle of attack and strength criteria.

It should be noted that the biggest issue is then to select from results provided by the lifting line method with lifting surface corrections at the hydrodynamic design stage the best combination in respect with:

- The pitch [P];
- The camber [c];
- The chord length [c_L];
- Thickness [t].

However, the detailed design stage using the lifting line theory with lifting surface correction for the 800 TEU's containership propeller has been performed with 'home-made' software developed at "University of Galati, *Dunarea de Jos*" programmed in *Turbo-Pascal* code.

Following tables present the results containing the most significant information useful for further calculations.

THE LIFTING LINE THEORY WITH LIFTING SURFACE CORRECTIONS RESULTS (1)						
r/R	**RAKE** *[RD]	**SKEW** *[RD] (mean value for all sections)	**CHORD LENGTH** *[RD]	**PITCH** *[RD]	**MAXIMUM CAMBER** *[RD]	**MAXIMUM THICKNESS** *[RD]
	$\overline{x}_R$ [mt]	$\overline{c}_S$ [°]	c [mts]	φ [mts]	$\overline{f}_M$ [mts]	$\overline{e}$ [mts]
0.150	0	21	1.75	4.7463	0.12	0.25
0.200	0	21	1.86100	4.7463	0.11000	0.2450
0.300	0	21	2.05960	5.0118	0.09100	0.2100
0.400	0	21	2.23800	5.0174	0.07500	0.1775
0.500	0	21	2.38820	5.0009	0.06240	0.1468
0.600	0	21	2.49750	5.0377	0.05530	0.1186
0.700	0	21	2.54230	5.0652	0.04950	0.0922
0.800	0	21	2.47400	5.0436	0.04470	0.0669
0.900	0	21	2.15640	4.9730	0.03850	0.0432
0.950	0	21	1.85000	4.9590	0.03020	0.0310
0.975	0	21	1.45000	4.9550	0.02150	0.0245
0.985	0	21	1.09000	4.9530	0.01750	0.0225
1.000	0	21	0.00000	4.9506	0.0104	0.0208

Table 15.1. Detail design stage results made with the lifting line theory (1).

*[RD] = radial distribution.

THE LIFTING LINE THEORY WITH LIFTING SURFACE CORRECTIONS RESULTS (2)			
SHIP VELOCITY	V_S	[knot]	18.6491
		[mt/sec]	9.59340
TOTAL SHIP RESISTANCE	R_T	[kN]	599.9121
THRUST	T	[kN]	706.4622
TORQUE	Q	[kN*mt]	611.7910
THRUST COEFFICIENT	k_T		0.21200
TORQUE COEFFICIENT	k_Q		0.0354
OPEN-WATER EFFICIENCY	η_0	[%]	0.6204
ADVANCE COEFFICIENT	J		0.6550
DELIVERED POWER	P_D	[kW]	8218.6500
MINIMUM EXPANDED AREA RATIO	$\frac{A_E}{A_0}$		0.8598
PITCH	φ	[mt]	5.0097

Table 15.2. Detail design stage results made with the lifting line theory (2).

Making a comparison between results obtained during preliminary stage of design shown Table 14 (results for propeller design at preliminary stage) and those obtained in detailed design phase with lifting line theory (Tables 15.1 and 15.2). Remarking some exceptions explained later on, we may determine that, due to their similitude, we have reliable results.

Exceptions:

a) Real ship velocity: at the beginning of the detailed design stage of the propeller, we have established that our propeller would theoretically provide the design speed (Vs = 18.5 knot). Conversely, after calculations performed with lifting line theory, we have discovered that now, there is an increment of 0.15 knots, which represents 0.8% of deviation. Nevertheless, this difference is inside tolerance value (± 0.2 knots).

b) Expanded Area Ratio: During preliminary stage of propeller design, we have encountered that the minimum blade area permitted in order to avoid dangerous cavitation (more than 5%) determined with Burrill's diagrams was A.E.R.=0.8120. Now, after calculations done in detailed propeller design phase with the lifting line theory software, we have found different value of E.A.R. (A.E.R.=0.8591) which represents around 6% of error.

Although there are some differences, according to lifting line theory with lifting surface corrections procedure, reliable results have been obtained to be then used for having at the end as we have said before, a "wake-adapted propeller" for the containership; all of this, by creating now, the propeller geometry.

5.3.2 The geometry of the propeller.

Many options regarding airfoil sections are available nowadays. The two most airfoil profiles used within the marine sector with the circulation theory are *NACA-16 and *NACA-66. For our case we have selected NACA-0066 profile.

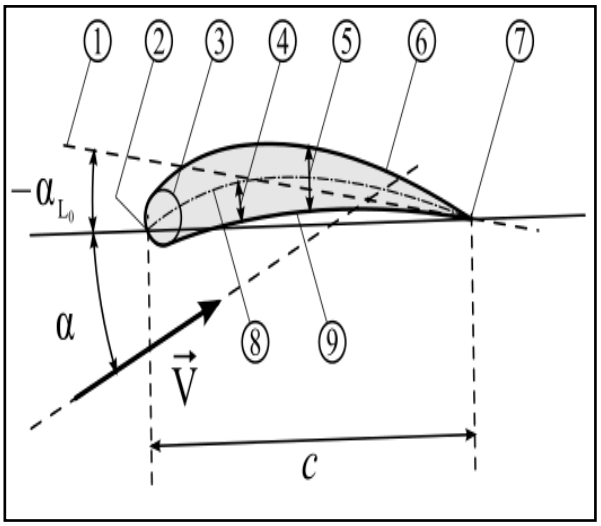

1. Zero lift line.
2. Leading edge.
3. Nose circle.
4. Camber.
5. Thickness.
6. Upper surface.
7. Trailing edge.
8. Main camber line.
9. Lower surface.

Figure 33. Airfoil geometry.

*The **NACA airfoils** are airfoil shapes for aircraft wings developed by the National Advisory Committee for Aeronautics (NACA). The shape of the NACA airfoils is described using a series of digits following the word "NACA". Developed by the advent of aerodynamic theory and experimentations (wind tunnel).

A propeller section at a given radius is the intersection between the blade and a circular cylinder of the selected radius. Later on, the section is presented as two dimensional profiles.

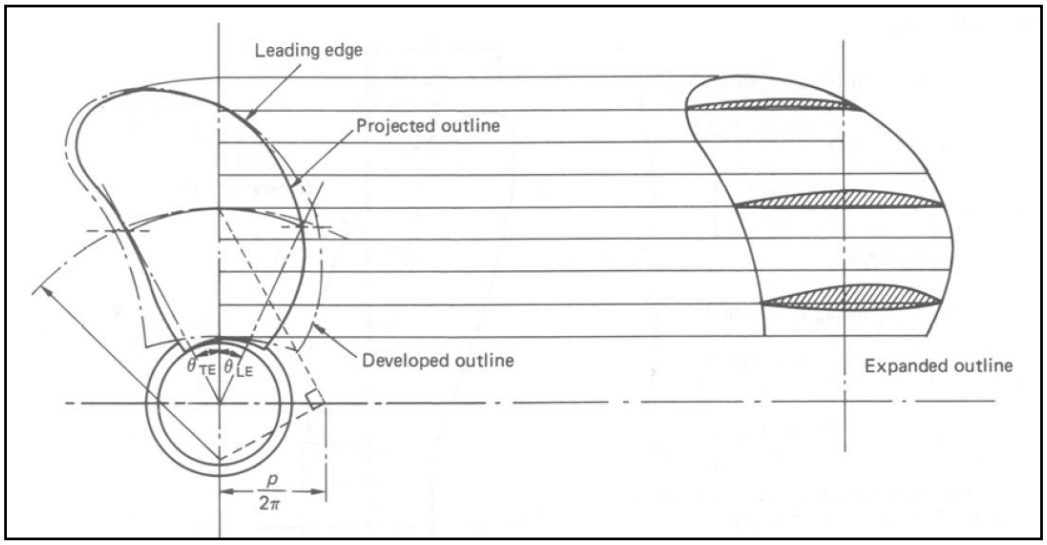

Figure 34. Representation of a propeller section at radii section given by r/R.

Then, there are three possibilities to proceed on propeller geometry design once detailed design procedure with lifting line theory has been finished, these are:

1. Given in technical drawings including a profile view; an expanded blade outline with details of the section shapes; the pitch distribution if it is not uniform and the transverse view which shows the projection outline and developed outline of the blade.

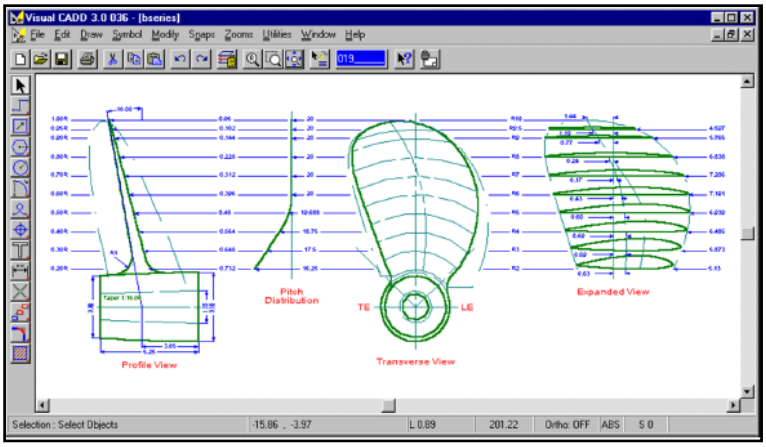

Figure 35. Example of propeller geometry in technical drawing.

2. By offset points data file,

2.1 Given directly in orthogonal coordinate system (x, y, z) which may be directly read by a C.A.D software (~.dat / ~.txt file). C.A.D. software reads these coordinates and gives automatically all offset points on each r/R section of the propeller to then, create the geometry based on this file.

NACA3DGAA: Bloc de notas

Archivo Edición Formato Ver Ayuda

```
20       24
     777.808283     200.503990     333.637097
     780.306821     212.706660     325.993005
     779.970456     220.102824     321.045650
     778.710193     225.926324     316.974540
     775.303789     235.980642     309.562109
     764.423298     256.598671     292.698965
     738.592954     288.906664     260.861077
     680.171828     334.871045     198.436250
     550.928649     381.660510      76.490637
     411.687041     387.691905     -34.792948
     265.119299     366.931182    -129.911780
     189.350249     349.942747    -170.457140
     111.788371     330.344334    -205.883908
```

Figure 36. Offset point data file extract (original).

2.1.1 We have first read the offset points with RHINO-5 software to later on, continue with the 3-D design using UNIGRAPHIPCS NX-6.

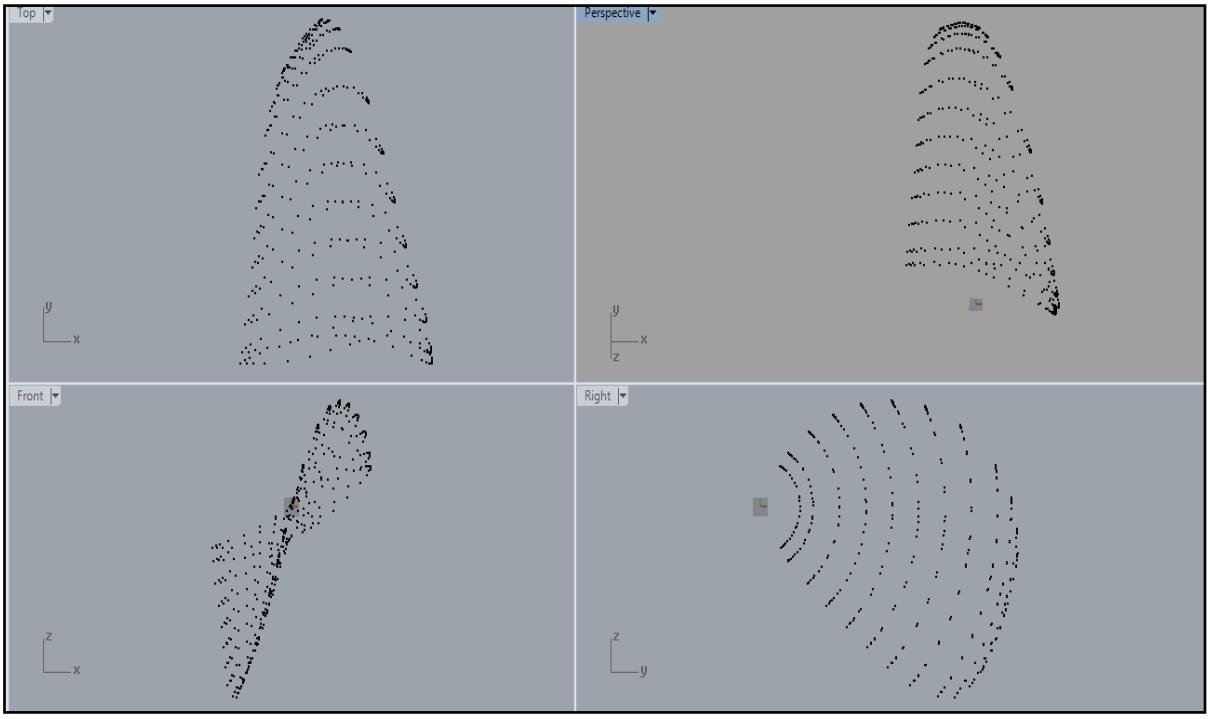

Figure 37. Propeller blade offset points for all r/R sections made on RHINO-5.

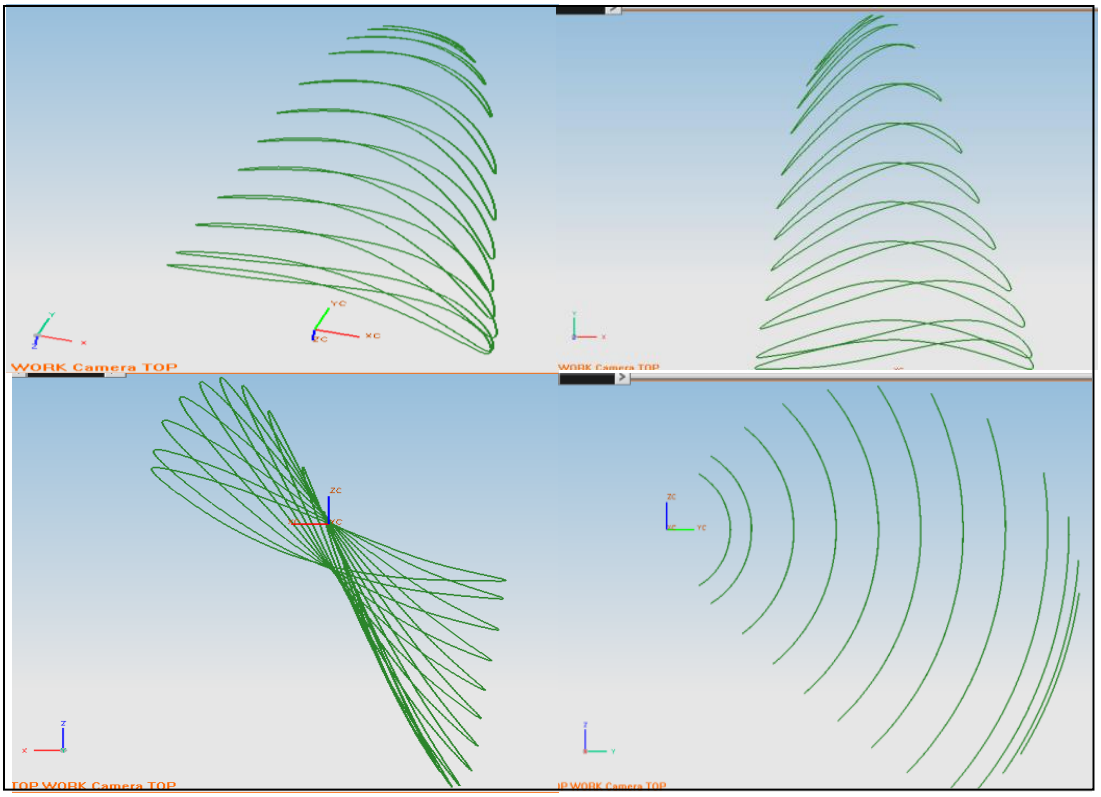

Figure 38. Propeller blade offset points after linkage between them for all r/R sections made on UNIGRAPHICS NX-6.

2.2 Provided by the lifting line method software as cylindrical coordinates $(x = \rho cos\varphi, y = \rho sin\varphi, z)$ for being transferred to orthogonal coordinate system (x,y,z) with following expressions by using on our case, the *Non-dimensional distribution for standard profiles* for NACA-66:

- For the upper side:

$$\bar{x}^{+} = \bar{x}_R + \left(\bar{c}_s + \bar{c}\bar{\xi}\right)sin\varphi + \left(\bar{f}_M F_c + \bar{e}F_T\right)cos\varphi \tag{43.1}$$

$$\theta^{+} = \frac{1}{r}\left[\left(\bar{c}_s + \bar{c}\bar{\xi}\right)cos\varphi - \left(\bar{f}_M F_c + \bar{e}F_T\right)sin\varphi\right] \tag{43.2}$$

- For the lower side:

$$\bar{x}^{-} = \bar{x}_R + \left(\bar{c}_s + \bar{c}\bar{\xi}\right)sin\varphi + \left(\bar{f}_M F_c - \bar{e}F_T\right)cos\varphi \tag{44.1}$$

$$\theta^{-} = \frac{1}{r}\left[\left(\bar{c}_s + \bar{c}\bar{\xi}\right)cos\varphi - \left(\bar{f}_M F_c - \bar{e}F_T\right)sin\varphi\right] \tag{44.2}$$

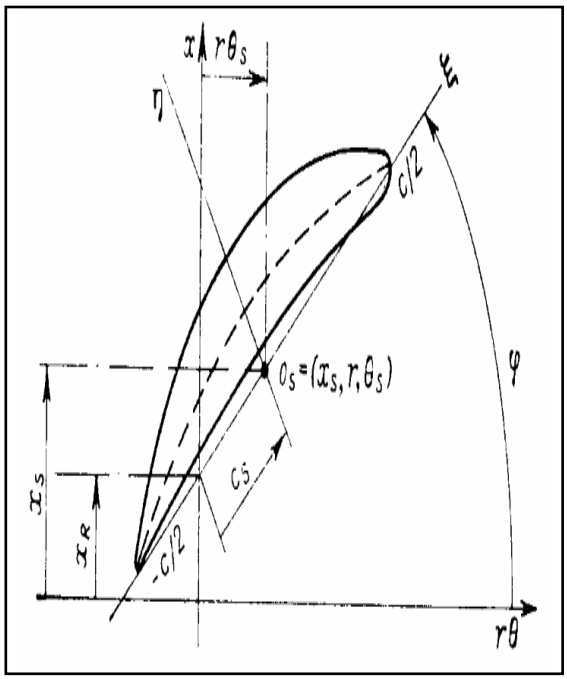

Figure 39. Wing section nomenclature.

Where all coefficients defined below are depending on the radius of the propeller geometry at different radii section r/R:

$\bar{c}_s$ = skew radial distribution;

$\bar{x}_R$ =rake radial distribution;

φ = pitch radial distribution;

c = chord length radial distribution;

$\bar{e}$ = maximum thickness radial distribution;

$F_c(\bar{\xi}, r)$= type of camber distribution;

$F_T(\bar{\xi}, r)$ = type of thickness distribution.

$\bar{f}_M$ = maximum camber radial distribution;

$\bar{\xi}$	$(1-\bar{\xi})/2$	$F_C(\bar{\xi})$	$F_T(\bar{\xi})$
1(LE)	0	0	0
0.995	0.0025	0.0235	0.0445
0.99	0.005	0.0423	0.0665
0.985	0.0075	0.0595	0.0812
0.975	0.0125	0.0907	0.1044
0.95	0.025	0.1586	0.1466
0.9	0.05	0.2712	0.2066
0.85	0.075	0.3657	0.2525
0.8	0.1	0.4482	0.2907
0.7	0.15	0.5869	0.3521
0.6	0.2	0.6993	0.4000
0.5	0.25	0.7905	0.4363
0.4	0.3	0.8635	0.4637
0.3	0.35	0.9202	0.4832
0.2	0.4	0.9615	0.4952
0.1	0.45	0.9881	0.5000
0	0.5	1	0.4962
-0.1	0.55	0.9971	0.4846
-0.2	0.6	0.9786	0.4653
-0.3	0.65	0.9434	0.4383
-0.4	0.7	0.8892	0.4035
-0.5	0.75	0.8121	0.3612
-0.6	0.8	0.7027	0.3110
-0.7	0.85	0.5425	0.2532
-0.8	0.9	0.3586	0.1877
-0.9	0.95	0.1713	0.1143
-00.95	0.975	0.0823	0.0748
-1(TE)	1	0	0.0333

Table 16. Non-dimensional distribution for standard profile for NACA-66.

3. By spline surface descriptions.

Due to output data files given after the detailed design with the lifting line theory and surface corrections was performed , we have continue the propeller geometry design by using the offset points data file (~.txt).

5.3.2.1 The skew distribution.

An important characteristic for the propeller, the skew angle has to be performed. Among some advantages of propellers having skew are a decrement regarding propeller induced pressure forces as well as the reduction bearing forces and torques.

$$\frac{SKEW}{R} = R_S - \sqrt{R_S - (r - 0.2)^2} \tag{45}$$

$$R_S = \frac{0.32}{SKEW_{VIRF}} + \frac{SKEW_{VIRF}}{2} \tag{46}$$

$$SKEW_{VIRF} = \frac{\theta_S}{cos_{\beta i}} = 21^{o} \tag{47}$$

$SKEW_{VIRF}$ = ranges between 20^{o} to 30^{o}, highly skewed propellers vary between 25^{o} to 30^{o}. The most common value is 21^{o}.

			THE SKEW DISTRIBUTION	
r/R	R_S	$\frac{SKEW}{R}$	X_a [mt]	$c - X_a$ [mt]
0.150	10.51524	-0.00442	0.875	0.87500
0.200	10.51524	-0.01256	0.9305	0.78050
0.300	10.51524	-0.04133	1.0171	0.81710
0.400	10.51524	-0.08679	1.0680	0.76800
0.500	10.51524	-0.14903	1.0778	0.67780

0.600	10.51524	-0.22817	1.0383	0.53830
0.700	10.51524	-0.32436	0.9339	0.33390
0.800	10.51524	-0.43778	0.7348	0.03480
0.900	10.51524	-0.56864	0.3631	-0.43690
0.950	10.51524	-0.64069	0.0804	-0.81960
0.975	10.51524	-0.67839	-0.1915	-1.14150
0.985	10.51524	-0.69378	-0.4018	-1.37680
1.000	10.51524	-0.71721	-0.9941	-1.97910

Table 17. Skew distribution results.

Where,

X_a = corresponds to distance between the leading edge and the generator line (vertical axis).

$c - X_a$ = corresponds to the distance between the trailing edge and the vertical axis.

c = chord.

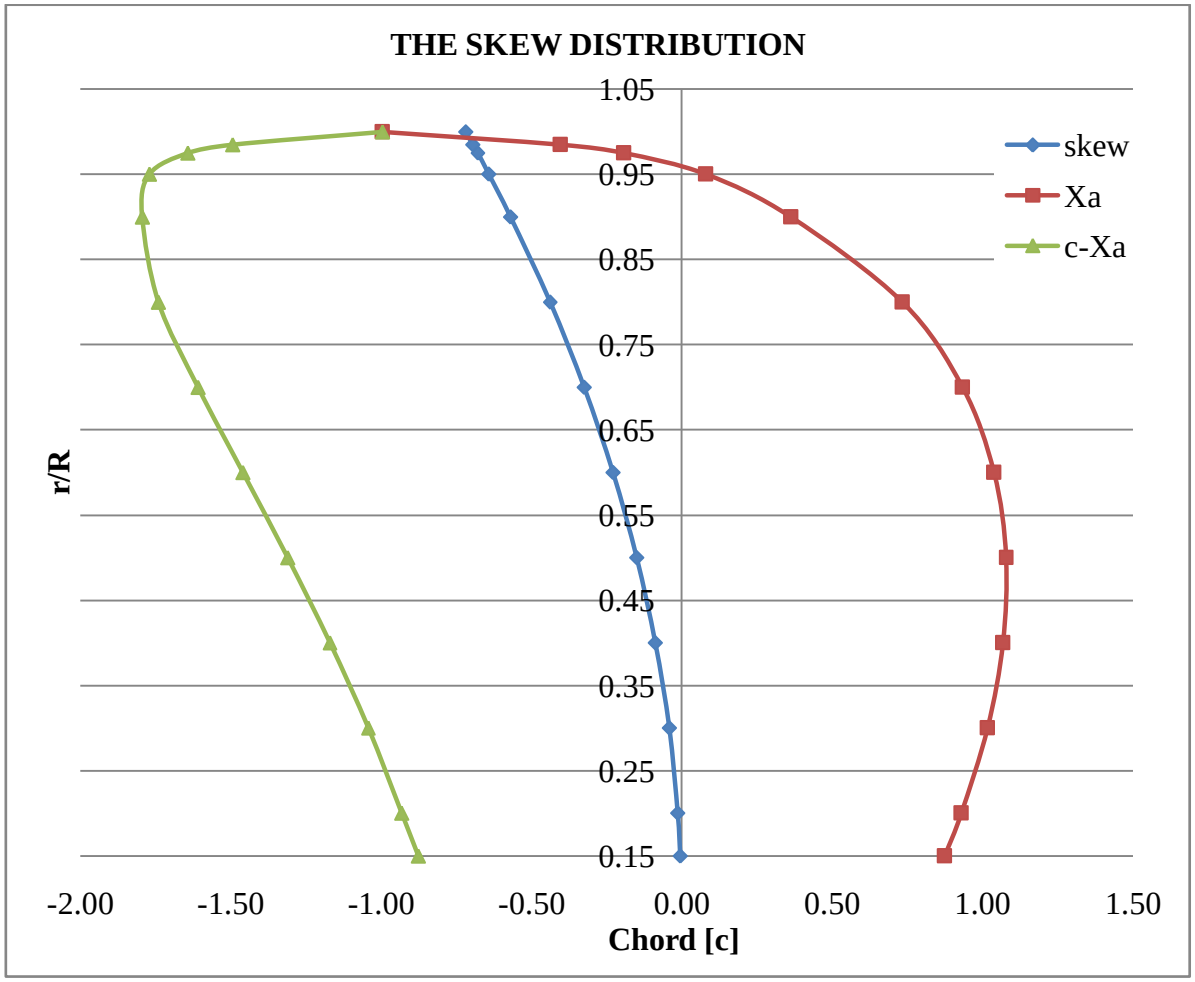

Figure 40.1. Blade profile with the skew distribution

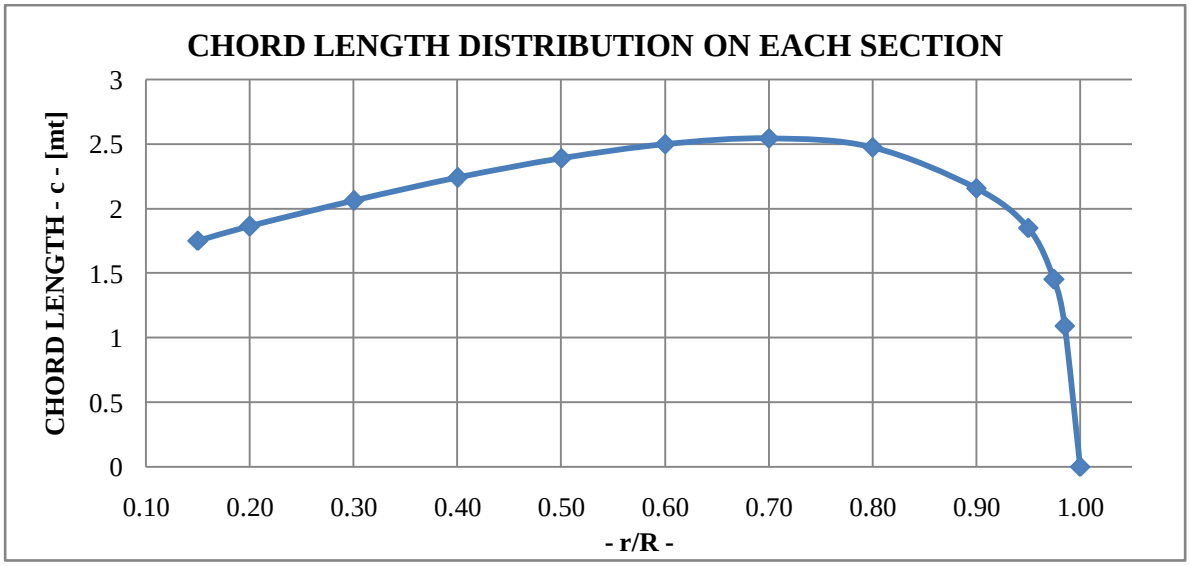

Figure 40.2. Chord length distribution on each section.

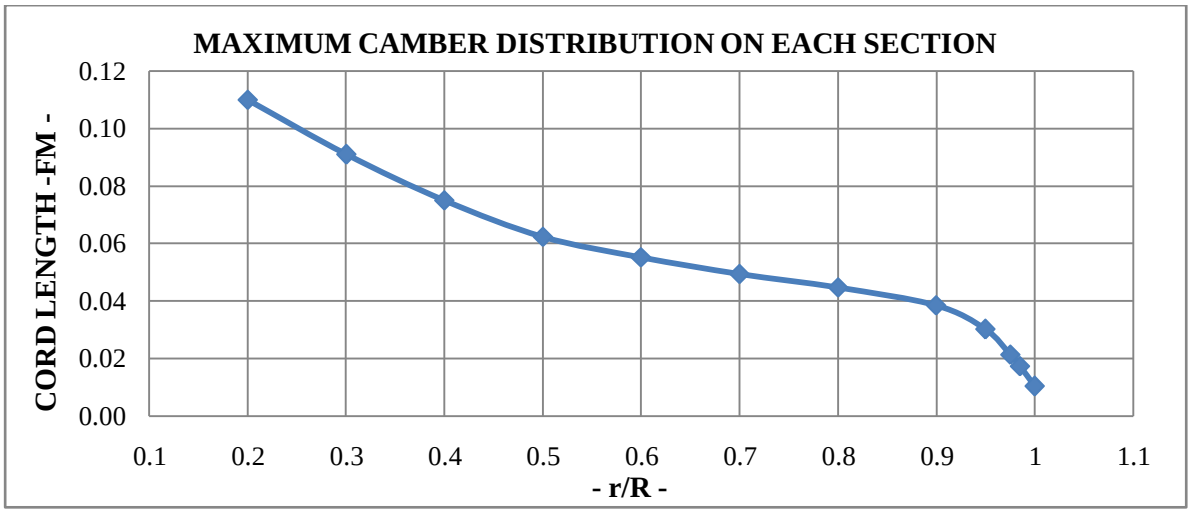

Figure 40.3. Camber distribution on each section.

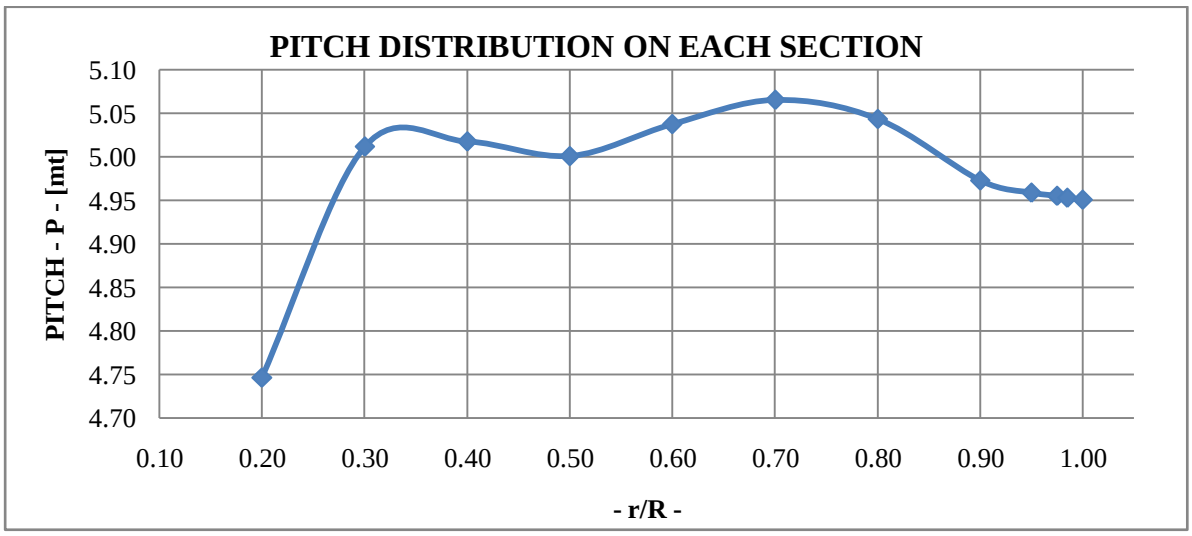

Figure 40.4. Pitch distribution on each section.

5.3.2.2 Final geometry.

The generation of the blade surface, as well as the volume of entire propeller including the hub has been performed in 3-D with *UNIGRAPHICS NX-6* software.

Hub diameter,

$$\frac{d_{hub}}{D_{opt}} = 0.17 \tag{48}$$

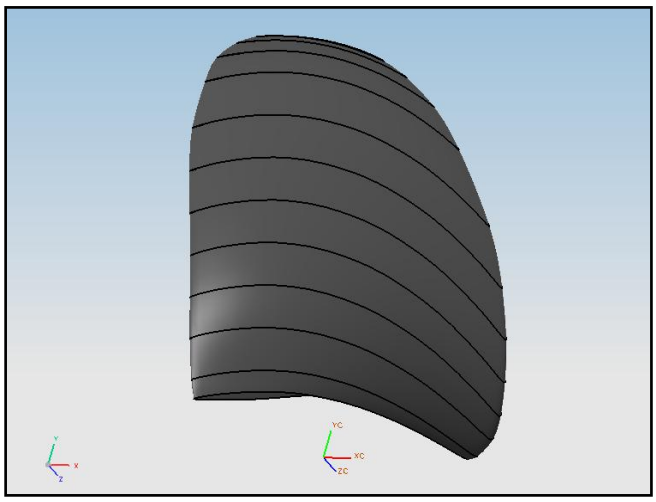

Figure 41.1. Blade surface.

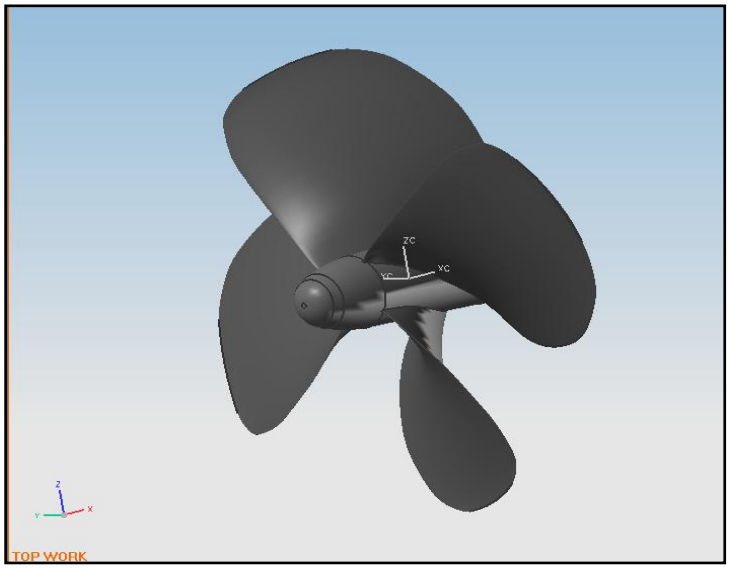

Figure 42.2 Final propeller 3-D geometry.

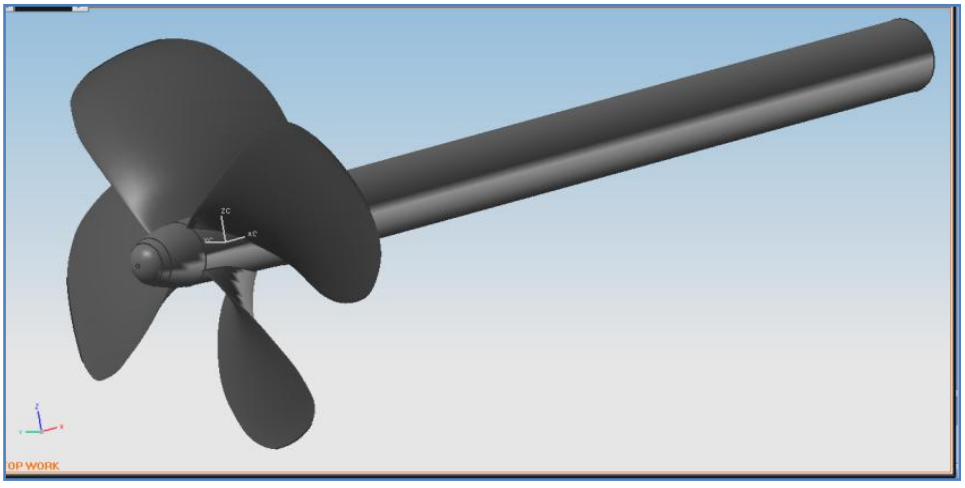

Figure 42.3. Final 3-D geometry (2).

6. THIRD STAGE: ANALYSIS OF THE DESIGN; HYDRODYNAMIC PROPELLER PERFORMANCES.

On the third stage of propeller design, the geometry is analyzed in all operating conditions. For this, it is required the detailed geometry with its characteristics and also, taking into account the effective wake distribution.

The objectives on the evaluation of the hydrodynamic propeller performance which are investigated via computational analysis or experimental tests (model test/full scale test) in off design conditions (steady and non-steady flow). Due to time consuming and expensive investigations, analytical and numerical methods are used for studying the behavior of the propeller in off design conditions.

The output data by analyzing the propeller on steady flow conditions will be then:

- Computations of the open water characteristics;
- Computation of the pressure distribution on propeller blades operating in uniform flow and/or by varying circumferentially the mean fluid flow.

The output data by analyzing the propeller on non-steady flow conditions will be then,

- Calculation of the pressure distribution on propeller blades in various blade locations; cavitation prediction;
- Computation of the unsteady forces and moments acting on the propeller shaft (bearing forces);
- Computation of the hull pressure fluctuations.

When computing with non-uniform flow the velocity changes in magnitude and direction at each revolution and thus a cyclic fluctuation in blade occurs.

During this chapter, we will perform the analysis of the propeller 3-D geometry by using steady fluid flow conditions without varying radially the mean fluid flow on different radii sections [r/R].

6.1 NUMERICAL ANALYSIS OF THE PROPELLER IN STEADY FLOW CONDITIONS WITH COMPUTATIONAL FLUID DYNAMICS.

6.1.1 Shipflow-5.0.

It is a potential and viscous flow commercial solver used for numerical simulations.

In order to run a SHIPFLOW computation, a command file must first be created in a command window (NOTEPAD++) where the user is capable to program using commands pre-established before by the code. The command file tells SHIPFLOW which modules should be executed. Each module has a specific set of commands which are unique to its operation. When specifying these commands it is necessary to tell SHIPFLOW:

- Which module you have chosen;
- Where you are beginning to define the commands;
- Where you have ended your command definition;

This is accomplished by the module delimiter commands. In our case the delimiter commands are [XFLOW] and [END].

Commands [XPAN] and [XCHAP] stated by default (by SHIPFLOW); declare if the user is employing either potential and/or viscous flow theory.

[XCHAP] is a finite volume RANS (Reynolds-Averaged Navier-Stokes) solver with a *'k-ω SST turbulence model'*. In SHIPFLOW calculations, it is used for example, in the stern where the viscous effects are important.

For our particular case, [XCHAP] has been selected for analyzing the propeller performances and to provide its open-water characteristics employing the Propeller-Open water" [POW] function which govern these computations.

```
xflow
   titl ( titl="7500, propeller B-879 ")
   prog ( xchap )
   hulltype ( POW )
   fluid (density = 1025.0, viscosity = 1.188e-6, gravity = 9.81)
```

Figure 43. SHIPFLOW-5.0 setting up.

6.1.1.1 The geometry.

The propeller 3-D geometry is replaced by default for SHIPFLOW-5.0 code as an actuator disk (sink-disk) representation having same diameter [D_{opt}] employing the variable named as [PROPELLER]. It also specifies the position of a propeller.

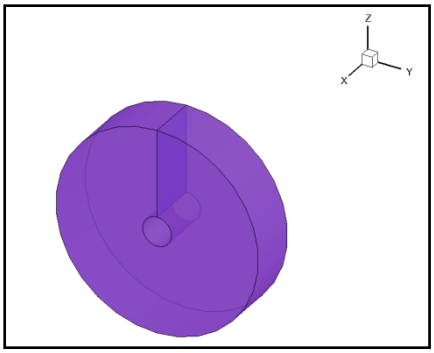

Figure 44. Propeller representation for SHIPFLOW-5.0 software.

```
propeller (  id="prop", dpro=5.20, dhub=0.886,xsh=0., zsh=0.,rotdir=1,
          nbla=4, numb=9,jv=0.8649,ear=0.879,
              r_rt=[0.2,0.3,0.4,0.5,0.6,0.7,0.8,0.9,1.0],
          p_d=[0.9145,0.9656,0.9667,0.9635,0.9706,0.9759,0.9717,0.9581,0.9538],
          c_d=[0.3585,0.3968,0.4312,0.4601,0.4812,0.4898,0.4766,0.4154,0.0],
          t_d=[0.0472,0.0404,0.0342,0.0282,0.0228,0.0177,0.0129,0.0083,0.0040],
          camb=[0.1100,0.0910,0.0750,0.0624,0.0553,0.0495,0.0447,0.0385,0.0104] )
```

Figure 45.General form of [PROPELLER] command.

[PROPELLER] must include information obtained by the lifting line theory such as:

- DPRO: propeller diameter (meters).
- DHUB: hub diameter (dimensionless).
- XSH, YSH, ZSH: propeller location.
- ROTDIR: propeller rotation direction.
- NBLA: number of blades.
- JV: propeller advance ratio. ($V_S / D_{opt} N$)
- NUMB: number of data points.
- R_RT: propeller radii sections (able to compute only 10 values);
- *P_D: pitch ratio of the corresponding blade section;
- *C_D: length of blade section of the corresponding blade section;
- *T_D: Maximum blade thickness of the corresponding blade section;
- *CAMB: Camber of the corresponding blade section;

*: divided by propeller diameter.

6.1.1.2 Propeller fluid domain.

The domain has a cubic form ([BOX] command) containing the disk (propeller) with dimensions based on the final diameter of the propeller [D_{opt}].

The structure of the program in the command file written in the executer (NOTEPAD++ command window) uses a [BOX] command to specify the domain by using *'low'* and *'high'* function (coordinates) which declare where the cubic domain will start and will finish respectively with its final dimension *'dim'*.

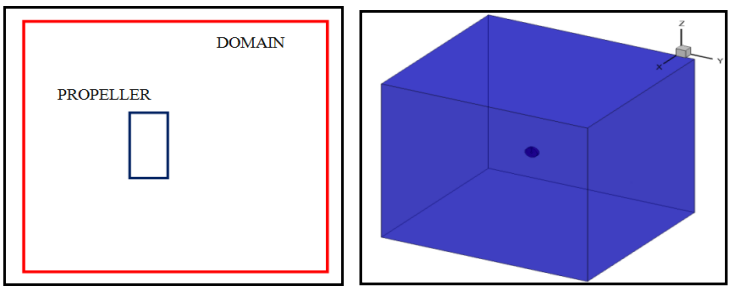

Figure 46. Fluid domain: 2-D and 3-D view respectively.

```
box ( low= [-2.0,-2.54,-2.54],high=[2.54, 2.54,.54],dime=[121,51,51],
```

Figure 47.General form of [BOX] command.

6.1.1.3 Discretization.

6.1.1.3.1The space: meshing.

SHIPFLOW code creates a rectilinear grid for [XCHAP] command where the user is capable to modify the generated mesh. On our case we have determined a refinement (stretching) in the middle of each face as it is shown on following figures.
[XCHAP] controls the propeller open-water calculation.

```
20 stretching( id="middlex", middle, s0=0.15, s1=0.8, ds0=0.35)
21 stretching( id="middlez", middle, s0=0.20, s1=0.8, ds0=0.15)
22 box ( low= [-2.0,-2.54,-2.54],high=[2.54, 2.54,.54],dime=[121,51,51],
23 str1="middlex", str2="middlez",str3="middlez",
```

Figure 48. Mesh creation and refinement declaration.

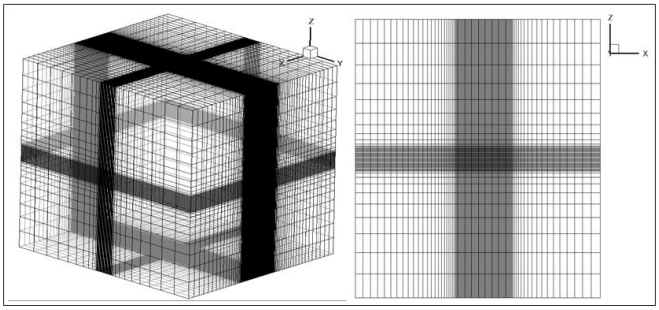

Figure 49. Mesh configuration: 3-D view (left); 2-D ‘x-z’ face view (right)

Referring the propeller grid, it is presented as structured mesh type as well.

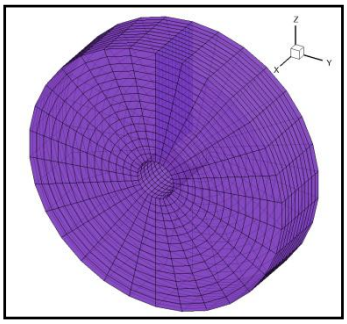

Figure 50. Propeller gird.

The propeller grid is put inside the box grid.

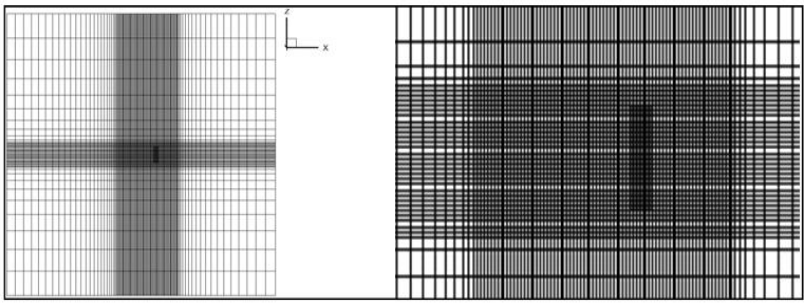

Figure 51. Side view; domain with propeller meshed.

On previous we can observe that the propeller is located not in the middle due to the fluid will flow from right to left. Because of this, we will analyze the behavior of the propeller after the fluid ‘traverse’ the actuator disk.

On the other hand the refinement is done in order to get more accurate results on the zones of interest which are before and after the propeller having more refinement on the ‘exit’ on one of the propeller face.

6.1.1.3.1.1 Boundary conditions.

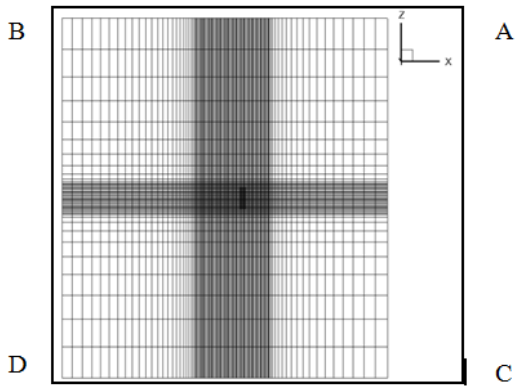

Figure 52. 2-D boundary conditions schema.

- Velocity inlet (INFLOW): condition declared on 'AC' face where the flow will enter in the domain parallel to the body (from left to right) by running different advance coefficient [J] values declared before on the command file.
- Pressure outlet (OUTFLOW): condition declared on 'BD' face where the flow "will exit"
- Walls: conditions declared on the rest of the faces where "slip" condition is assumed in slip wall normal velocity is zero but the tangential velocity is not zero (v=0,u is nonzero). The slip wall condition is for cases where viscous effects at the wall are negligible and/or the mesh size is much bigger than the boundary layer thickness.
- Body: known automatically with [POW] function.

```
str1="middlex", str2="middlez",str3="middlez",
bc11="INFLOW", bc12="OUTFLOW", bc21="SLIP",
bc22="SLIP",bc31="SLIP", bc32="SLIP")
symm( nosym )
```

Figure 53. Declaration of boundary conditions.

6.1.1.3.2. The equations: numerical simulation.

6.1.1.3.2.1 Turbulence model selection.

[XCHAP] is a finite volume code that solves the Reynolds averaged Navier-Stokes (viscous equations) equations. It uses several turbulence models *(EASM, k-*w *BSL, k-*w *SST)*. The solver can be used in a zonal or a global approach.

For our case, *k*-ω shear stress transport (SST) model has been employed for [POW] function (given as a default). One of the advantages of the *k*-ω formulation is the near wall treatment for low-Reynolds number computations.

The way that SHIPFLOW-5.0 will solve this problem is: the surface of the actuator disk which simulates the propeller will be solved using potential flow theory while the rest of the domain will employ the viscous flow theory.

6.1.1.4 Assumptions.

For the fluid we have,

SALT WATER		
DENSITY	kg/mt^3	1,025
KINEMATIC VISCOSITY [ν]	mt^2/sec	1.188x10-6

Table 18. Fluid properties.

See figure 43. SHIPFLOW-5.0 setting up for reference.

6.1.1.5 Results.

6.1.1.5.1 The open-water characteristics diagram.

To know the hydrodynamic performances of the designed propeller for different velocities we have built its open-water characteristics diagram plotting thrust [K_T] and torque [K_Q] coefficients and its open-water efficiency [η_0] for the resultant pitch ratio [P/D=0.9634] where P =5.0097 (given by the lifting line theory result).

SHIPFLOW-5.0 software provides automatically, after computations of [POW] have finished, an output data file (~.dat) which contains information about each result obtained of [K_T] and

[K_Q] for each advance coefficient [J] determined before in the command file by the user including also the optimum [J] value given by the lifting line theory calculation as well.

ADVANCE COEFFICIENT	VELOCITY [mt/sec]	RESULTS BY SHIPFLOW				
		TOTAL FORCES AND MOMENTS		THRUST COEFF	TORQUE COEFF	OPEN-WATER EFFICIENCY
		THRUST	TORQUE			
		T	Q	Kt	10*Kq	η0
J	mt/sec	kN	kN-mt			
0.1	1.1003	1204.06	865.64	0.3602	0.4990	11.49%
0.2	2.2006	1130.18	826.59	0.3381	0.4765	22.59%
0.3	3.3008	1050.20	781.65	0.3142	0.4506	33.29%
0.4	4.4011	954.64	726.33	0.2856	0.4187	43.43%
0.5	5.5014	846.44	660.42	0.2532	0.3807	52.93%
0.6	6.6017	724.15	582.79	0.2167	0.3360	61.58%
0.655	**7.2068**	**650.65**	**534.79**	**0.1947**	**0.3083**	**65.83%**
0.7	7.7020	587.24	492.67	0.1757	0.2840	68.92%
0.8	8.8022	436.71	390.55	0.1307	0.2251	73.89%
0.9	9.9025	269.41	271.34	0.0806	0.1564	73.81%
1	11.0028	98.34	139.91	0.0294	0.0807	58.06%

Table 19. SHIPFLOW results.

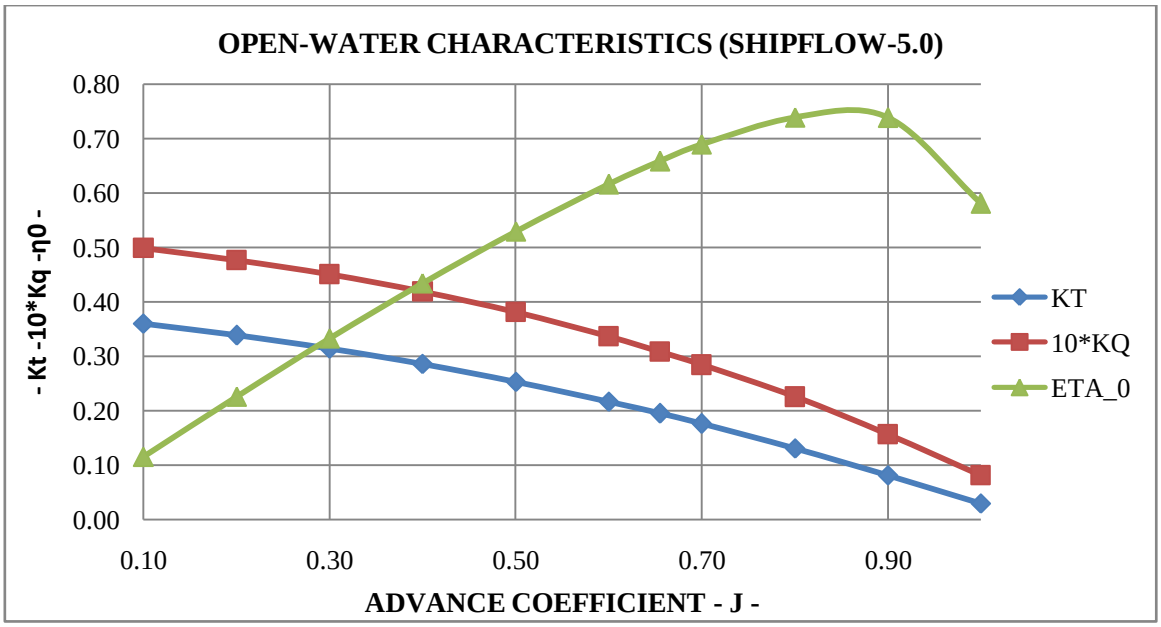

Figure 54. K_T, K_Q, η_0 diagram; results from SHIPFLOW.

6.1.2 Ansys-Fluent.

For the hydrodynamic performances of the propeller employing C.F.D. algorithms departing from the 3-D geometry including the fluid domain, both modeled in UNIGRAPHICS NX-6 PLM software. Then, the discretization has been performed ((1) space and (2) equations); 1) the mesh has been generated with WORKBENCH-13.0 platform in FLUENT-13.0 module employing finite volume methods. Later on, boundary conditions have been defined within the same mesher module of FLUENT-13.0; 2) then; the simulation has been performed with its particular assumptions of the issue such as choosing the numerical simulation, turbulence model and so on. Finally post-processing and results are shown.

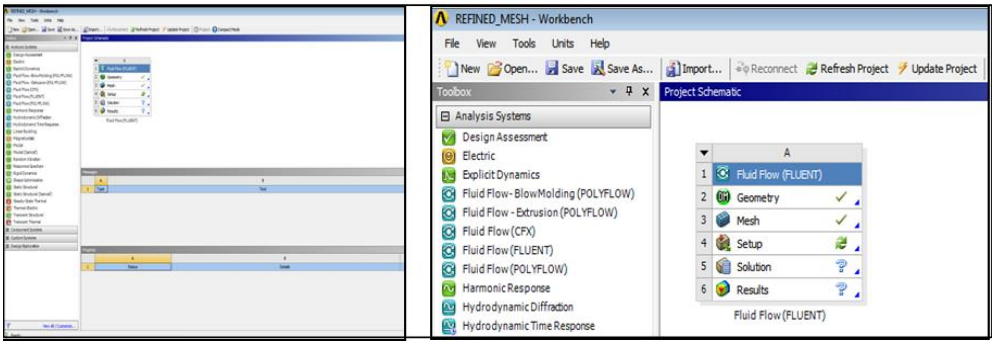

Figure 55. WORKBENCH-13.0 platform screen view.

6.1.2.1 Propeller fluid domain.

The domain will have a cylindrical form containing the 3-D geometry of the propeller with dimensions based on the final diameter of it. The propeller geometry as well as its domain has been designed with UNIGRAPHICS NX-6.

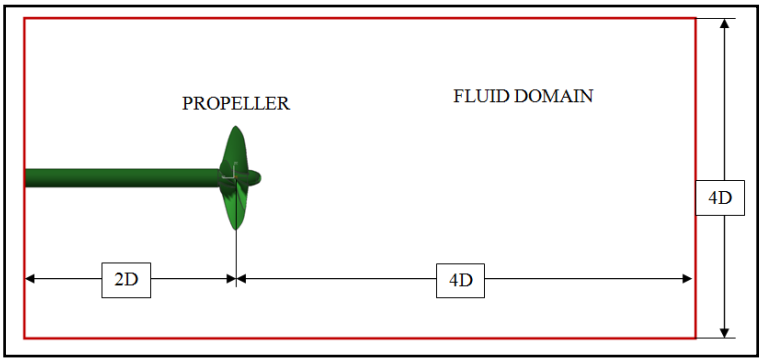

Figure 56. 2-D fluid domain dimensions schema.

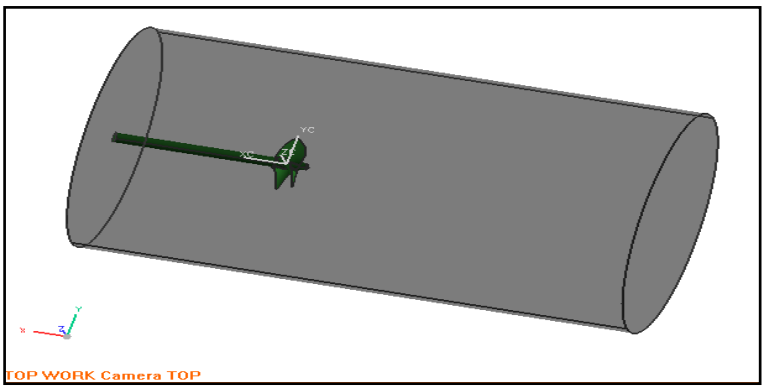

Figure 57. 3-D Propeller geometry surrounded by the fluid domain cylinder.

Later on, the volume of the propeller is necessary to be subtracted from the fluid domain with a boolean operation.

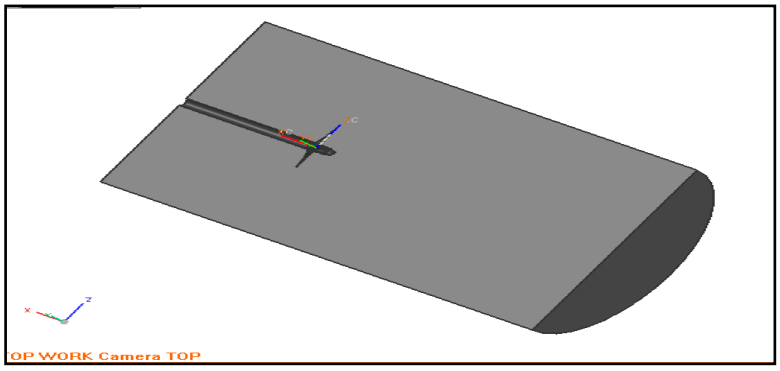

Figure 58. Body subtracted from fluid domain.

6.1.2.2 Discretization.

6.1.2.2.1 The space: meshing.

The mesh has been generated with WORKBENCH-13.0 platform in FLUENT-13.0 module employing finite volume methods. The grid was created by default with FLUENT-13.0 mesher as well having following mesh details:

MESH TYPE		DEFAULT - FINE
RELEVANCE		REFINED
MINIMUM SIZE OF ELEMENT	[mm]	50
MAXIMUM SIZE OF ELEMENT	[mm]	950
GROWTH RATE		DEFAULT (1.10)

TRANSITION		SLOW
ELEMENT TYPE		TETRAHEDICAL
TOTAL NO. OF ELEMENTS (CELLS)		2601932
TOTAL NO. OF NODES		450291

Table 20. Mesh details.

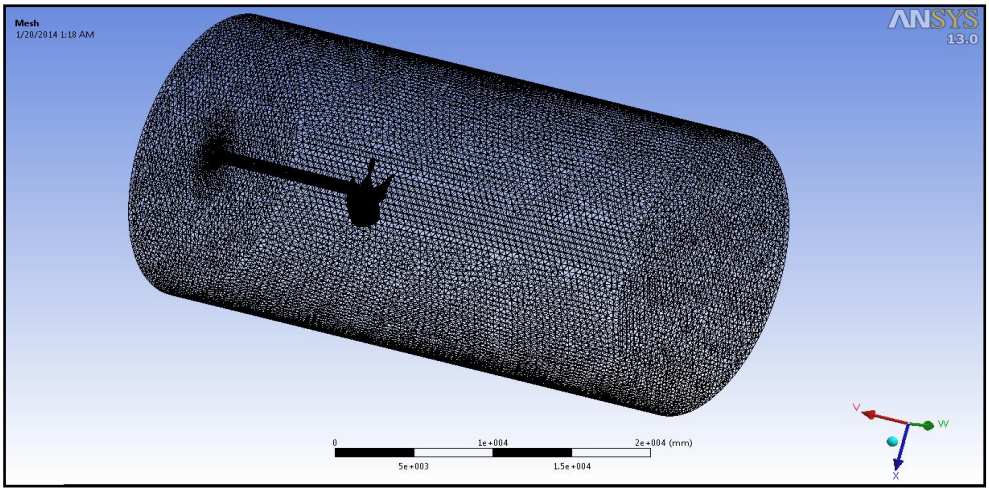

Figure 59. Mesh generation on propeller and fluid domain.

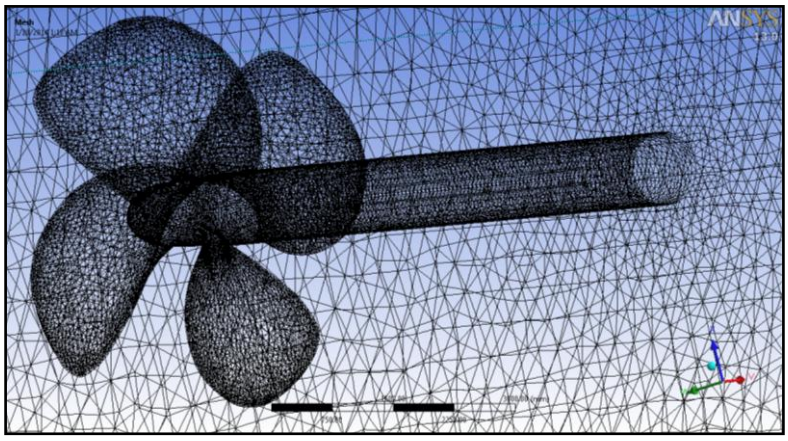

Figure 60. Mesh generation on propeller with refinement.

6.1.2.2.1.1 Boundary conditions.

The resolution of the problem depends largely on the boundary conditions imposed to which the fluid is subjected. To comprehend how the simulation will be run, following boundary conditions have been taken into account:

- Velocity inlet $\frac{\partial \varphi}{\partial x} = u$: condition declared on 'AC' face where the flow will enter in the domain parallel to the body (from left to right) by running different velocities given by the advance coefficient formulae [J] computed from *J=0.1~1.4* and fixing optimum diameter [$D_{opt} = 5.20\ mt$] and revolution rate [*n =2.12rps*] values.
- Pressure outlet: condition declared on 'BC' face where the flow "will exit" (a reference pressure in order to the fluid keeps its course, this case the value is cero static pressure).
- Wall (boundary surface of the domain): limits of declared domain with non-slip wall (non-slip shear condition, normal velocity on walls is cero, we do not take into account on it).
- Body: propeller geometry; taken as 'stationary' wall with no slip shear condition.

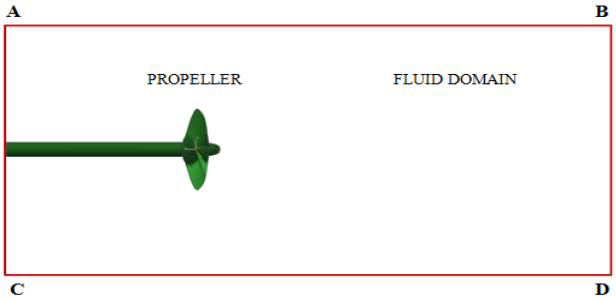

Figure 61. 2-D boundary conditions schema.

Based on previous schema, boundary conditions have been applied to the 3-D model.

6.1.2.2.2 The equations: numerical simulation

6.1.2.2.2.1 Turbulence model selection.

For our study case we have selected from several options offered by the Reynolds Average Navier Stokes methods (RANS) and the 'eddy-viscosity turbulence models' the **'Realizable k-ε turbulence model'.** It is the simplest and complete turbulence model which uses 2-

equation models in which the solution of 2 separate transport equations allow the turbulent velocity and length scales to be independently determined; where [k] is established as the first transported variable determines the energy in the turbulence and is called *"turbulent kinetic energy"*; [ε] is the second transported variable named as the turbulent dissipation which determines the rate of dissipation of the turbulent kinetic energy obtained by equilibrium condition ($P_k = \varepsilon$).

6.1.2.3 Assumptions.

For the fluid we have,

SALT WATER		
DENSITY	kg/mt^3	1,025
KINEMATIC VISCOSITY [v]	mt^2/sec	1.188x10-6

Table 21. Fluid properties.

It is declared as:

1) Ideal fluid:
    a. Incompressible.
    b. Inviscid.

6.1.2.3.1 Fluent.

The fluid has being considered as rotational along its pass through the domain. The rotation type of the fluid is stated as FLUENT calls 'moving reference frame' with a fixed angular celerity [ω] of 127 RPM.

The propeller body is then kept as stationary while the effect of the rotational movement of the propeller has been applied to the fluid zone.

The pressure velocity coupling method has been selected as *'simple',* due to it is applicable for a steady state flow condition.

The discretization method is then selected as *'standard'* for the momentum, turbulent kinetic energy and the turbulent dissipation rate.

6.1.2.4 Results.

6.1.2.4. The open-water characteristics.

To know the hydrodynamic performances of the designed propeller for different speeds we have built its open-water characteristics diagram plotting thrust [K_T] and torque [K_Q] coefficients and its open-water efficiency [η_0] for the resultant pitch ratio [P/D=0.9634] where P =5.0097 (given by the lifting line theory result).

By reading total forces and moments from all simulations performed in FLUENT code, they were converted in thrust and torque coefficients as well as the open-water efficiency for each of them with known expressions respectively (equations 15, 15.1 and 15.2).

ADVANCE COEFFICIENT	VELOCITY [mt/sec]	FLUENT 6.3.26				OPEN-WATER EFFICIENCY
		TOTAL FORCES AND MOMENTS		THRUST COEFF	TORQUE COEFF	
		THRUST	TORQUE			
		T	Q			
J	mt/sec	kN	kN-mt	Kt	Kq	η0
0.10	1.1003	1507.733	1105.074	0.4511	0.0637	11.27%
0.20	2.2006	1493.332	1095.289	0.4468	0.0631	22.52%
0.30	3.3008	1178.153	887.35	0.3525	0.0512	32.90%
0.40	4.4011	1011.127	778.359	0.3025	0.0449	42.92%
0.50	5.5014	843.714	668.23	0.2524	0.0385	52.15%
0.60	6.6017	676.348	556.214	0.2024	0.0321	60.27%
0.655	7.2068	736.191	596.612	0.2203	0.0344	66.76%
0.70	7.7020	660.843	545.835	0.1977	0.0315	70.00%
0.80	8.8022	340.37	325.615	0.1018	0.0188	69.08%
0.90	9.9025	159.237	199.161	0.0476	0.0115	59.44%
1.00	11.0028	141.369	186.806	0.0423	0.0108	62.51%

Figure 22. FLUENT results.

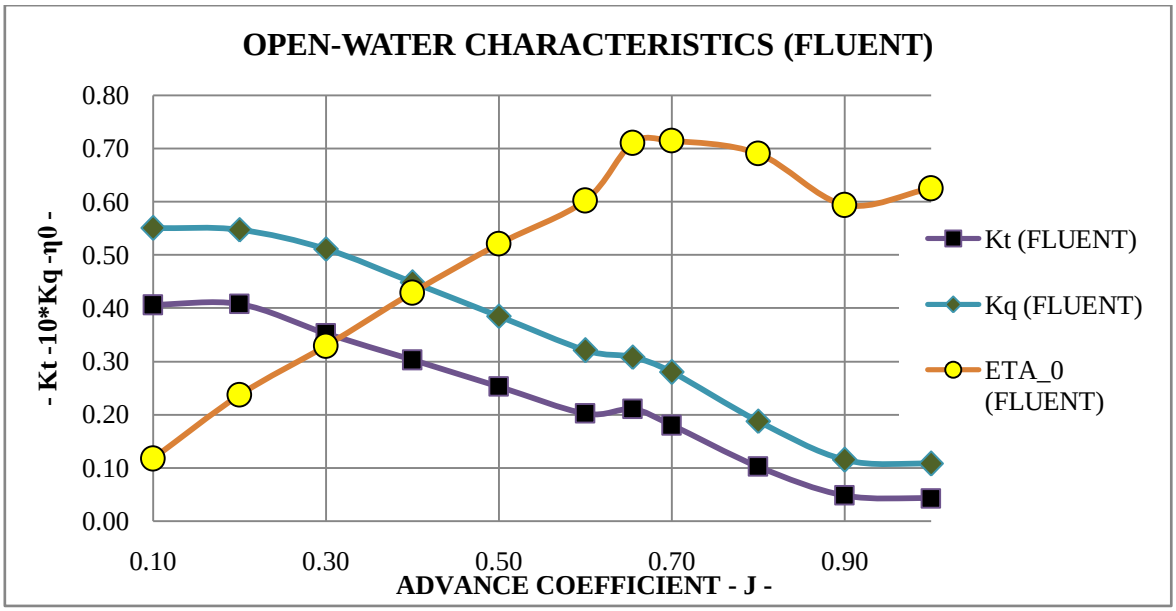

Figure 62. K_T, K_Q, η_0 diagram; results from FLUENT.

As we can observe on previous figure, for [J] values between 0.20 to 0.60 approximately, it gives congruent results while small and big [J] values there exist no accuracy.

6.1.2.4.2 Thrust [t] and torque [q] for design speed [V_S].

Input data taken from detailed design with the lifting line method

- $V_S = 18.649\ knot.$
- $V_A = 7.2068 \frac{mt}{sec}$
- $N = 127\ RPM$
- $J = 0.655$

Once the solution has converged and the chart of drag coefficient is stable as we can see on figure 63, we have found following results regarding total force and total moment.

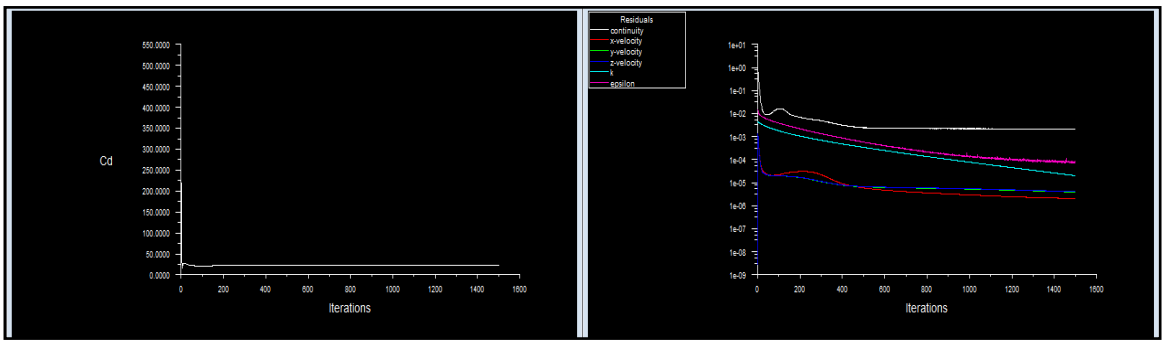

Figure 63. Drag coefficient diagram (left); convergence diagram (right).

After 1500 iterations we have,

1. Total force (Thrust): the axial forces (‘x’ axis) on the propeller ,

PRESSURE FORCE	VISCOUS FORCE	TOTAL FORCE
[kNewton]	[kNewton]	[kNewton]
736.858	-0.666582	736.191

Table 23.1. Total force results with CFD-methods.

2. Total moment (Torque): the moment produced by the rotation of the fluid flow around the propeller is,

PRESSURE MOMENT	VISCOUS MOMENT	TOTAL MOMENT
[kN-mt]	[Kn-mt]	[kN-mt]
596.336	0.27630347	596.612

Figure 23.2. Total moment results with CFD-methods.

The difference between results obtained by the lifting line method with lifting surface corrections and C.F.D. methods (in open-water characteristics) is then,

		LIFTING LINE THEORY	CFD –ANALYSIS open-water chrc)	DIFFERENCE	ERROR [%]
TOTAL THRUST	[kNewton]	706.4622	736.191	29.7288	4.21
TOTAL TORQUE	[kN-mt]	611.791	596.612	15.179	2.48

Table 23.3. Comparison results and error percentage.

As a conclusion we could say that the fact that the propeller remains stationary and the fluid rotational [N=127 RPM] influences the accuracy on the result. On the other hand, the error margin on torque and torque could be due not only to the turbulence model but also due to the parameters defined in the used turbulence *model k-epsilon Realizable with standard Wall Functions*.

Another parameter to take into account is that previous comparison done regarding results total forces and moments is in theory, nor correct due to the lifting line theory results were obtained based on which the propeller is designed for the given wake distribution radially varied; on contrary, computations performed in FLUENT were done based on the global wake value (open-water characteristics).

In order to be more precise, we may run a simulation varying the velocity of the flow radially on each [r/R] section.

6.1.2.4.3 Analysis on pressure field

We cannot depreciate the study on pressure field presented on the blades for the proposed design. Based this analysis on the momentum theory as well as the wing theory and the distribution of pressure over an airfoil employing post-processing.

Coming back to the propeller theory, the momentum theory declares that: the production of thrust thanks to propeller (regarded as an actuator disk) based on axial (and rotational) changes acting in the fluid flow (see propeller theory, page 57). In other words, it describes that the flow experiences a decrement in pressure while it reaches the propeller up to the propeller itself. Knowing Bernoulli's principle, the velocity of the fluid is then increased when it is close to the disk. Right after when the fluid 'touches' the blade, there exists a sudden increment (again) of the pressure because of the tangential shear stress generated by the rotation of the propeller (see figure 21).

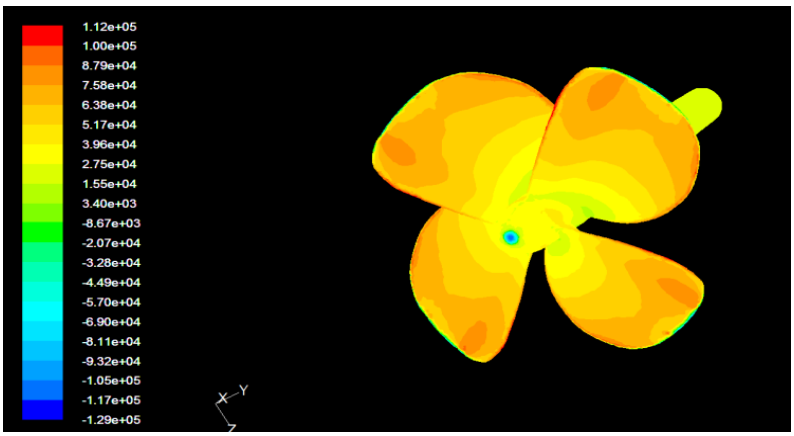

Figure 64.1. Pressure distribution over the face of the propeller at J=0.655.

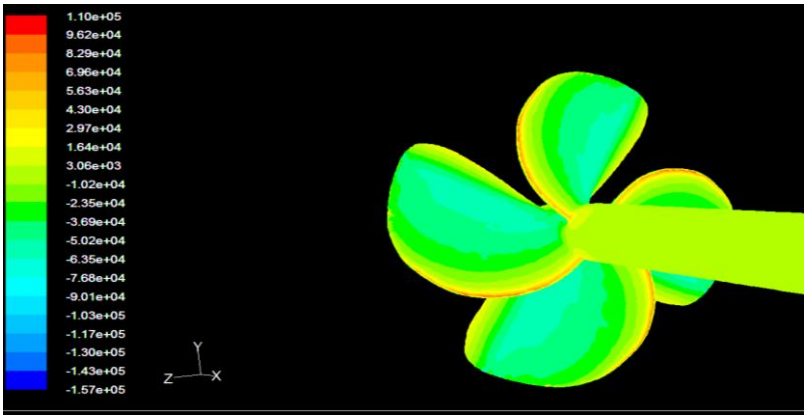

Figure 64.2. Pressure distribution over the back of the propeller at J=0.655.

As we can observe on figure 64.1, the pressure is relatively high due to the thrust generated for each blade while turning.

Looking on pressure field, it would provide important information from design point view. Whit this treatment of information, the designer is able to know where high pressures would be encounter. On the other hand pressure distribution on the propeller can let you know about risk of cavitation; pressure below boiling water point will provoke this phenomenon. If this occurs, we may face other problems such as noise, vibrations, erosion and so on.

6.2 COMPARISON: THE OPEN-WATER CHARACTERISTICS DIAGRAM SHIPFLOW –FLUENT.

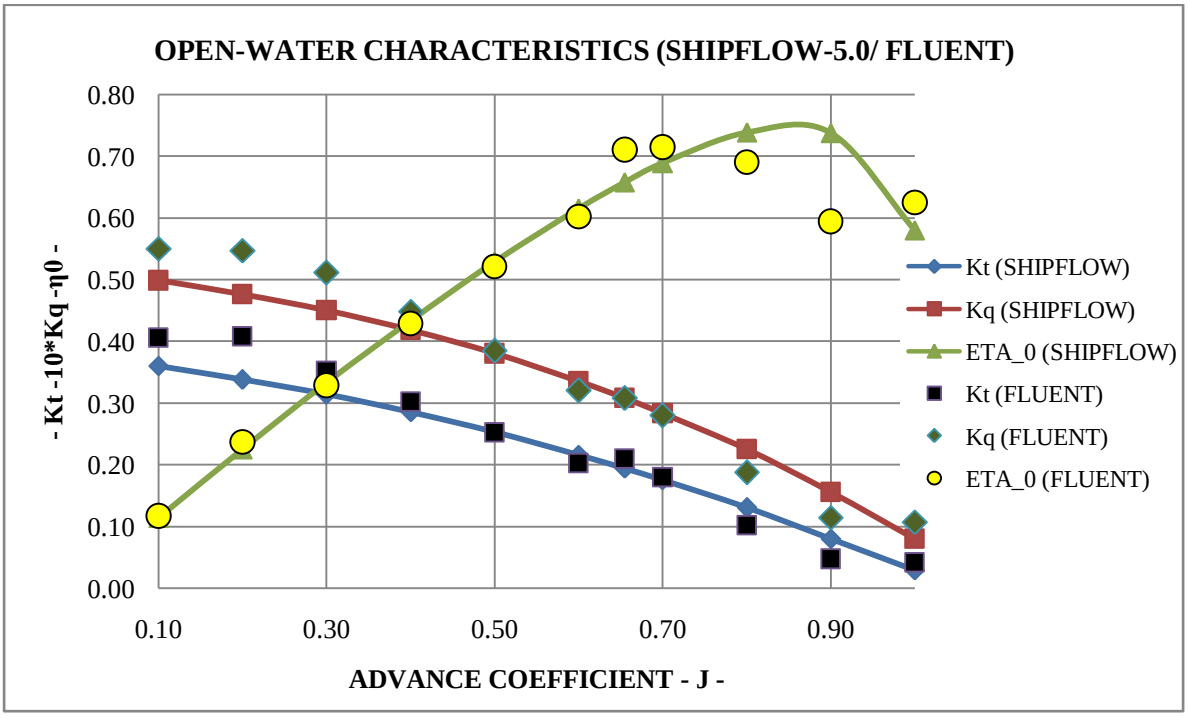

Figure 65. Open water characteristics comparison between SHIPFLOW-5.0 and FLUENT.

Comparing results obtained from two different CFD method software, it can be seen that there are similitude regarding open water characteristics calculations. For advance coefficient values between 0.20 to 0.60 approximately, they have similar tendency while for bigger [J] values, FLUENT code gives no reliable information.

Regarding this behavior from FLUENT results, one conclusion could be referred to the grid, due to the used mesh was created with default refined characteristics.

It should be noted also that SHIPFLOW-5.0 computes the open-water characteristics based on calculations performed with the Lifting line theory with surface correction; in contrary as we said previously, in FLUENT code we have built our open-water characteristics diagram based on the global wake coefficient, this means, one velocity imposed on the fluid and not varied radially for each [r/R] section of the propeller; that is why also, we could find some mistakes.

7. CONCLUSIONS.

Designing the propeller through systematic series is a topic which we cannot avoid it. It permits us to get an idea about the device but, due to its disadvantages explained before that result from selecting a propeller belonging to a systematic series, there is no justification for waiving the propeller design by direct calculation using lifting line methods with surface corrections which provides feasible results.

Considered the propeller design as an iterative procedure having one objective: to provide maximum thrust to propel the vessel with minimum power consumption without vibration, cavitation and other restrictive conditions. This iterative process concludes after the designed propeller is analyzed with numerical simulations to later on, built on scale and tried out. Once this examination is approved, we can determine that the design is finished. But, we cannot assure the expected hydrodynamic performances until the real propeller be checked on real conditions.

More and more, the design techniques have to improve continuously by applying modern methods in order to predict the hydrodynamic performances of propellers in its real environment. The implementation of computational fluid dynamics codes for performing analysis in off design conditions provides reliable information in order to validate the design.
The use of numerical algorithms during the last part of the propeller design loop for performing the study of the behavior of the proposed propeller on this thesis had the objective first, being involved with numerical methods for getting the knowledge of these kind of simulations regarding propeller design as well as to understand how one issue can be solved on different manners. There were discrepancies regarding results due to, the lack of experience about numerical simulations (the physics of it) and the ability to manipulate these tools as well as the selection of different parameters for example, type of grid selected in FLUENT for example, from personal point of view. Even these results were not the expected; it is a good starting point for further analysis employing computational fluid dynamics on this field.

REFERENCES.

1	Amoraritei,M. *,"Ship propulsion lectures",* 2013,UGAL, RO.
2	U. Politecnica de Catalunya, *"Resistance & Propulsion lectures"*, 2012, U.P.C., SPAIN.
3	V. Lewis, Edward, "PNA Volume II- Resistance, Propulsion and Vibration", SNAME
4	Ghose, J.P., Gokarn, R.P., *"Basic ship propulsion",* 2004, Allied Publishers, INDIA.
5	F. Molland Anthony; R. Tumirck Stephen; A. Hudson, Dominic. *"Ship resistance and propulsion: practical estimation of propulsive power",* 2011, Cambridge Press University, USA.
6	Crlton, John*, "Marine propellers and propulsion*", 2nd. ed, 2007, B-H publications, USA.
7	f. Molland, Anthony, *"The maritime engineering reference book"*, 2008, B-H publications, USA.
8	Schneekluth, H., Bertram. V.,*"Ship design for efficiency and economy"*, 2nd ed., 1998, B-H publications, USA.
9	Bertram, V. *"Practical ship hydrodynamics",* 2000, B-H publications, USA.
10	D.G.M. Watson, *"Practical ship design"*, volume I, Ocean Eng. series editors, SCOTLAND.
11	Alvarino C. R., Azpiroz A., J.J., Meizoso F. M.*, "El proyecto basico del buque mercante",* 2000, Fondo editorial de Ing. Naval, Colegio oficial de Ing. Navales, SPAIN.
12	Breslin P., John, Andersen, Poul, *"Hydrodynamics of ship propellers",* 1993, Cambridge University Press, USA.
13	Holtrop, J and Mennen, G.G.J.*, "An approximate power prediction method"*, 1982.
14	Bernitsas, M.M., Ray, D., Kinley, P., *"Kt, Kq and efficiency curves for the Wageningen B-series propellers",* 1987, University of Michigan, USA.
15	Amoraritei, M., *"Theoretical study on propulsive performances and exciting forces induced by ship propeller",* 20010, The annals of Dunarea de Jos, UGAL, ROMANIA
16	Amoraritei, M., *"Developments in the design of ship propeller",* 2005, Workshop on vortex dominated flows, ROMANIA.
17	Amoraritei M., "*Numerical simulation and analysis of flow around marine propeller",* 2006, International conference on fluid dlow technologies, September 6-9.

18	MAN Diesel & Turbo, "*Basic Principles of ship propulsion",* MAND&T publications, DENMARK.
19	Gaafary, M.M., El-Kilani, H.S., Moustafa, M.M*., "Optimum design of B-series marine propellers",* 2010, Alexandria Eng. Journal, Alexandria University, EGYPT.
20	Kuiper, G., *"New developments and propeller design",* 2010, 9th Intnl. Conference on Hydrodynamics, THE NETHERLANDS
21	FLOWTECH, "SHIPFLOW-5.0", User Manuals, FLOWTECH products, SWEEDEN.
22	ANSYS, "ANSYS-FLUENT", User manuals and workshops, USA.

ACKNOWLEDGEMENTS.

This thesis was developed in the frame of the European Master Course in “Integrated Advanced Ship Design” named “EMSHIP” for “European Education in Advanced Ship Design”, Ref.: 159652-1-2009-1-BE-ERA MUNDUS-EMMC.